Quantum Critical Systems from AdS/CFT

Jie Ren

A Dissertation
Presented to the Faculty
of Princeton University
in Candidacy for the Degree
of Doctor of Philosophy

Recommended for Acceptance
by the Department of
Physics
Advisers: Steven S. Gubser and Christopher P. Herzog

June 2013

Abstract

The AdS/CFT (anti-de Sitter/conformal field theory) correspondence enables us to construct some strongly coupled quantum field theories by means of general relativity, and this approach provides new universality classes of condensed matter systems. In this dissertation, we will consider three systems.

The first system (chapter 2) is the Reissner-Nordstrom (RN)-AdS_4 black hole at finite temperature. By solving the Dirac equation for a massive, charged spinor in this background, we find that the fermions have a Rashba-like dispersion relation, and the Fermi surface has a spin-orbit helical locking structure. We use an improved WKB method that takes into account the spin-orbit coupling. The effective potential has a potential well with a barrier. The quasibound states in the potential well can tunnel through the barrier into the horizon, giving an imaginary part to the mode.

The second system (chapter 3) is the two-charge black hole in AdS_5 at zero temperature, which gives an analytically solvable model for the holographic Fermi surface. Descending from type IIB supergravity, the two-charge black hole describes N coincident D3-branes with equal, nonzero angular momenta in two of the three independent planes of rotation orthogonal to the D3-brane world volume. The IR geometry of the extremal two-charge black hole is conformal to $AdS_2 \times \mathbb{R}^3$, and the electric field vanishes in the near horizon limit.

The third system (chapter 4) is the extremal RN-AdS_5 black hole, in which quantum criticality is studied by solving the Klein-Gordon equation. The Green's function near quantum critical points is analytically obtained. There are two types of instability: the first one is triggered by a zero mode, and gives a hybridized critical point; the second one is triggered by the instability of the IR geometry, and gives a bifurcating critical point.

Acknowledgements

I am very grateful to my two advisors, Profs. Steven S. Gubser and Christopher P. Herzog, for their guidance and inspiration.

I thank Profs. I. R. Klebanov and A. M. Polyakov for their excellent courses. I thank Profs. F. D. M. Haldane, D. A. Huse, I. R. Klebanov, and especially A. M. Polyakov for discussions.

I thank Prof. M. Z. Hasan and his graduate student Matthew Xia for my experimental project about angle-resolved photoemission spectroscopy (ARPES), which turned out to be very related to my research on AdS/CFT.

I thank my other fellow students, without whose help I probably could not pass the prelims.

Contents

Chapter 1

Introduction to applied AdS/CFT

1.1 What is in common among water, CO_2, and a magnet?

Theoretical physics tries to understand nature in terms of a few simple principles. As an example, water, CO_2, and a magnet are seemingly different things, but they all have a second-order phase transition with the same critical exponents; they belong to the same universality class. Close to the critical points A, B, and C illustrated in figure 1.1, they are described by the same quantum field theory (QFT) with the action[1]

$$S = \int d^d x \left(\frac{1}{2} (\partial_\mu \phi)^2 + \frac{1}{2} m^2 \phi^2 + \frac{\lambda}{4!} \phi^4 \right). \tag{1.1}$$

In $d > 4$ dimensions, the theory is non-renormalizable, which implies that it is only well-defined under a certain energy scale, and in the low energy limit, quantum effects can be neglected and the mean field theory can be used. In $d < 4$ dimensions, the theory is super-renormalizable, which implies that in the high energy limit, the theory becomes free, while in the low energy limit, the theory becomes strongly coupled, and

[1] Written in Euclidean signature. The statistical mechanics in d spatial dimensions at finite temperature is equivalent to a quantum field theory in d spacetime dimensions at zero temperature.

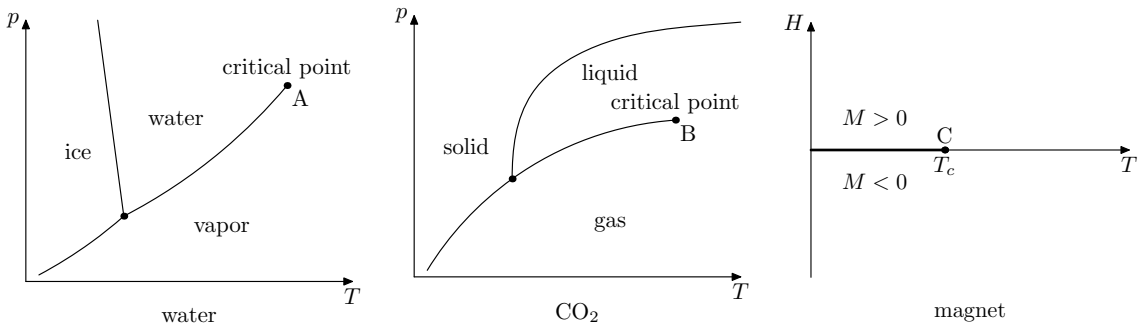

Figure 1.1: Schematic plot of phase diagrams for water, CO_2, and a magnet. Here T is the temperature, p is the pressure, and H is the magnetic field. There is a second-order phase transition at critical points A, B, and C.

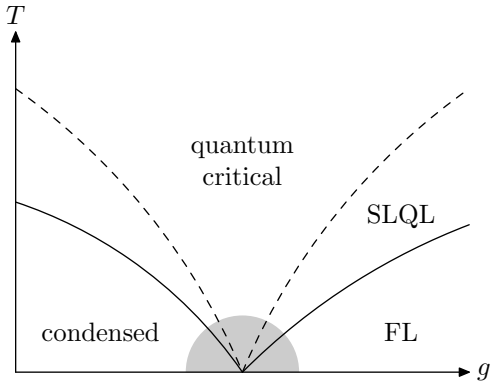

Figure 1.2: (Adapted from ref. [2].) Schematic plot of the phase diagram near a quantum critical point. FL stands for Fermi liquid, and SLQL stands for semi-local quantum liquid.

the standard technique of perturbation in λ is not valid. In this case, the theory flows to an infrared-stable fixed point when $d < 4$ [1]. Another example of a strongly coupled system is the Yang-Mills theory. In the high energy limit, the theory is asymptotically free, while in the low energy limit, the theory is strongly coupled and has a mass gap.

Understanding different phases of quantum matter by their phase transitions is a significant and challenging task in modern physics [3]. In general, the quantum phase transition happens by tuning a parameter to a quantum critical point at the absolute zero temperature. At nonzero temperature, the quantum critical point will become a quantum critical region. Studying the quantum phase transition at zero temperature

can give key insights to understand the quantum critical region at nonzero temperature. The quantum phase transition can happen for both insulators and metals. Figure 1.2 shows a typical phase diagram. The special feature for metals is that they have a Fermi surface. The metal in the quantum critical region is called the strange metal, which is a strongly interacting system. A puzzle about the strange metal behavior is that the resistivity grows linearly with temperature. Another phase, unconventional superconductivity (without a quasiparticle description), will appear at the quantum critical region.

It is a formidable task to understand strongly interacting QFTs in general. It is desirable to start from some simple, computable models. The AdS/CFT correspondence, or gauge/gravity duality, provides us a tool to study some quantum critical systems in terms of classical gravity [4, 5, 6]. This duality maps some strongly interacting systems, which are difficult to study by conventional methods, to a classical gravity system, which is well-established as Einstein's general theory of relativity. The gravity has one more dimension; this extra dimension plays the role of the energy scale. To make the duality work, we also need to take the "large N" limit, which means that the gauge theory has a large number of local degrees of freedom. These models are not realistic in nature, but they capture many essential features of the real world systems, such as unconventional superconductors and quantum chromodynamics (QCD).

1.2 The AdS/CFT dictionary

Generally, the holographic principle states that some quantum theories of gravity in $(d+1)$-dimensional spacetime is equivalent to a quantum field theory in d-dimensional spacetime without gravity. The first example of the AdS/CFT correspondence states that the type IIB superstring theory on $AdS_5 \times S^5$ is equivalent to the $\mathcal{N} = 4$ SU(N)

super-Yang-mills theory on the boundary of AdS_5 [7]. Another example is that the M-theory on $AdS_4 \times S^7/\mathbb{Z}_k$ is equivalent to the $\mathcal{N} = 6$ $\mathrm{SU}(N)_k \times \mathrm{SU}(N)_{-k}$ super-Chern-Simons theory (ABJM theory) on the boundary of AdS_4 [8].

Under certain conditions, the quantum theory of gravity can be approximated by the classical theory of gravity. In the first example above, the parameters in the gravity side are the AdS radius L, the string length l_s, and the Planck length l_p; the parameters in the gauge theory side are the 't Hooft coupling $\lambda = g_{\mathrm{YM}}^2 N$ and the number of colors N. They have the following relations

$$\left(\frac{L}{l_s}\right)^4 \sim \lambda, \qquad \left(\frac{L}{l_p}\right)^4 \sim N. \tag{1.2}$$

In the $\lambda \to \infty$ and $N \to \infty$ limits, the strings are weakly coupled and can be described by classical gravity. Starting from

$$Z_{\mathrm{string}} = Z_{\mathrm{CFT}}, \tag{1.3}$$

in the strong coupling and large N limits, we have

$$Z_{\mathrm{CFT}}[J] \approx e^{S_{\mathrm{grav}}}, \tag{1.4}$$

where the equations of motion in the bulk are solved with boundary conditions depending on the source J [9, 10]. Supergravities on AdS_5, AdS_4, and AdS_7 can be used as consistent truncations of the type IIB superstring and M-theory [11].

Some entries of the AdS/CFT dictionary are

bulk	$\longleftrightarrow$	**boundary**
fields		local operators
spin		spin
mass		scaling dimension Δ
metric $g_{\mu\nu}$		energy-momentum tensor $T^{\mu\nu}$
gauge field A_μ		conserved current J^μ
gauge symmetry		global symmetry
black hole		deconfined phase at temperature T
Euclidean black hole		confined phase
charged black hole		system at chemical potential μ

To study a system at finite temperate and density, the simplest geometry is the Reissner-Nordström (RN) black hole in AdS space. The action is

$$S = \int d^{d+1}x\sqrt{-g}\left(R + \frac{d(d-1)}{L^2} - \frac{1}{4}F_{\mu\nu}F^{\mu\nu}\right). \tag{1.5}$$

The metric ansatz of Poincaré coordinates is

$$ds^2 = \frac{L^2}{z^2}\left(-f(z)dt^2 + dx^2 + \frac{dz^2}{f(z)}\right). \tag{1.6}$$

The solution for the AdS_{d+1} charged black hole with chemical potential μ is

$$f(z) = 1 - (1+\tilde{\mu}^2)\Big(\frac{z}{z_h}\Big)^d + \tilde{\mu}^2\Big(\frac{z}{z_h}\Big)^{2(d-1)}, \tag{1.7}$$

$$A(z) = \mu\Big[1 - \Big(\frac{z}{z_h}\Big)^{d-2}\Big]dt, \tag{1.8}$$

where

$$\tilde{\mu}^2 = \frac{d-2}{2(d-1)}\mu^2. \tag{1.9}$$

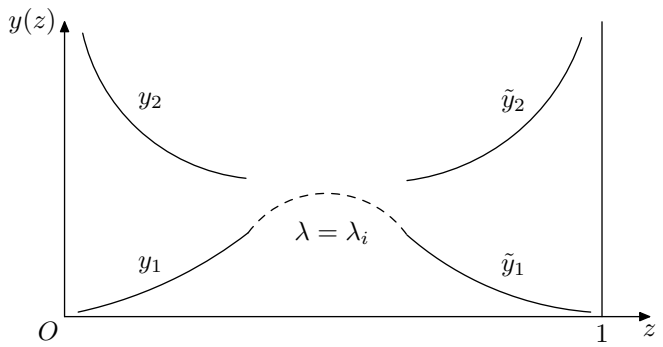

Figure 1.3: Boundary value problem. For the RN-AdS black hole in Poincaré coordinates, the AdS boundary is at $z = 0$, and the horizon is at $z = 1$.

The Hawking temperature is

$$T = \frac{d - (d-2)\tilde{\mu}^2 z_h^2}{4\pi z_h}. \tag{1.10}$$

The retarded Green's function can be obtained by solving the equations of motion in the bulk with in-falling boundary condition at the horizon [12]. The poles of the Green's function correspond to the quasinormal modes in the bulk. In the equations of motion, the horizon is always at a singular point, and the AdS boundary can be at either a singular point or an ordinary point. The prescribed behaviors at the horizon and the AdS boundary determine the quasinormal modes, which are eigenvalues from a boundary value problem illustrated in figure 1.3. In the following, we assume the black hole is at finite temperature. At $T = 0$, the near horizon behavior will be changed.

1.2.1 Klein-Gordon equation in AdS space

To obtain the Green's function for a scalar operator in the dual CFT, we will solve the Klein-Gordon equation for a scalar field Φ. After the Fourier transform

$$\Phi(z, x^\mu) = \int \frac{d\omega d^{d-1}\mathbf{k}}{(2\pi)^d} e^{-i\omega t + i\mathbf{k}\cdot\mathbf{x}} \phi(z), \tag{1.11}$$

the equation of motion for ϕ is

$$\phi'' + \left(\frac{f'}{f} - \frac{d-1}{z}\right)\phi' + \left(\frac{(\omega + qA_t)^2}{f^2} - \frac{k^2}{f} - \frac{m^2}{z^2 f}\right)\phi = 0, \tag{1.12}$$

where q is the charge of the scalar, and m^2 is above the Breitenlohner-Freedman (BF) bound [13]: $m^2 \geq m^2_{\rm BF} = -d^2/4$. To obtain the retarded Green's function, we impose the in-falling boundary condition at the horizon $z = 1$:

$$\phi = (1-z)^{-i\omega/4\pi T}(1 + \cdots), \tag{1.13}$$

where $T = |f'(1)|/4\pi$ for the coordinates eq. (1.6), and "$\cdots$" denotes higher orders of $(1-z)$. The asymptotic behavior near the AdS boundary $z = 0$ is

$$\phi = Az^{\Delta_-}(1 + \cdots) + Bz^{\Delta_+}(1 + \cdots), \tag{1.14}$$

where

$$\Delta_\pm = -\frac{d}{2} \pm \sqrt{\frac{d^2}{4} + m^2}. \tag{1.15}$$

In the standard quantization, the retarded Green's function is

$$G = (2\Delta_+ - d)\,\frac{B}{A}. \tag{1.16}$$

When $-d^2/4 \leq m^2 \leq -d^2/4 + 1$, there is an alternative quantization, by which the Green's function is $G \sim A/B$ [14].

1.2.2 Dirac equation in AdS space

To have a fermionic operator O_Ψ in a dual field theory, we consider a spinor Ψ in gravity with the action[2]

$$S_\Psi = -i \int d^{d+1}x \sqrt{-g} \bar{\Psi}(\gamma^\mu D_\mu - m)\Psi, \tag{1.17}$$

where Ψ is a spinor of mass m and charge q, and $\bar{\Psi} = \Psi^\dagger \gamma^{\underline{t}}$. Vielbein indices are underlined, and related to coordinate indices by $\gamma^{\underline{a}} = e^{\underline{a}}{}_\mu \gamma^\mu$. The covariant derivative is

$$D_\mu = \partial_\mu + \frac{i}{4}\omega_{\mu,\underline{ab}}\gamma^{\underline{ab}} - iqA_\mu, \tag{1.18}$$

where ω is the spin connection, $\gamma^{\underline{ab}} = \frac{1}{2}[\gamma^{\underline{a}}, \gamma^{\underline{b}}]$, and A_μ is a gauge field.

We choose the gamma matrices according to ref. [16]. Consider the Euclidean Clifford algebra, $\{\tilde{\gamma}^a, \tilde{\gamma}^b\} = \delta^{ab}$ in D dimensions. In the case $D = 2$, we take $\tilde{\gamma}^0 = \sigma_3$ and $\tilde{\gamma}^1 = \sigma_2$. Given a Clifford algebra $\tilde{\gamma}^a$ in $D = 2n$ dimensions, a Clifford algebra in $D + 2 = 2n + 2$ dimensions is

$$\tilde{\Gamma}^0 = \mathrm{id} \otimes \sigma_3, \qquad \tilde{\Gamma}^1 = \mathrm{id} \otimes \sigma_2, \qquad \tilde{\Gamma}^a = \tilde{\gamma}^{a-2} \otimes \sigma_1. \tag{1.19}$$

For odd dimensions, in the usual way we identify $\tilde{\gamma}^{2n+1}$ with the product of other gamma matrices (up to a factor of i). The Lorentzian Clifford algebra can be recovered by multiplying one of the $\tilde{\gamma}^a$ by i. We choose $\gamma^{\underline{t}} = i\tilde{\gamma}^1$, $\gamma^{\underline{z}} = \tilde{\gamma}^0$, $\gamma^{\underline{x}} = \tilde{\gamma}^2$, $\cdots$. For AdS_4, the gamma matrices are

$$\gamma^{\underline{t}} = \begin{pmatrix} i\sigma_2 & 0 \\ 0 & i\sigma_2 \end{pmatrix}, \qquad \gamma^{\underline{z}} = \begin{pmatrix} \sigma_3 & 0 \\ 0 & \sigma_3 \end{pmatrix}, \qquad \gamma^{\underline{x}} = \begin{pmatrix} \sigma_1 & 0 \\ 0 & -\sigma_1 \end{pmatrix}, \qquad \gamma^{\underline{y}} = \begin{pmatrix} 0 & -i\sigma_1 \\ i\sigma_1 & 0 \end{pmatrix}. \tag{1.20}$$

[2]Appropriate boundary terms should be added to make the variational principle well-posed and cancel any divergences. See, for example, the appendix of ref. [15].

Assuming the metric is diagonal and depends only on the radial coordinate z, the spin-connection term in the Dirac equation can be eliminated by using the rescaled spinor $\tilde{\psi} = (-gg^{zz})^{1/4}\Psi$. The equation of motion for $\tilde{\psi}$ is

$$[\gamma^\mu(\partial_\mu - iqA_\mu) - m]\tilde{\psi} = 0. \tag{1.21}$$

The Fourier transform of $\tilde{\psi}$ is

$$\tilde{\psi}(x^\mu, z) = \int \frac{d^4k}{(2\pi)^4} e^{ik_\mu x^\mu} \psi_k(z), \tag{1.22}$$

where $k^\mu = (\omega, \mathbf{k})$. Because of rotational symmetry, we assume without loss of generality that the spatial momentum is in the x direction. We also assume that A_t is the only nonzero component of A. By plugging a single Fourier mode $\tilde{\psi} \sim e^{-i\omega t + ikx}\psi(z)$ into eq. (1.21), we obtain the equation of motion for ψ:

$$\left[-i\sqrt{-g^{tt}}\gamma^{\underline{t}}(\omega + qA_t) + \sqrt{g^{zz}}\gamma^{\underline{z}}\partial_z + i\sqrt{g^{xx}}\gamma^{\underline{x}}k - m\right]\psi = 0. \tag{1.23}$$

For AdS_{d+1}, ψ is a 2^n-component spinor where $n = \lfloor (d+1)/2 \rfloor$. We write ψ as

$$\psi_\alpha = \begin{pmatrix} u_{1\alpha} \\ \\ u_{2\alpha} \end{pmatrix}, \tag{1.24}$$

where $\alpha = 1, 2, \cdots, 2^{n-1}$. For the choice of gamma matrices as eq. (1.20), eq. (1.23) reduces to two decoupled equations

$$\left[\sqrt{-g^{tt}}\sigma_2(\omega + qA_t) + \sqrt{g^{zz}}\sigma_3\partial_z - i(-1)^\alpha\sqrt{g^{xx}}\sigma_1 k - m\right]\psi_\alpha = 0, \tag{1.25}$$

where ψ_α are the 2^{n-1} two-component spinors appearing in the 2^{n-1} spinor equations, respectively, with momentum alternating between $+k$ and $-k$. Therefore the second

block of equations, i.e., the one for ψ_2, is related to the first black by $k \to -k$. A third block (if present) is identical to the first, the fourth block to the second, and so on.

A way to generalize the system eq. (1.17) is to add a dipole coupling as [17, 18]:

$$\bar{\Psi}(\not{D} - m - ip\not{F})\Psi, \tag{1.26}$$

where $\not{F} = \frac{1}{2}\gamma^{\mu\nu}F_{\mu\nu}$. For the RN-$AdS_{d+1}$ solution, $\not{F} = -(d-2)\mu z^{d-1}\gamma^{\underline{zt}}$. By defining $\mu_p \equiv (d-2)\mu p$, the Dirac equation (1.25) is simply changed by $(-1)^\alpha k \to (-1)^\alpha k - \mu_p z^{d-2}$.

To obtain the retarded Green's function, we impose the in-falling boundary condition at the horizon $z = 1$:

$$u_{1\alpha} = (1-z)^{-i\omega/4\pi T}(1 + \cdots), \tag{1.27}$$

$$u_{2\alpha} = (1-z)^{-i\omega/4\pi T}(1 + \cdots). \tag{1.28}$$

The asymptotic behavior near the AdS boundary $z = 0$ is

$$u_{1\alpha} = b_\alpha z^{r_1}(1 + \cdots) + d_\alpha z^{r_2}(1 + \cdots), \qquad r_1 = m, \quad r_2 = 1 - m \tag{1.29}$$

$$u_{2\alpha} = a_\alpha z^{s_1}(1 + \cdots) + c_\alpha z^{s_2}(1 + \cdots), \qquad s_1 = -m, \quad s_2 = m + 1 \tag{1.30}$$

where "$\cdots$" denotes higher orders of z. If $m > 1/2$, the term $b_\alpha z^m$ will become subleading compared to $d_\alpha z^{1-m}$ in eq. (1.29). If $m = 1/2,\ 3/2,\ 5/2,\ \cdots$, we need to multiply a $\ln z$ before the subleading terms. If $m = 1,\ 2,\ 3,\ \cdots$, we may still need a $\ln z$ if the Dirac equation is coupled to a gauge field.

The Green's function is[3]

$$G_R(\omega,k)=\begin{pmatrix} G_1\mathbb{1} & & \\ & G_2\mathbb{1} & \\ & & \ddots \end{pmatrix}, \qquad G_\alpha = i\frac{b_\alpha}{a_\alpha}, \tag{1.31}$$

where $\mathbb{1}$ is the a 2×2 unit matrix. In the following chapters, we sometimes denote G as the Green's function and it refers to G_1. When $m \leq 1/2$, there is an alternative definition of the Green's function by $G_\alpha = -ia_\alpha/b_\alpha$. The simple diagonal form of the Green's function is due to the fact that only block-diagonal gamma matrices appear in the Dirac equation (1.23). If A_y is present, the Green's function will not be diagonal, which implies that the up spins and down spins are mixed by a magnetic field. Another example is that when there is electric dipole coupling as $\bar{\psi}\gamma_5 \not{F}\psi$ [20]. The prescription when the Green's function is not diagonal can be found in ref. [16].

1.2.3 Vector and tensor perturbations

The correlation functions of vector and tensor perturbations can be obtained by using gauge invariant variables [21]. The conductivity is obtained from the retarded current-current correlation function

$$\tilde{G}_{\mu\nu}(x-y) = i\theta(x^0-y^0)\langle[J_\mu(x),J_\nu(y)]\rangle. \tag{1.32}$$

The Fourier transform is denoted by $G_{\mu\nu}(p)$, where $p^2 = -\omega^2 + \boldsymbol{k}^2$. At zero temperature, all components of $G_{\mu\nu}$ are determined by a scalar function $\Pi(p^2)$ as $G_{\mu\nu} = (\eta_{\mu\nu} - p_\mu p_\nu/p^2)\Pi(p^2)$. At finite temperature, the Lorentz invariance is broken, and

[3]Note that different choice of gamma matrices may lead to different AdS/CFT prescription for the Green's function. The "$-i$" factor in eq. (1.31) is needed for eq. (1.20). For the case without the "$-i$" factor, the leading term "1" in eq. (1.28) will be replaced with "i". A way to check the consistency is that whether $\mathrm{Im}(G) > 0$ is always held. Another way to check is by the exact result $G = i$ when $m = 0$ and $k = 0$ [19].

$G_{\mu\nu}$ can be split into transverse and longitudinal parts:

$$G_{\mu\nu}(p) = P^T_{\mu\nu}\Pi^T(\omega, \boldsymbol{k}) + P^L_{\mu\nu}\Pi^L(\omega, \boldsymbol{k}). \tag{1.33}$$

In general, we need to turn on all the perturbations

$$\tilde{A}_\mu = e^{-i\omega t + i\mathbf{k}\cdot\mathbf{x}} A_\mu, \qquad \tilde{g}_{\mu\nu} = e^{-i\omega t + i\mathbf{k}\cdot\mathbf{x}} g_{\mu\nu}. \tag{1.34}$$

To calculate the conductivity, we need to turn on the perturbations $e^{-i\omega t}A_x(z)$ and $e^{-i\omega t}g_{tx}(z)$. After eliminating g_{tx}, we obtain a single equation for A_x as

$$A_x'' + \left(\frac{f'}{f} - \frac{d-3}{z}\right) A_x' + \left(\frac{\omega^2}{f^2} - \frac{A_t'^2 z^2}{f}\right) A_x = 0. \tag{1.35}$$

1.3 Brief review and summary

Charged black holes in asymptotically AdS space can be regarded as the dual description of some strongly interacting fermionic systems at finite charge density, such as non-Fermi liquids. This is an application of the gauge/gravity duality, which allows us to calculate the Green's function by solving the bulk Dirac equation. There are several charged black hole systems we may choose, and each of them corresponds to a distinctive quantum critical system. Here I will discuss three most influential geometries, which are the RN black hole in AdS, the electron star, and a dilatonic black hole. Each of them captures some key features of the finite density systems, but also has some disadvantages. The study of the gauge/gravity duality by these three geometries helps us to gain more insights to the quantum critical systems.

A well-studied example is the RN black hole in AdS as the geometry [22, 23, 24]. The most consequent result is that the dispersion relation of excitations near the Fermi surface is determined by the IR geometry. The solution of the Green's function

contains both UV and IR data. The IR Green's function can be exactly solved as $\mathcal{G}_k(\omega) \sim \omega^{2\nu_k}$, due to the IR geometry containing an AdS_2 factor. If $\nu_k > 1/2$, the excitations near the Fermi surface are stable, i.e., there are quasiparticles with long enough lifetime, and thus the system describes the Fermi liquid. If $\nu_k < 1/2$, the excitations near the Fermi surface are unstable, i.e., there are no quasiparticles, and thus the system describes the non-Fermi liquid. If $\nu_k = 1/2$, a delicate cancelation between the UV and IR data gives a marginal Fermi liquid, which was proposed to explain the unconventional superconductors before [25]. Moreover, ν_k can become imaginary, which indicates an instability due to the pair production in the near horizon region.

The RN black hole system also has some disadvantages. First, the system has nonzero entropy at zero temperature, which suggests that this geometry is not the true ground state. Second, the pair production in the near horizon region will backreact on the metric and change the geometry eventually. After we take into account the backreactions of the bulk fermions, the IR geometry will be changed into Lifshitz geometry [26]. Third, the matching between the UV and IR data can only be done numerically.

The electron star is constructed by taking into account the backreactions of the fermions [27]. This geometry is close to the realistic case, at a price that heavy numerical calculations will be needed to solve the Einstein's equations and the Dirac equation. The IR geometry has a Lifshitz scaling with dynamical critical exponent z. The result shows that this system also has Fermi surfaces, but the excitations near the Fermi surface are more stable than the RN black hole system for $\omega \lesssim k^z$. The properties of the system can be qualitatively seen by the effective potential for the Dirac equation. For certain parameters, the effective potential of the Dirac equation has a potential well with a barrier. The quasibound states in the well can tunnel through the barrier to the horizon, which will lead to an instability. As a result, these quasinormal modes have a small imaginary part. However, the WKB method used in

previous works could not explain the sign of this imaginary part, because the effect of spin on the Green's function was not taken into account.

In chapter 2, we study the Green's function of a gauge invariant fermionic operator in a strongly coupled field theory at nonzero temperature and density using a dual gravity description. The gravity model contains a charged black hole in four dimensional anti-de Sitter space and probe charged fermions. In particular, we consider the effects of the spin of these probe fermions on the properties of the Green's function. There exists a spin-orbit coupling between the spin of an electron and the electric field of a RN black hole. On the field theory side, this coupling leads to a Rashba like dispersion relation. We also study the effects of spin on the damping term in the dispersion relation by considering how the spin affects the placement of the fermionic quasinormal modes in the complex frequency plane in a WKB limit.

In ref. [28], another improved geometry, a charged dilatonic black hole in AdS_5 as a consistent truncation of the type IIB supergravity, is studied as the ground state of the gravity dual to a fermionic system. At low temperature, the entropy and the specific heat are proportional to the temperature, like the Fermi liquid. An exact value of the Fermi momentum k_F, which indicates the existence of the Fermi surface, was found for a special choice of parameters. In general, the Fermi momentum cannot be analytically solved in the first two geometries. The exact value of k_F solved in the third geometry indicates that it has more elegance besides its favorable thermodynamical property and demands further study.

In chapter 3, we find exact, analytic solutions of the Dirac equation for a charged, massless fermion in the background of a charged, dilatonic black hole in AdS_5. The black hole descends from type IIB supergravity, where it describes D3-branes with equal angular momenta in two of the three independent planes of rotation orthogonal to the world-volume. The Green's function near the Fermi surface for a strongly coupled fermionic system can be extracted holographically from an exact solution of

the Dirac equation at zero frequency but nonzero momentum. There can be several Fermi momenta, and they take the form $k_F = q - n - 1/2$ (in units of the chemical potential), where q is the charge of the spinor, and n is a non-negative integer that labels the Fermi surfaces. Much as for holographic Fermi surfaces based on the RN-AdS_5 solution, the dispersion relation of the excitations near the Fermi surface is determined by the geometry close to the horizon, and one can obtain Fermi liquid, marginal Fermi liquid, and non-Fermi liquid behaviors depending on the value of k_F.

The main difference between the RN black hole and the charged dilatonic black hole is due to the IR geometry. In the RN-AdS_5 black hole system, the IR geometry is $AdS_2 \times \mathbb{R}^3$, and the electric field is constant at the horizon. In our system, the IR geometry is conformal to $AdS_2 \times \mathbb{R}^3$, and the electric field vanishes at the "horizon," which is a naked singularity. In terms of the dynamical critical exponent z and the hyperscaling violation exponent θ, this IR geometry corresponds to the limit $z \to \infty$ with $\eta = -\theta/z = 1$ [29, 27]. There is still flux behind the horizon due to the dilaton field. The two systems are similar in that the dispersion relation of the excitation near the Fermi surface is determined by the IR scaling dimension. The two systems are different in that ν_k for the RN black hole could become imaginary, while in our system ν_k is always real, which implies that the instability near horizon in the RN black hole system is absent in our system.

In chapter 4, we find exact, analytic solutions of the Klein-Gordon equation for a scalar field in the background of the extremal RN-AdS_5 black hole. The Green's function near a quantum critical point for a strongly coupled system can be extracted holographically from an exact solution for the scalar at zero frequency (ω), but arbitrary momentum (k), mass, and charge. By examining the Green's function near $\omega = 0$, there are two types of instability: the first one is triggered by a zero mode, and gives a hybridized critical point; the second one is triggered by the instability of the IR geometry, and gives a bifurcating critical point. The two types of instability can

happen at the same time, and give a mixed critical point. Without tuning an extra parameter, only the second type of instability can happen at $k = 0$. At the critical point with the superfluid velocity, the scalar can develop either type of instability, depending on the parameters. The zero mode can also be obtained by tuning a double trace deformation. The phase diagrams can be analytically drawn.

Appendix A includes some notes on how to take advantage of the Heun function and the hypergeometric function in solving the equations of motion.

Chapter 2

The spin of holographic electrons at nonzero density and temperature

This chapter is a lightly edited version of ref. [30], which was written in collaboration with Christopher P. Herzog.

2.1 Introduction

Through gauge/gravity duality [7, 9, 10], a charged spinor field in an asymptotically anti-de Sitter (AdS) space in a classical limit can be used to model strongly interacting fermions in field theory. While the start of this program can be traced back to refs. [31, 32] which solve the Dirac equation in pure AdS space, with refs. [33, 19, 34] there has been a resurgence of interest in the subject focused on fermions at nonzero charge density in the hope of modeling strongly interacting cousins of Fermi liquids. These so-called non-Fermi liquids are believed to underly some of the interesting physics of heavy fermion compounds and high temperature superconductors. Initial gauge/gravity duality studies focused on charged black hole backgrounds. By tuning

the parameters of the fermionic field, both Fermi liquid and non-Fermi liquid behavior can be obtained [22].

These holographic models of strongly interacting fermions appear to be delicate to construct. The charged black hole is subject to a wide variety of potential instabilities in the zero temperature limit. For example, if the field theory contains an operator dual to a charged scalar field in the bulk, the black hole can develop scalar hair in a holographic superfluid phase transition [35, 36, 37, 38]. If a four fermion interaction term with the right sign is added to the Dirac Lagrangian, there can be a Bardeen-Cooper-Schrieffer phase transition at low temperatures in the bulk [39]. Even with no extra terms in the Lagrangian, if the fermions have a large enough charge, the condensation of a Fermi sea in the bulk will modify the geometry, producing an electron star at low temperatures [40, 41, 27]. The field theories dual to these electron stars exhibit the usual Fermi liquid behavior. In contrast, the non-Fermi liquid behavior found by [22] occurs in the limit where the Fermi sea outside the black hole is very small.

The delicate nature of these systems aside, they seem to be promising toy models to address some of the questions surrounding strongly correlated electron systems. The current paradigm surrounding these toy models appeals to ideas of confinement in large N gauge theories [24, 42, 43, 44]. The charge of the black hole should be carried by deconfined degrees of freedom – non-gauge invariant fermions behind the horizon. The added Dirac field is dual to a confined degree of freedom, i.e. a gauge invariant fermion or mesino. Just as in QCD where the mesons and baryons interact weakly with each other in a large N limit, these mesinos form a Fermi liquid which by definition is effectively weakly interacting. It is the conjectured fermions behind the horizon which lead to non-Fermi liquid like behavior.

Our goals in this chapter are modest. We would like to provide a more careful consideration of spin physics and spin-orbit coupling in these holographic systems

than has appeared heretofore in the literature. A qualitative discussion of spin-orbit effects appears in ref. [45] in the context of coupling fermions to a d-wave holographic superconductor, but we shall try to be more quantitative and precise here. By spin orbit coupling, we mean that a bulk charged fermion moving perpendicular to an applied electric field experiences an effective magnetic field that splits the degeneracy between the two spin states.

Let us start with an electrically charged black hole in AdS_4 at nonzero temperature to which we add a spinor field. Using the standard gauge/gravity duality dictionary, we may compute the quasinormal mode (QNM) spectrum of the spinor field which will allow us to deduce where the retarded Greens function for the dual gauge invariant fermionic operator has poles [12, 46]. When the charge of the black hole is large enough, the imaginary parts of many of these quasinormal modes will be small, and we plot in figure 2.1a the real part of the freqency of these modes versus momentum. One may think of these curves as dispersion relations for fermionic quasiparticles in the field theory. Alternately, one may think of these curves as locations where the field theory may have a nonzero density of states. (To compute the actual density of states, we need the full Green's function including the residues of the poles, and these residues may vanish at special points.) The system is rotationally symmetric, and one can envision the full k dependence by rotating the graph around the ω-axis. The details of this numerical computation are presented in section 2.3.

The similarity between figure 2.1a and figure 2.1b is one of the central observations of this chapter. Figure 2.1a resembles four copies of figure 2.1b. Figure 2.1b is the dispersion relation for a nonrelativistic two dimensional electron gas with a spin orbit (or Rashba) coupling. The Rashba Hamiltonian can be written

$$H = \frac{k^2}{2m_{\text{eff}}} - \lambda \vec{\sigma} \cdot (\hat{z} \times \vec{k}) - \mu \,, \tag{2.1}$$

where λ is the Rashba coupling constant, μ a chemical potential, $\vec{\sigma}$ the Pauli matrices, m_{eff} the electron effective mass, and $\hat{z}$ the unit vector perpendicular to the gas.

From the bulk spacetime point of view, the similarity between these two figures is straightforwardly explained. Electrons with the dispersion relation (2.1) can be produced by a two dimensional slab-like geometry with a strong electric field perpendicular to the slab. On the gravity side, the charge of the black hole provides the electric field. The slab lies between the boundary of AdS on one side and the horizon on the other. More precisely, deriving a Schrödinger equation for the spinor field, one finds a potential barrier between the well in which the spinors live and the horizon. Tunneling through the barrier produces the small negative imaginary part of the QNMs.

For the 2+1 dimensional field theory, this similarity naively presents a puzzle. The usual derivation of the Hamiltonian (2.1) is intrinsically 3+1 dimensional and relies on the presence of the electric field and a notion of spin-orbit coupling. In the context of heavy fermion compounds and strange metals, one anticipates that spin should be essentially an internal $SU(2)$ symmetry of the electrons. There are no strong magnetic or electric fields in these compounds, and the Fermi surface or surfaces should be spin degenerate. There is no obvious mechanism for breaking the $SU(2)$ symmetry of these strongly interacting fermions at nonzero density.

The solution to this puzzle is that by the rules of the AdS/CFT correspondence, the dual field theory is intrinsically relativistic. Spin is not an internal symmetry but instead implies a corresponding transformation rule under the Lorentz group. In 2+1 dimensions, angular momentum dualizes to a scalar. Massive free fermions satisfying the Dirac equation $(\gamma^\mu p_\mu - im)\psi = 0$ carry a spin determined by the sign of their mass $\frac{1}{2}\text{sgn}(m)$ (see for example [47]).[1] In contrast, massless fermions, because the little group is too small, carry no spin at all. We believe that the fermions in our field

[1] In our conventions, the gamma matrices obey $\{\gamma^\mu, \gamma^\nu\} = 2\eta^{\mu\nu}$ where $\eta^{\mu\nu} = (- + +)$.

theory are massless for two reasons. The first is that the field theory is conformal and a mass term breaks scale invariance. The second is that while a mass term for the fermions breaks parity in 2+1 dimensions, the state we consider in the field theory appears to be parity invariant. In support of this claim, note that the Hamiltonian (2.1) is invariant under the parity operation that sends $(k_x, k_y) \to (-k_x, k_y)$ and $\psi \to \sigma_x \psi$.

There is an alternate intrinsically 2+1 dimensional way of motivating the Hamiltonian (2.1). Our black hole background is dual to a conformal theory at nonzero chemical potential μ and temperature. The presence of energy and charge density identifies a preferred Lorentz frame $u^\mu = (1, 0, 0)$. From an effective field theory point of view, it is natural to expect a modified Dirac equation of the form [48]

$$[(1 + F)p_\mu + (-\mu + G)u_\mu]\, \gamma^\mu \psi = 0\,, \tag{2.2}$$

where $p^\mu = (\omega, k_x, k_y)$ is the four momentum and F and G are arbitrary functions of ω and $k = \sqrt{k_x^2 + k_y^2}$. Note we have not included a bare mass in this expression. Choosing gamma matrices $\gamma^t = i\sigma_z$, $\gamma^x = \sigma_x$ and $\gamma^y = \sigma^y$ and setting F and G to zero, we recover (2.1) without the k^2 term and with $\lambda = 1$. (In other words, the Rashba coupling itself is the Hamiltonian for a massless relativistic fermion in 2+1 dimensions.) To add the k^2 term, we may posit that $G(\omega, k) \sim k^2$ which is allowed by the symmetries. To get the different bands in figure 2.1a, we may additionally posit the existence of several species of massless fermions with different charges q_i, replacing μ with μq_i in (2.1). Ideally, we would like to derive this effective Dirac equation from an action, but we do not know how.

One may object on technical grounds to the nonextremal black hole background used to produce figure 2.1a. From earlier work on the electron stars [40, 41, 27], for the large charge, low mass fermion chosen, it is clear that the bulk Fermi sea will

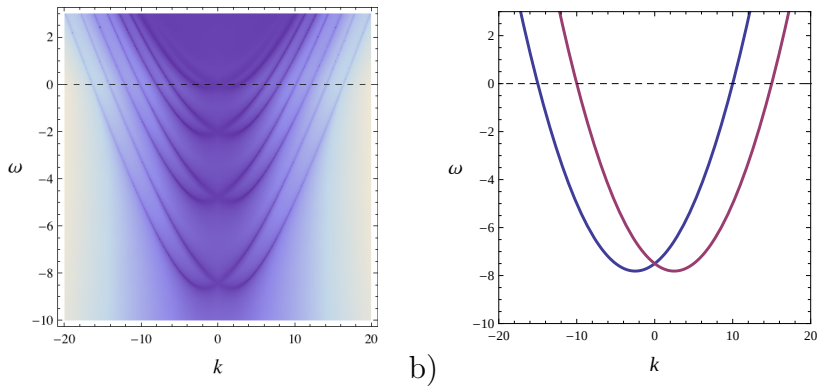

Figure 2.1: (a) The dispersion relation in the boundary theory for a bulk fermion with charge times chemical potential divided by temperature $\mu q/4\pi T = 25$ and mass times AdS radius $mL = 2$. (b) The dispersion relation for a fermion with a Rashba type coupling. The Fermi surface in both cases is indicated by the dashed line.

cause a back reaction of the black hole background. In principle, one should use the numerically computed electron star metrics to produce figure 2.1a. However, the phase transition between the charged black hole and the electron star is third order [41], and there are many qualitatively similar features between the charged black hole and electron star backgrounds. Using the numerical electron star metrics, which are only exact in an Oppenheimer-Volkoff approximation, should not change the story in a qualitative way.[2]

We begin this chapter by revisiting the Dirac equation in these charged black hole and electron star backgrounds in section 2.2. We show, using the Pauli-Lubanski pseudovector, how to identify the different spin components of the fermion. Next in section 2.2.1, we review how to compute the QNMs of a spinor field in these backgrounds, and connect the QNMs to poles of the retarded Green's function in the dual field theory. Section 2.2.2 reviews how to convert the Dirac equation into an effective Schrödinger equation for the spinor for use in a WKB approximation. The WKB limit will give us qualitative insight into the nature of this spin-orbit coupling. Finally, in section 2.3, we employ the machinery set up in the earlier sections to

[2]See [42, 49] for progress going beyond the Oppenheimer-Volkoff approximation. Note that in the Oppenheimer-Volkoff approximation, the electrons are heavy and the spin splitting is very small.

compute the QNMs of the spinor in a charged black hole in AdS_4, giving the details behind figure 2.1a. Section 2.3.1 contains a discussion of the numerical solution of the Dirac equation, while 2.3.2 discusses the Dirac equation in a WKB limit. The WKB calculation contains some unusual features which we discuss at length. We are able to show how the WKB approximation gets the sign of the imaginary part of the quasinormal modes correct. Making use of Heun polynomials, appendix A.1 contains some exact analytic solutions of the Dirac equation for a charged spinor in a black hole in AdS_5.

2.2 The Dirac Equation Revisited

To have a gauge invariant fermionic operator O_Ψ in a dual field theory, we consider a spinor Ψ in a curved spacetime with the action

$$S_\Psi = -i \int d^{d+1}x\sqrt{-g}\,\overline{\Psi}(\gamma^\mu D_\mu - m)\Psi\,, \tag{2.3}$$

where Ψ is a spinor of mass m and charge q, and we follow the convention of section 1.2.2.

With AdS/CFT applications in mind, we make the following simplifying assumptions on the metric and gauge field. We assume a translationally and rotationally invariant metric of the form

$$ds^2 = g_{tt}dt^2 + g_{xx}(dx^2 + dy^2 + \ldots) + g_{zz}dz^2\,, \tag{2.4}$$

where the diagonal metric components $g_{\mu\mu}(z)$ depend only on a radial coordinate z. Additionally, we assume that A_t is the only nonzero component of the vector potential and that it is a function only of the radial coordinate z. In other words, there is a radial electric field whose strength may vary as a function of the radial direction.

The type of spacetimes we have in mind are Reissner-Nordström (RN) black holes and electron stars in AdS, both of which obey this set of assumptions.

Given these assumptions, the Dirac equation takes a particularly simple form. The spin-connection term in the Dirac equation can be eliminated by using the rescaled spinor $\tilde{\psi} = (-gg^{zz})^{1/4}\Psi$. The equation of motion for $\tilde{\psi}$ is eq. (1.21). Because of rotational symmetry, we assume without loss of generality that the spatial momentum is in the x direction. By plugging a single Fourier mode $\tilde{\psi} \sim e^{-i\omega t+ikx}\psi(z)$ into eq. (1.21), we obtain the equation of motion for ψ as eq. (1.23). Because we have set momentum in the y direction to zero, the Dirac equation for the four component spinor ψ decouples into equations for two-component spinors $\psi = (\psi_+, \psi_-)^T$:

$$\left[\sqrt{-g^{tt}}\sigma_2(\omega + qA_t) + \sqrt{g^{zz}}\sigma_3\partial_z \pm i\sqrt{g^{xx}}\sigma_1 k - m\right]\psi_\pm = 0\,. \tag{2.5}$$

We argue that $\psi_\pm$ correspond to fermions with opposite spin. To see the spin direction, consider the Pauli-Lubanski pseudovector

$$W_{\underline{a}} = \frac{1}{2}\epsilon_{\underline{abcd}}J^{\underline{bc}}P^{\underline{d}}\,, \tag{2.6}$$

where $J^{\underline{ab}} = \frac{i}{4}[\gamma^{\underline{a}}, \gamma^{\underline{b}}]$ and $P^{\underline{a}} = -iD^{\underline{a}}$. We will show that $\psi = (\psi_+, 0)$ and $\psi = (0, \psi_-)$ are eigenstates of $W_{\underline{y}}$. Acting on $e^{-i\omega t+ikx}\psi(z)$, $P^{\underline{a}} = -ie^{\underline{a}}{}_{\mu}g^{\mu\nu}D_\nu$ is given by

$$P^{\underline{a}} = (\sqrt{-g^{tt}}(\omega + qA_t),\, -i\sqrt{g^{zz}}\partial_z,\, \sqrt{g^{xx}}k,\, 0)\,. \tag{2.7}$$

Thus we obtain $W_{\underline{y}} =$

$$\frac{i}{2}\begin{pmatrix} -i\sqrt{g^{zz}}\partial_z & \sqrt{g^{xx}}k - \sqrt{-g^{tt}}(\omega + qA_t) & 0 & 0 \\ \sqrt{g^{xx}}k + \sqrt{-g^{tt}}(\omega + qA_t) & i\sqrt{g^{zz}}\partial_z & 0 & 0 \\ 0 & 0 & i\sqrt{g^{zz}}\partial_z & \sqrt{g^{xx}}k + \sqrt{-g^{tt}}(\omega + qA_t) \\ 0 & 0 & \sqrt{g^{xx}}k - \sqrt{-g^{tt}}(\omega + qA_t) & -i\sqrt{g^{zz}}\partial_z \end{pmatrix}. \tag{2.8}$$

We find then that the Dirac equation (2.5) can be written in terms of the $W_{\underline{y}}$ component of the Pauli-Lubanski pseudovector:

$$W_{\underline{y}} \begin{pmatrix} \psi_+ \\ \psi_- \end{pmatrix} = \frac{1}{2} m \begin{pmatrix} \mathbb{1} & 0 \\ 0 & -\mathbb{1} \end{pmatrix} \begin{pmatrix} \psi_+ \\ \psi_- \end{pmatrix}, \tag{2.9}$$

which means that the spin of ψ_+ is in the y-direction, and the spin of ψ_- is in the opposite direction. Because we assumed that the momentum is in the x-direction, and the system has rotational invariance, the direction of spin is always perpendicular to the plane defined by the momentum and the radial direction z. The Dirac equation decouples into these spin eigenstates.

This decoupling of spin eigenstates is in good agreement with flat space, nonrelativistic intuition [45]. Starting with a massive fermion moving in the x-direction, the fermion in its own rest frame will experience both an electric field in the radial z-direction and a magnetic field in the y-direction. This magnetic field will induce an energy splitting between the y-spin up fermion and the y-spin down fermion. The WKB limit we consider later will further strengthen this non-relativistic intuition. There is also a possible coupling between the curvature and the spin.

2.2.1 From quasinormal modes in the bulk to dispersion relations in the boundary

In this section, we would like to take advantage of the well known AdS/CFT relation between QNMs of the bulk spacetime and poles in the Greens functions of the dual field theory [12]. To that end, we begin by discussing the QNM boundary conditions for the Dirac equation (2.5).

We will assume that our metric in the limit $z \to 0$ is asymptotically of anti-de Sitter form:

$$g_{tt} \sim g_{xx} \sim g_{zz} \sim \frac{1}{z^2}\,. \tag{2.10}$$

There are two linearly independent solutions of the two component Dirac equation which approach the boundary as

$$\chi_1 \sim \begin{pmatrix} z^m \\ 0 \end{pmatrix} \quad \text{and} \quad \chi_2 \sim \begin{pmatrix} 0 \\ z^{-m} \end{pmatrix}. \tag{2.11}$$

We apply the "Dirichlet" boundary condition that the χ_2 solution vanish. Using these boundary conditions, the relation between the scaling dimension of the dual operator O_Ψ and the mass of the spinor is $\Delta = m + d/2$ [31]. The unitarity bound on the scaling dimension restricts us to $m \geq -1/2$.[3]

As the "Dirichlet" boundary condition is Hermitian, the quasinormalness of the modes comes from the boundary condition applied in the interior of the geometry. We assume that $g_{tt} \to 0$ at some $z_h > 0$, and at this horizon, the phase velocity of the spinor wave function is in the positive z-direction. For example, for a non-extremal blackhole, we may take the time and radial metric components to vanish as $-g_{tt} \sim g^{zz} \sim 4\pi T(z_h - z)$ where T is the Hawking temperature. In this case, our ingoing boundary condition is

$$\psi_\pm \sim (z_h - z)^{-i\omega/4\pi T} \begin{pmatrix} 1 \\ 1 \end{pmatrix}. \tag{2.12}$$

One may also consider more exotic situations, for example the Lifshitz geometry in the interior of the electron star [40].

[3]Using the "Neumann" boundary condition, we may consider spinors with dimension $\Delta = -m + d/2$ and $m \leq 1/2$.

Solving the Dirac equation with "Dirichlet" boundary conditions at $z = 0$ and ingoing boundary conditions at the horizon is only possible for a discrete set of complex frequencies ω called QNMs. As we tune k in the Dirac equation, a given QNM will trace out a curve in the complex ω plane. Provided the imaginary part of the QNM is small, this curve is essentially a dispersion relation for a quasi-stable particle.

To relate the QNMs to poles in the fermionic two-point function in the dual field theory, let us briefly recall how to compute these two-point functions. The first step is to solve the Dirac equation with ingoing boundary conditions at the horizon and arbitrary boundary conditions at $z = 0$, yielding a solution of the form $\psi_\pm = b_\pm \chi_1 + a_\pm \chi_2$ for each spin component where $a_\pm$ is interpreted as proportional to a source in the dual field theory and $b_\pm$ as an expectation value. The retarded Green's function is in reality a 2×2 matrix, but our choice of momentum has diagonalized it. Through the theory of linear response, the retarded Green's function is $G_R^{\alpha\beta} = i\delta_{\alpha\beta} b_\alpha / a_\beta$ [16]. If a_α vanishes, G_R will have a pole.

2.2.2 A Schrödinger form for the Dirac equation

While at least three papers have considered the WKB limit of the Dirac equation in this AdS/CFT context [22, 27, 24], these papers have largely ignored the effects of the spin of the electron. Our focus here shall be on the spin.

The WKB approximation in this case assumes that the dimensionful parameters m, ω, qA_t, and k are large compared to the scale $\partial_z \ln \psi_\pm$ over which the wave function varies. We may capture this limit by introducing a small parameter $\hbar$ multiplying ∂_z in the Dirac equation,

$$\left[\hbar\sqrt{g^{zz}}\sigma_3\partial_z - m + \sqrt{-g^{tt}}\sigma_2(\omega + qA_t) \pm i\sqrt{g^{xx}}\sigma_1 k\right]\psi_\pm = 0\,, \tag{2.13}$$

and then expanding in $\hbar$.

Our first step is to convert the Dirac equation into Schrödinger form. As noted in this AdS/CFT context by [22], there is no unique procedure. Given an equation in Schrödinger form, one has the usual freedom to reparametrize the coordinate $y = f(z)$ and rescale the wave function $\phi \to Z\phi$ subject to the constraint $Z^2 f'$ is a constant. However, there is an additional functional degree of freedom associated with converting a Dirac equation into Schrödinger form; one can introduce the scalar wave function $\phi_\pm$ such that

$$\psi_\pm = \begin{pmatrix} \alpha\,\phi_\pm + \hbar\beta\,\partial_z\phi_\pm \\ \gamma\,\phi_\pm + \hbar\delta\,\partial_z\phi_\pm \end{pmatrix}. \tag{2.14}$$

The condition that $\phi_\pm$ satisfies a Schrödinger type equation $-\partial_z^2\phi_\pm + V\phi_\pm = 0$ puts three constraints on the functions α, β, γ, and δ, but leaves a family of potentials $V(z)$ parametrized by an undetermined function [50].

One simple choice is to select $\phi_\pm$ to be proportional to the first component of the two component spinor $\psi_\pm$:

$$\psi_\pm = \begin{pmatrix} \sqrt{Z_{\pm k}}\,\phi_\pm \\ i\frac{\sqrt{g_{zz}}m\sqrt{Z_{\pm k}}\,\phi_\pm - \hbar\,\partial_z(\sqrt{Z_{\pm k}}\,\phi_\pm)}{Z_{\pm k}} \end{pmatrix} \tag{2.15}$$

where we have introduced a normalization factor

$$Z_k \equiv (g_{zz})^{1/2}\left[\sqrt{-g^{tt}}(\omega + qA_t) - \sqrt{g^{xx}}k\right]. \tag{2.16}$$

Given these substitutions, $\phi_\pm$ satisfies a Schrödinger equation of the form

$$-\partial_z^2\phi_\pm + V_{\pm k,m}\phi_\pm = 0\,, \tag{2.17}$$

where the potential function is

$$V_{k,m}(z) \;=\; \frac{1}{\hbar^2}\left(g_{zz}m^2 - Z_{-k}Z_k\right) - \frac{mg_{zz}}{\hbar}\frac{\partial_z(\sqrt{g^{zz}}Z_k)}{Z_k} + \sqrt{Z_k}\partial_z^2\frac{1}{\sqrt{Z_k}}\,. \quad (2.18)$$

Note that the spin dependence of the potential enters only at subleading order. At leading order in $\hbar$, $V_{k,m}$ is independent of the sign of k.

At leading order in $\hbar$, the spinor potential $V_{k,m}$ is exactly what one obtains for a charged scalar particle in this curved spacetime. If we start with the scalar wave equation $(D_\mu D^\mu - m^2)\Phi = 0$ and let $\Phi = e^{-i\omega t+ikx}Z(z)\phi(z)$ where $Z = \sqrt{g_{zz}}(-g)^{-1/4}$, then we obtain $-\partial_z^2\phi + V_s\phi = 0$ where

$$V_s(z) \;=\; \frac{1}{\hbar^2}\left(g_{zz}m^2 - Z_{-k}Z_k\right) + Z\partial_z^2\frac{1}{Z}\,, \quad (2.19)$$

and we have introduced factors of $\hbar$ analogously to the spinor case.

There is an important difference between the scalar and the spinor case. The normalization factor Z_k may vanish at a point in spacetime where the energy of the particle is equal to the local chemical potential plus a k dependent correction. At such a point, the spinor potential $V_{k,m}$ will have singularities at subleading order in $\hbar$. We will see in the next section how these subleading singularities mean that while scalar QNMs can lie in the upper half plane, the spinor QNMs will not.

Before getting into the details, we can say something about the number of zeroes Z_k possesses in the interval $0 < z < z_h$. In general, we will associate the boundary value of A_t with a chemical potential: $A_t(0) = \mu$; at the horizon we set $A_t(z_h) = 0$. Given the boundary conditions described in section 2.2.1 for the metric $g_{\mu\nu}$, close to the horizon we find that $Z_k \sim \omega/4\pi T(z_h - z)$. At the boundary, we find instead that $Z_k(0) = \omega + q\mu - k$. Thus, if $\omega + q\mu - k$ and ω are of the same sign, there will be an even number of zeroes between the boundary and the horizon. If they have opposite sign, there will be an odd number. In the cases we consider below, $q\mu > k - \omega$, and

so the parity of the number of zeroes is determined by the sign of ω, odd if $\omega < 0$ and even if $\omega > 0$.

Before continuing to an example, we would like to point out another simple choice of Schrödinger equation. We can let $\phi_\pm$ be proportional to the second component of $\psi_\pm$ rather than the first. To compute this alternate Schrödinger equation, we do not need to do the calculation again. Note instead that eq. (2.13) is invariant under $k \to -k$, $m \to -m$, and $\psi_\pm \to \sigma_1 \psi_\pm$. Thus the Schrödinger equation for the second component is given by replacing $V_{k,m}$ with $V_{-k,-m}$. Interestingly, this symmetry implies that the potentials $V_{k,m}$ and $V_{-k,-m}$ have the same quasinormal mode spectrum (being careful to exchange the boundary conditions on the two components of $\psi_\pm$ as well). The existence of this second isospectral potential allows for some cross checks when we perform a WKB analysis below.

2.3 An Example: AdS-Reissner-Nordström Black Hole

To study a fermionic system at nonzero temperature and density, we use the RN black hole as the background geometry, solve the Dirac equation coupled to a U(1) gauge field, and obtain the QNMs. We will solve the Dirac equation both numerically and using WKB. Our main interest is the location of the poles of the Green's function. Most of our results are for the $m = 2$ spinor in AdS_4.

We consider a charged black hole in AdS_4 in the Poincaré patch for which the metric has the form

$$ds^2 = \frac{L^2}{z^2}\left(-f(z)dt^2 + dx^2 + dy^2 + \frac{dz^2}{f(z)}\right). \tag{2.20}$$

The conformal boundary is at $z = 0$, and the horizon is at $z = z_h$, where $f(z_h) = 0$. We set $L = 1$ and $z_h = 1$, which are allowed by two scaling symmetries [38]. The charged black hole solution and its probe limit are as follows:

$$\text{RN-}AdS_4\text{:} \qquad f = 1 - \left(1 + \frac{\mu^2}{4}\right) z^3 + \frac{\mu^2}{4} z^4 \qquad \text{with} \quad A_t = \mu(1 - z)\,; \tag{2.21}$$

$$\text{probe limit:} \qquad f = 1 - z^3 \qquad \text{with} \quad A_t = \mu(1 - z)\,. \tag{2.22}$$

We work in the probe limit $\mu = 0$ and $\mu q = \mu_q$ held fixed. In this limit, the electric field does not backreact on the geometry. If we use the full solution to the RN black hole, the qualitative features will not change, as we will discuss at the end of section 2.3.1.

2.3.1 Numerics

To solve the Dirac equation (2.5) numerically in this spacetime, we approximate the ingoing solution by a Taylor series near the horizon $z = 1$, integrate numerically to a point near the boundary $z = 0$, and fit the numerical solution to the boundary expansion $\psi_\pm = b_\pm \chi_1 + a_\pm \chi_2$. The numerical integration was performed using Mathematica's NDSolve routine [51]. As we are interested in QNMs and the corresponding Green's function singularities, we focus on the value of the source $a_\pm$.

Figure 2.2 presents a density plot of $|a_+|$ as a function of complex ω. We see that the poles of the Green's function in the complex ω plane have the following features:

- As we increase the chemical potential μ_q, there are more and more poles along the negative real ω axis. Decreasing μ_q moves these poles to the right. Once they cross the imaginary axis, they begin to move away from the positive real axis. See figure 2.2.

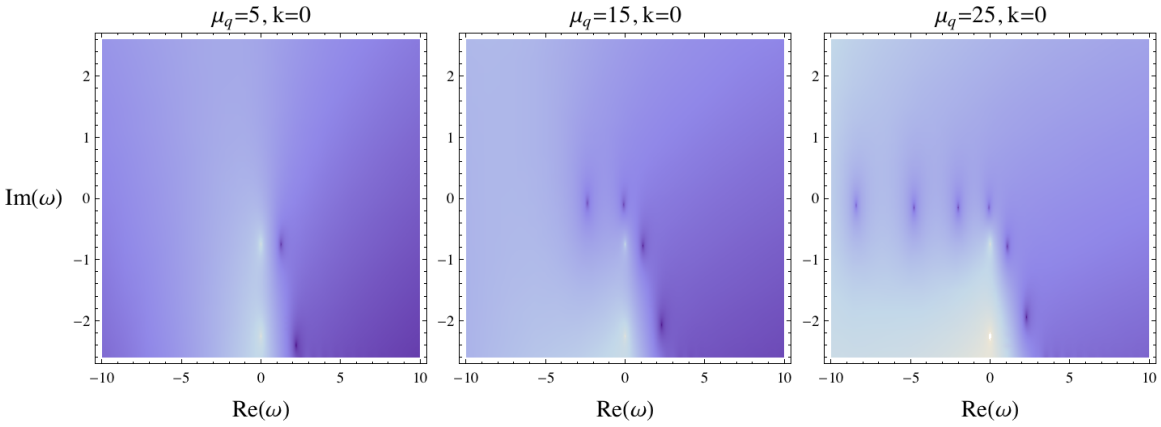

Figure 2.2: Motion of the poles in the complex ω plane as we increase μ_q. From left to right, $\mu_q = 5$, 15, 25. Other parameters are $m = 2$ and $k = 0$.

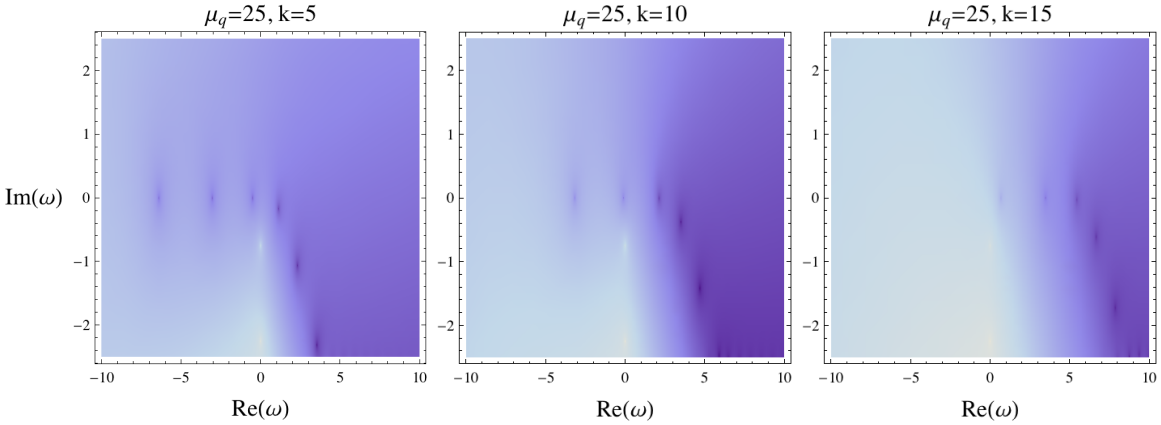

Figure 2.3: Motion of the poles in the complex ω plane as we increase k. From left to right, $k = 5$, 10, 15. Other parameters are $m = 2$ and $\mu_q = 25$.

- If we fix μ_q and increase the momentum k, the poles move to the right. As $\omega = 0$ corresponds to the Fermi surface, when a pole crosses the imaginary axis, we obtain a Fermi momentum k_F. See figure 2.3.

We can obtain many Fermi momenta $k_F^{(n)}$ and many Fermi surfaces. The poles close to the real ω axis correspond to quasibound states, and the number of them at $k = 0$ equals the number of Fermi surfaces. The number of Fermi surfaces grows linearly with the chemical potential, which can be seen by comparing figure 2.2 and figure 2.11 in the next section (or equivalently tables (2.39) and (2.39)).

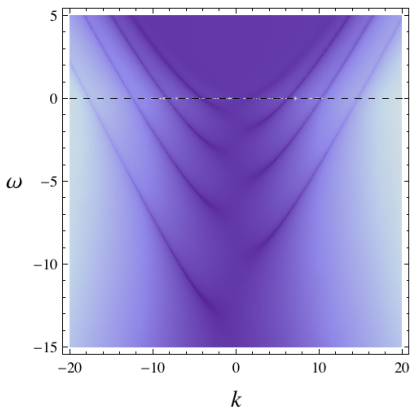

Figure 2.4: Dispersion relation for a massless fermion with $\mu_q = 20$. Its mirror image $k \to -k$ is for the opposite helicity. There are no poles in the Green's function at $k = 0$.

For the other spin ($k \to -k$), the poles will be in slightly different locations. The spin splitting can be seen more obviously by looking at figure 2.1. The figure is a plot of the dispersion relation and was constructed by superposing density plots of $|a_+|$ and $|a_-|$ in the k-ω plane. The density plot of $|a_+|$ corresponds to the parabolas on the left and $|a_-|$ to the parabolas on the right.

For comparison, we also plot the dispersion relation for a massless $m = 0$ bulk fermion in figure 2.4. (Here only $|a_+|$ is plotted. The density plot for the other spin component $|a_-|$ is the mirror image.) Unlike the massive case, there do not seem to be well defined quasiparticles close to the $k = 0$ axis. For the $m = 0$ case there are no poles in the Green's function at $k = 0$ and $m = 0$. This fact can be checked analytically by solving the Dirac equation to obtain $G_R(\omega, k = 0) = i$ [22]. From a bulk point of view, the absence of these poles is presumably related to the absence of a rest frame for a massless particle. As can be seen in figure 2.4, poles do appear for $k \neq 0$. For the field theory dual, the interpretation is more obscure. Ref. [49] relates the absence to strong interactions with a background continuum of states existing inside an "IR lightcone". Why then the interactions are suppressed for larger bulk masses still needs to be explored.

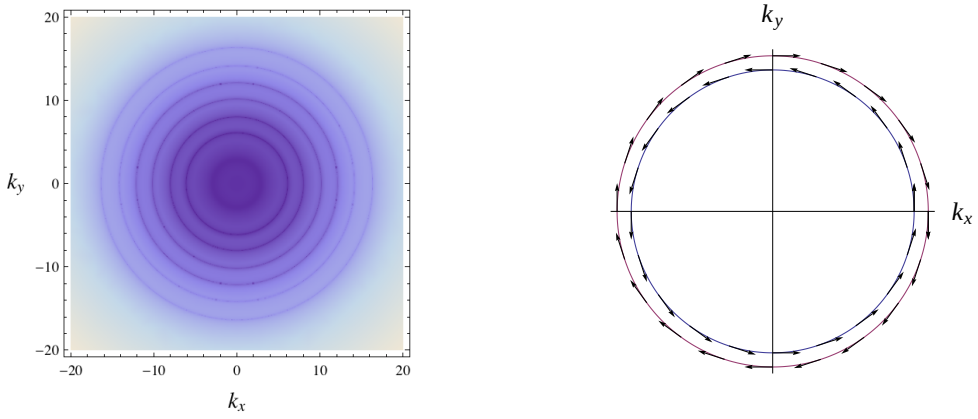

Figure 2.5: The left plot shows the Fermi surfaces with spin splitting. The parameters are $m = 2$ and $\mu_q = 25$. The right plot illustrates the directions of spin for massive bulk fermions.

Figure 2.5 (left) shows the location of the Fermi surfaces in momentum space and also demonstrates the spin splitting effect. As we discussed above, the spin of the bulk spacetime fermions is perpendicular to the momentum and the electric field. Thus the bulk Fermi surfaces are spin polarized, as shown schematically in figure 2.5 (right). A similar effect has been studied in spin Hall systems [52] and observed in experiments [53] for electrons that while confined to a plane still have a three dimensional spin.

Note that for the 2+1 dimensional field theory fermions, the spins shown in figure 2.5 (right) are misleading. From a purely 2+1 dimensional perspective, we argued in the introduction that the fermions are both massless and spinless. The extra degrees of freedom producing the second Fermi surface come from the hole states. The dispersion relation for the hole states has been bent upward, emptying out the infinite Fermi sea and producing a second Fermi surface.

Before moving on to WKB, we promised a discussion of the validity of our probe approximation. The temperature for the charged black hole solution eq. (2.21) is

$$T = \frac{12 - \mu^2}{16\pi} \,. \tag{2.23}$$

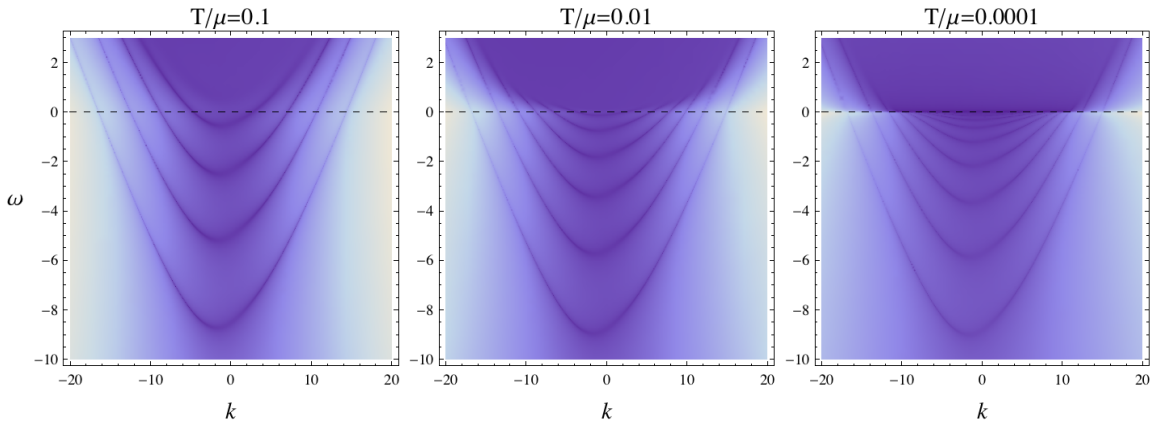

Figure 2.6: Temperature dependence of the dispersion relation with fixed $\mu_q = 25$. This is the only plot that uses the full solution of the RN black hole in this chapter. The chemical potential for the three plots are $\mu \approx 1.7665$, 3.2218, 3.4615 (from left to right). The extremal case corresponds to $\mu = 2\sqrt{3} \approx 3.4641$. These are spin up fermions.

If we lower the temperature by increasing the chemical potential μ, more Fermi surfaces will appear, but the size of the outer Fermi surface will remain roughly the same, as figure 2.6 shows. By comparing figure 2.6 and figure 2.1a, we can see that if we consider the high temperature regime, i.e., $T/\mu > 0.1$, there is no essential difference between the full RN solution and the probe limit in eq. (2.22).

2.3.2 WKB

The rough picture of the WKB analysis of the Schrödinger equation (2.17) with the spinor potential function $V_{k,m}$ (2.18) is easily explained. Schematically, we may write our potential as

$$V_{k,m} = \frac{V_0}{\hbar^2} + \frac{V_1}{\hbar} + V_2 \,. \tag{2.24}$$

Considering only the leading order term $V_0 = g_{zz}m^2 - Z_k Z_{-k}$, there is a barrier at the conformal boundary $z = 0$ provided $m^2 > 0$. At the horizon $z = 1$, the potential V_0 is unbounded below provided $\omega^2 > 0$. For intermediate values $0 < z < 1$ and appropriate choices of k, μ, and q, one may find a potential well where $V_0 < 0$ separated from the horizon by a barrier where $V_0 > 0$ (see figure 2.7). For discrete

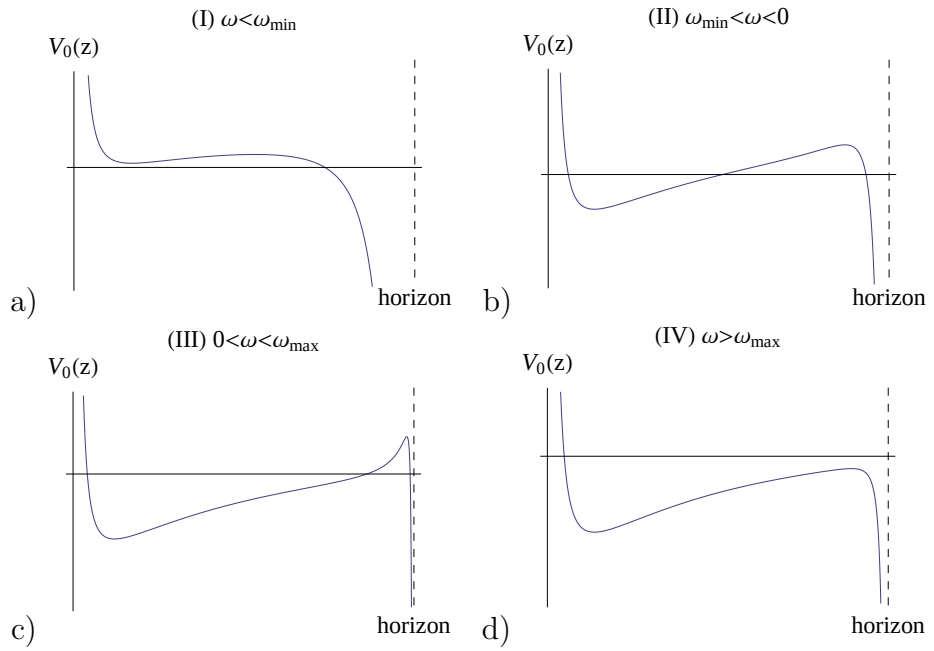

Figure 2.7: The leading order potential V_0 for the spinor or scalar when $\omega \neq 0$. There exist quasi-bound states when $\omega_{\min} < \omega < \omega_{\max}$.

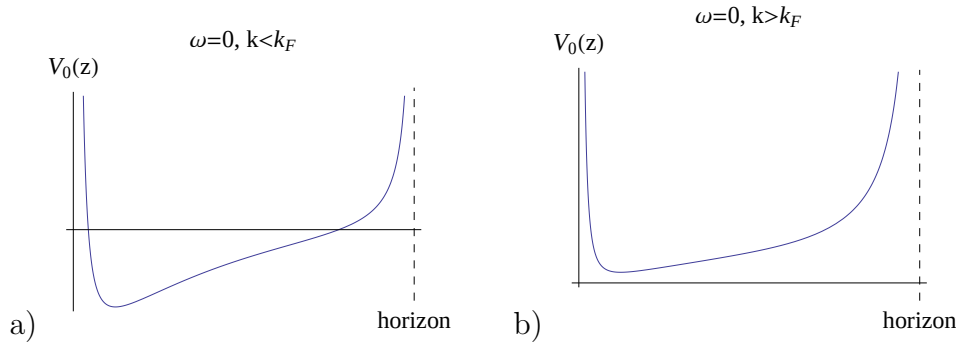

Figure 2.8: The leading order potential V_0 for the spinor or scalar when $\omega = 0$. There exists a bound state provided k is not too large.

choices of ω, the wave function will satisfy a Bohr-Sommerfeld type quantization condition, and the potential well will support quasi-bound states. Tunneling through the barrier to the horizon gives ω a small imaginary part. Note in the special case $\omega = 0$ shown in figure 2.8, the potential at the horizon becomes a barrier, suggesting that the quasinormal modes have very small imaginary part close to the origin.

The detailed picture of this WKB analysis is more intricate. At leading order in $\hbar$, the Schrödinger potentials for the spinor and scalar are identical, and the results

will be independent of the spin that is this chapter's main focus. Moreover, there is an important qualitative difference in the QNM spectrum for the spinor and scalar that is not captured at this leading order. The charged scalar QNMs may lie in the upper half of the complex ω plane signaling a perturbative instability [36, 37], while the spinor QNMs will not. Yet, as we will see, the leading order WKB analysis would put the spinor QNMs in the upper half plane as well.

To capture the effects of spin, we will keep the first subleading term in the $\hbar$ expansion of $V_{k,m}$. Our WKB wavefunction is then

$$\phi_{\rm WKB} = \frac{1}{V_0^{1/4}} \exp\left(\pm\frac{1}{\hbar}\int \sqrt{V_0}\left(1+\hbar\frac{V_1}{2V_0}\right)dz\right). \tag{2.25}$$

The classical turning points are defined in terms of the zeroes of V_0.

To set up the WKB problem, let $z_1 < z_2$ be the turning points bounding the classically allowed region. Similarly, let $z_2 < z_3$ bound the potential barrier. We begin by writing formal expressions for the WKB wave functions to the left and right of the three points z_1, z_2, and z_3 valid to next to leading order in $\hbar$:

$$\phi_1 = \frac{1}{V_0^{1/4}}\left(A_1 e^{\frac{1}{\hbar}\int_z^{z_1}\sqrt{V_0}(1+\hbar V_1/2V_0)dz} + B_1 e^{-\frac{1}{\hbar}\int_z^{z_1}\sqrt{V_0}(1+\hbar V_1/2V_0)dz}\right), \tag{2.26}$$

$$\phi_2 = \frac{1}{(-V_0)^{1/4}}\left(A_2 e^{\frac{i}{\hbar}\int_{z_1}^{z}\sqrt{-V_0}(1+\hbar V_1/2V_0)dz} + B_2 e^{-\frac{i}{\hbar}\int_{z_1}^{z}\sqrt{-V_0}(1+\hbar V_1/2V_0)dz}\right), \tag{2.27}$$

$$\phi_3 = \frac{1}{(-V_0)^{1/4}}\left(A_3 e^{\frac{i}{\hbar}\int_{z}^{z_2}\sqrt{-V_0}(1+\hbar V_1/2V_0)dz} + B_3 e^{-\frac{i}{\hbar}\int_{z}^{z_2}\sqrt{-V_0}(1+\hbar V_1/2V_0)dz}\right), \tag{2.28}$$

$$\phi_4 = \frac{1}{V_0^{1/4}}\left(A_4 e^{\frac{1}{\hbar}\int_{z_2}^{z}\sqrt{V_0}(1+\hbar V_1/2V_0)dz} + B_4 e^{-\frac{1}{\hbar}\int_{z_2}^{z}\sqrt{V_0}(1+\hbar V_1/2V_0)dz}\right), \tag{2.29}$$

$$\phi_5 = \frac{1}{V_0^{1/4}}\left(A_5 e^{\frac{1}{\hbar}\int_{z}^{z_3}\sqrt{V_0}(1+\hbar V_1/2V_0)dz} + B_5 e^{-\frac{1}{\hbar}\int_{z}^{z_3}\sqrt{V_0}(1+\hbar V_1/2V_0)dz}\right), \tag{2.30}$$

$$\phi_6 = \frac{1}{(-V_0)^{1/4}}\left(A_6 e^{\frac{i}{\hbar}\int_{z_3}^{z}\sqrt{-V_0}(1+\hbar V_1/2V_0)dz} + B_6 e^{-\frac{i}{\hbar}\int_{z_3}^{z}\sqrt{-V_0}(1+\hbar V_1/2V_0)dz}\right). \tag{2.31}$$

Figure 2.9 portrays a typical potential with the regions labeled in which the six WKB wave functions are valid.

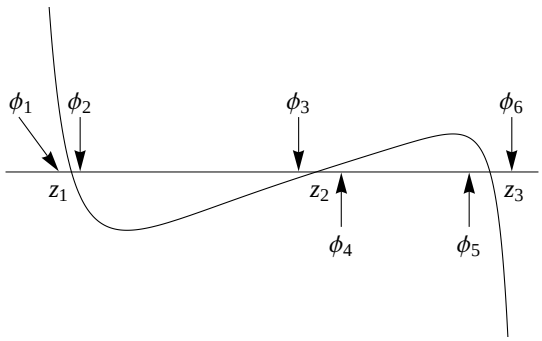

Figure 2.9: A typical spinor or scalar potential at leading order in $\hbar$. The classical turning points are z_1, z_2, and z_3. The WKB wave functions ϕ_i correspond to eqs. (2.26)–(2.31)

The wave functions in adjacent regions will be related by connection matrices M_i such that $v_{i+1} = M_i v_i$ where $v_i = (A_i, B_i)^T$. Given these connection matrices, we can obtain a semi-classical quantization condition on ω by applying boundary conditions. We will take Dirichlet boundary conditions at $z = 0$ that $A_1 = 0$. At the horizon, we have ingoing boundary conditions that $\phi \sim (1-z)^{-i\omega/3}$. The WKB wave function (2.31) has the near horizon expansion $\phi_6 \sim A_6(1-z)^{-i|\omega|/3} + B_6(1-z)^{i|\omega|/3}$. Thus when $\omega > 0$ we should take $B_6 = 0$, and when $\omega < 0$ we should take instead $A_6 = 0$. The equation

$$v_6 = M_5 M_4 M_3 M_2 M_1 v_1 \tag{2.32}$$

then provides a Bohr-Sommerfeld like quantization condition on ω.

The matrices M_i are all well known. To go from a classically forbidden region to the classically allowed region, we use the standard WKB connection formula

$$M = \begin{pmatrix} \frac{i}{2} & 1 \\ \frac{1}{2} & i \end{pmatrix}. \tag{2.33}$$

Thus we find that $M_1 = M$ and $M_3 = M^{-1}$. To go from ϕ_2 to ϕ_3 or from ϕ_4 to ϕ_5, we make use of the fact that $\int_a^z f(z)dz = -\int_z^b f(z)dz + \int_a^b f(z)dz$:

$$M_2 = \begin{pmatrix} 0 & e^{-iL} \\ e^{iL} & 0 \end{pmatrix}, \qquad M_4 = \begin{pmatrix} 0 & e^{-K} \\ e^{K} & 0 \end{pmatrix}, \tag{2.34}$$

where

$$L \equiv \frac{1}{\hbar}\int_{z_1}^{z_2} \sqrt{-V_0}\left(1 + \hbar\frac{V_1}{2V_0}\right) dz\,, \qquad K \equiv \frac{1}{\hbar}\int_{z_2}^{z_3} \sqrt{V_0}\left(1 + \hbar\frac{V_1}{2V_0}\right) dz\,. \tag{2.35}$$

The connection matrix M_4 deserves closer scrutiny because the integral K is not always well defined. From eq. (2.18), we see that the potential term V_1 (for the ϕ_+ case) has the form

$$V_1 = -g_{zz}m\frac{\partial_z(\sqrt{g^{zz}}Z_k)}{Z_k}\,. \tag{2.36}$$

Thus V_1 will have a simple pole where Z_k vanishes. From the form of $V_0 = g_{zz}m^2 - Z_{-k}Z_k$, it is clear that Z_k will only vanish in a classically forbidden region where $V_0 > 0$. Thus, the integral L will never be singular in this way. Let $z = a_i$ be the locations of the simple poles of V_1. Near a_i, the integrand for K looks like $\frac{1}{2}(z-a_i)^{-1}$. We regulate the singularity by taking a small semi-circular detour in the complex z plane. The detour introduces a factor of $\pm i\pi/2$, depending on the choice of detour above or below the singularity. This extra phase factor introduces a relative minus sign between the two nonzero entries of M_4. We do not need to worry about the overall sign as it will not affect the quantization condition.

We can be more precise about where Z_k has zeroes. From (2.16), Z_k is manifestly positive in the region $0 < z < 1$ if both $\omega > 0$ and $k < 0$. Thus in this case, there will be no singularity to worry about. However, if $\omega < 0$ there will in general be one such value $z = a_1$ and if $\omega > 0$ and $k > 0$, there will be either zero or two such values.

Given the matrices M_i and the relation (2.32), we find the quantization condition on ω looks in general like

$$\cos L(\omega) + ice^{-2K(\omega)} \sin L(\omega) = 0\,. \tag{2.37}$$

In deriving (2.37), we made the implicit assumption that the turning points lie on the real axis. However, the quantization condition implies ω is not real, and if ω is not real, the turning points will in general not lie on the real axis. To get out of this apparent contradiction, we assume that $|ce^{-2K}| \ll 1$. Then the imaginary part of ω should be small, and we can use (2.37) to estimate it. We find the QNMs at ω_n, $n = 1, 2, 3, \ldots$, satisfy

$$L(\mathrm{Re}\,\omega_n) = \pi(n - 1/2)\,, \qquad \mathrm{Im}\,\omega_n \approx c\frac{e^{-2K}}{dL/d\omega}\bigg|_{\omega=\mathrm{Re}\,\omega_n}\,. \tag{2.38}$$

In all our examples, it is also true that $dL/d\omega > 0$. Thus the sign of the imaginary part is determined by the sign of ce^{-2K}.

Specializing to the ϕ_+ case for concreteness, there are several cases to consider.

- When $\omega > 0$ and $k < 0$, the singularities at $z = a_i$ are absent, and we find for both the scalar and spinor the quantization condition (2.37) with $c = -1/4$. These QNMs lie in the lower half plane.

- For the scalar when $\omega < 0$, the change in the WKB boundary conditions at the horizon leads to the relation (2.37) with $c = 1/4$. These QNMs lie in the upper half plane.

- For the spinor when $\omega < 0$, there is a pole in V_1 at $z = a_1$. Deforming the contour to avoid the pole adds a phase factor $\pi i/2$ to the integral K. Thus while $c = 1/4$ as in the scalar case, $e^{-2K} < 0$ is negative. These QNMs lie in the lower half plane.

- We may also consider the case where $\omega > 0$ and $k > 0$. In this case, Z_k may have no zeroes or two zeroes in the region $0 < z < 1$. If there are no zeroes, we reduce to the $\omega > 0$ and $k < 0$ case. If there are two zeroes, then $e^{-2K} > 0$ and the QNMs are still in the lower half plane.

At first order in $\hbar$, the WKB approximation already works pretty well. Below are tables comparing the first order WKB against numerical integration of the Dirac equation. For $m = 2$ and $\mu_q = 25$ we have the following results when $k = \pm 5$, illustrating the spin splitting:

$k = -5$	
numeric	WKB
$-7.90 - 0.00516i$	$-7.99 - 0.00504i$
$-4.23 - 0.00597i$	$-4.30 - 0.00587i$
$-1.42 - 0.00545i$	$-1.47 - 0.0052i$
$0.574 - 0.0390i$	$0.576 - 0.041i$

$k = 5$	
numeric	WKB
$-6.40 - 0.00398i$	$-6.48 - 0.00383i$
$-3.04 - 0.00476i$	$-3.10 - 0.00471i$
$-0.504 - 0.00471i$	$-0.540 - 0.0044i$

We have presented the same information graphically in figure 2.10.

For $m = 2$, $k = 0$, we also present results for $\mu_q = 50$ and $\mu_q = 75$.

$\mu_q = 50$	
numeric	WKB
$-26.35 - 0.172i$	$-26.77 - 0.135i$
$-20.84 - 0.248i$	$-21.25 - 0.18i$
$-16.29 - 0.281i$	$-16.66 - 0.19i$
$-12.41 - 0.292i$	$-12.74 - 0.18i$
$-9.03 - 0.290i$	$-9.34 - 0.17i$
$-6.10 - 0.278i$	$-6.37 - 0.16i$
$-3.57 - 0.255i$	$-3.80 - 0.14i$
$-1.44 - 0.218i$	$-1.63 - 0.12i$

$\mu_q = 75$	
numeric	WKB
$-45.98 - 0.214i$	$-46.50 - 0.165i$
$-39.14 - 0.313i$	$-39.64 - 0.227i$
$-33.41 - 0.361i$	$-33.87 - 0.24i$
$-28.43 - 0.385i$	$-28.87 - 0.24i$
$-24.02 - 0.394i$	$-24.42 - 0.23i$
$-20.05 - 0.394i$	$-20.42 - 0.22i$
$-16.45 - 0.388i$	$-16.80 - 0.21i$
$-13.18 - 0.377i$	$-13.51 - 0.195i$
$-10.20 - 0.362i$	$-10.50 - 0.18i$
$-7.50 - 0.343i$	$-7.77 - 0.17i$
$-5.06 - 0.319i$	$-5.31 - 0.15i$
$-2.90 - 0.288i$	$-3.11 - 0.13i$
$-1.05 - 0.240i$	$-1.23 - 0.11i$

The results are presented graphically in figure 2.11.

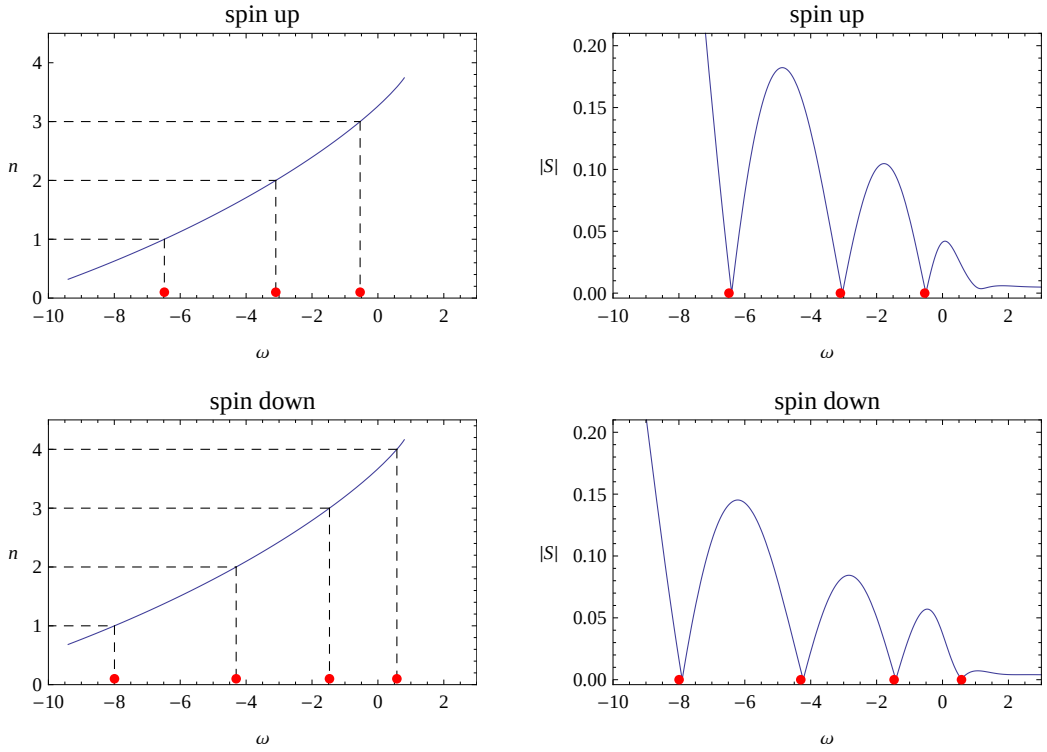

Figure 2.10: Normal modes obtained by the Bohr-Sommerfeld quantization, marked by red dots. The parameters are $m = 2$, $k = 5$, and $\mu_q = 25$. Here $|S| = |a_\alpha|$ is the source (denominator) of the Green's function.

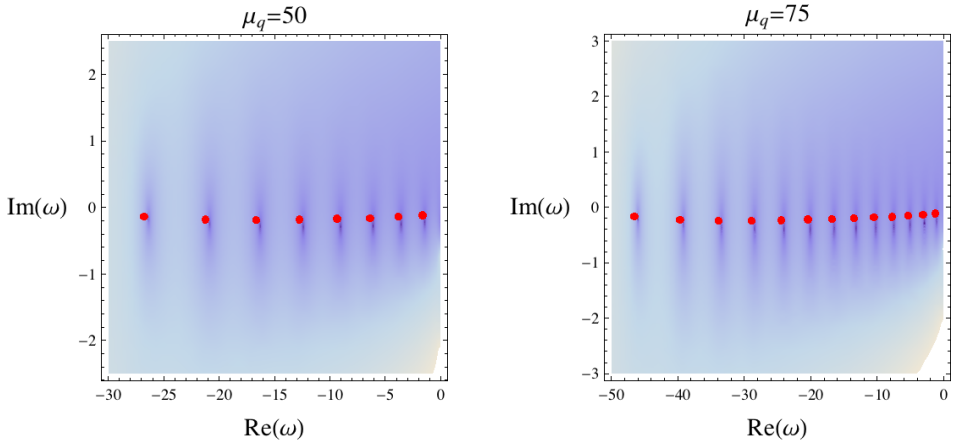

Figure 2.11: Quasibound states in the complex ω plane. The red dots are the quasinormal modes obtained by the generalized WKB formula. The parameters are $m = 2$, $k = 0$. Two values of μ_q are considered.

We will stop at first order in the WKB approximation, but there are some interesting complications that appear at second order. There exist second order poles in $V_{k,m}$ at $z = 0$, 1 and a_i that require a more careful consideration. Regardless of the background, the second order poles near $z = a_i$ have the universal form

$$V_{k,m} \approx \frac{3/4}{(z - a_i)^2} \,. \tag{2.39}$$

In our particular case, at the conformal boundary, we find that

$$V_{k,m} = \frac{m^2 - m\hbar}{\hbar^2 z^2} + O(z^{-1}) \,. \tag{2.40}$$

At the horizon, we have instead

$$V_{k,m} = -\left(\frac{1}{4} + \frac{16\omega^2}{\hbar^2(12 - \mu^2)^2}\right) \frac{1}{(1 - z)^2} + O(1 - z)^{-3/2} \,. \tag{2.41}$$

The issue with second order poles in the potential is that the naive WKB wave functions do not have the proper scaling behavior near such points. Langer [54] proposed a modification, justified by a rescaling of the wave function and redefinition of z, that boils down to adding by hand a term of the form $\frac{1}{4}(z - z_s)^{-2}$ to the potential for each second order pole z_s. These Langer modification factors are second order in our $\hbar$ expansion, and thus we have neglected them.

2.4 Discussion

We have tried to show in this chapter that spin affects in important ways the physics of holographic constructions involving fermions. The pole of the field theory fermionic Green's function obeys a Rashba type dispersion relation, indicating the importance of spin orbit coupling in the gravitational side of the construction. The spin also

plays an important role in determining the lifetimes of quasiparticles. Without the spin corrections in the WKB approximation, the fermionic dispersion relation would have an imaginary part of the wrong sign! That spin plays an important role in the bulk is ironic given that in a 2+1 dimensional field theory dual, we argued in the introduction that the fermions should be both massless and (hence) spinless.

This work leaves open several issues that we would like to return to at some point. One is a more thorough exploration of the parameter space of our model. We would like to understand better the qualitative difference between bulk fermions with large masses $mL \gtrsim 1$ and small masses $mL \lesssim 1$ illustrated by figures 2.1a and 2.4. While the gravity explanation is related to the absence of a rest frame for a relativistic particle, the field theory interpretation is less clear. The limit $\omega \to 0$ played an important role in previous works on the subject (see for example [22]), and we would like to see what our WKB formalism predicts for the magnitude of the imaginary part of the dispersion relation and the corresponding lifetime of the quasiparticles. (How does including $\hbar$ corrections change the results of [27]?) Third, it would be interesting to consider the $T \to 0$ limit in more detail.

It would also be interesting to work with a wider variety of backgrounds, for example the electron star or the holographic superconductor. We believe the qualitative nature of our story involving spin-orbit coupling and quasinormal mode placement will not change, but there may be other interesting effects. For example, with the d-wave superconductor studied in [45], it was precisely this spin-orbit coupling which gave rise to Fermi arcs.

Chapter 3

Analytic fermionic Green's functions from holography

This chapter is a lightly edited version of ref. [55], which was written in collaboration with Steven S. Gubser.

3.1 Introduction

Charged black holes in asymptotically anti-de Sittter (AdS) space can be regarded as the gravitational dual description of certain strongly interacting fermionic systems at finite charge density, such as non-Fermi liquids [33]. This is an application of the gauge/gravity duality [7, 9, 10], which allows us to calculate fermionic Green's function by solving the bulk Dirac equation [31, 32, 46]. A particularly well-studied example is the Reissner-Nordström (RN) black hole in AdS as the geometry [19, 34, 22, 23]. We will focus instead on a particular dilatonic black hole in AdS_5, explored originally in ref. [28]; see also ref. [56] for related work.

The dilatonic black hole in question is sometimes referred to as the two-charge black hole. From a five-dimensional point of view, this is because two of the three mutually commuting $U(1)$ subgroups of the $SO(6)$ gauge group of maximal gauged

supergravity are nonzero and equal, while the third is zero. From a ten-dimensional point of view, this black hole describes N coincident D3-branes with equal, nonzero angular momentum in two of the three independent planes of rotation orthogonal to the D3-brane world-volume. The dilatonic black hole enjoys several advantages over the better studied RN-AdS_5 black hole:

- The entropy and specific heat of the dilatonic black hole are proportional to temperature, as compared to a nonzero, $\mathcal{O}(N^2)$ entropy at extremality for the RN-AdS_5 black hole.

- Exact information about the position and properties of Fermi surfaces is available for the dilatonic black hole, for massless bulk fermion actions with no Pauli couplings. This stands in contrast with the RN-AdS_5 black hole, where one must resort to numerics to find k_F. (This is even true of ref. [57], in which numerical work led to strong evidence that the Fermi momenta are simple algebraic numbers.)

- Pair creation of fermions near the horizon, and back-reaction of the resulting fermionic matter, must distort the RN-AdS_5 geometry to some extent. But for the dilatonic black holes there is some evidence, to be explained below, that pair creation of fermions is suppressed.

A notable disadvantage of the dilatonic black hole is that its extremal limit—which will be our main focus—has a naked singularity. Any nonzero temperature cloaks the naked singularity with a horizon, but as temperature is taken to zero, the dilaton as well as curvature invariants become larger and larger at the horizon, until at zero temperature they diverge. Nevertheless it is straightforward to pick out physically reasonable boundary conditions for fermions: In particular, for $\omega = 0$ one can simply demand that the allowed solutions are regular as the naked singularity is approached.

The main aim of this chapter is to solve the massless Dirac equation,

$$\gamma^{\mu}(\nabla_{\mu} - iqA_{\mu})\Psi = 0, \tag{3.1}$$

in the extremal limit of the dilatonic black hole background, and to show that the corresponding Green's function exhibits one or more Fermi surfaces if $q > 1/2$. For $1/2 < q < 1$, there is only a single Fermi surface, and v_F is not well-defined. For $1 < q < 3/2$, there is still only a single Fermi surface, but v_F is well defined. For $q > 3/2$, there are additional Fermi surfaces at $k_F = q - n - 1/2$, where n is a positive integer. The outermost Fermi surface has the simplest properties: assuming $q > 1$, the Green's function near the Fermi surface takes the form

$$G = \frac{Z}{-\omega + v_F(k - k_F) - \Sigma(\omega, k_F)}, \tag{3.2}$$

where

$$\begin{aligned} k_F &= q - \frac{1}{2} \qquad v_F = \frac{4(q-1)}{4q-3} \\ \Sigma &= \frac{\Gamma(q+1/2)\Gamma(1-q)e^{i\pi(1-q)}}{2^{4q-5}\sqrt{\pi}(4q-3)\Gamma(q-1)\Gamma(q)}\omega^{2q-1} \\ Z &= \frac{8\Gamma(q+1/2)}{\sqrt{\pi}(4q-3)\Gamma(q-1)}. \end{aligned} \tag{3.3}$$

Formulas generalizing eq. (3.3) to Fermi surfaces with $n > 0$ can be found in section 3.4.

The organization of the rest of this chapter is as follows. In section 3.2, we solve the Dirac equation at $\omega = 0$ in terms of hypergeometric functions, and find the normal modes that determine the location of Fermi surfaces. In section 3.3, we study the near horizon geometry (hereafter IR for infrared), solving the Dirac equation and obtaining the IR Green's function. In section 3.4, we obtain the Green's function

near Fermi surface by matching the IR solution to a zero-frequency solution away from the IR. In section 3.5, we numerically solve the Green's function and explain the main features at general ω. In section 3.6, we conclude with some discussion.

3.2 Normal modes

The two-charge black hole in AdS_5 is determined by

$$\mathcal{L} = \frac{1}{2\kappa^2}\Big[R - \frac{1}{4}e^{4\alpha}F_{\mu\nu}^2 - 12(\partial_\mu\alpha)^2 + \frac{1}{L^2}(8e^{2\alpha} + 4e^{-4\alpha})\Big], \tag{3.4}$$

which is from a consistent truncation of the type IIB supergravity with three U(1) charges $Q_1 = Q_2 = Q$ and $Q_3 = 0$. The solution in the extremal case is

$$\begin{aligned} ds^2 &= e^{2A}(-hdt^2 + d\mathbf{x}^2) + \frac{e^{2B}}{h}dr^2 \\ A = \ln\frac{r}{L} + \frac{1}{3}\ln\left(1+\frac{Q^2}{r^2}\right) \qquad & B = -\ln\frac{r}{L} - \frac{2}{3}\ln\left(1+\frac{Q^2}{r^2}\right) \\ h = \frac{(r^2+2Q^2)r^2}{(r^2+Q^2)^2} \qquad & \alpha = \frac{1}{6}\ln\left(1+\frac{Q^2}{r^2}\right) \\ A_\mu dx^\mu = \Phi dt \qquad & \Phi = \frac{\sqrt{2}Qr^2}{(r^2+Q^2)L}. \end{aligned} \tag{3.5}$$

The "horizon" for this black hole is at $r = 0$, which is a spacetime singularity. For the non-extremal case, and its ten-dimensional lift, see ref. [28].

We will solve the Dirac equation for a massless spinor in the above background, but we keep the mass term at first. If the metric is diagonal and depends only on the radial coordinate r, the Dirac equation can be simplified by using the rescaled spinor $\tilde{\Psi} = (-gg^{rr})^{1/4}\Psi$. The equation of motion for $\tilde{\Psi}$ is

$$[\gamma^\mu(\partial_\mu - iqA_\mu) - m]\tilde{\Psi} = 0. \tag{3.6}$$

We assume that the momentum is in the x direction. By plugging a single Fourier mode $\tilde{\Psi} \sim e^{-i\omega t+ikx}\hat{\Psi}$ to eq. (3.6), the equation for $\hat{\Psi}$ is

$$\left[-i\sqrt{-g^{tt}}\gamma^{\underline{t}}(\omega + qA_t) + \sqrt{g^{rr}}\gamma^{\underline{r}}\partial_r + i\sqrt{g^{xx}}\gamma^{\underline{x}}k - m\right]\hat{\Psi} = 0. \tag{3.7}$$

We choose the following gamma matrices for AdS_5:

$$\gamma^{\underline{t}} = \begin{pmatrix} i\sigma_1 & 0 \\ 0 & i\sigma_1 \end{pmatrix} \qquad \gamma^{\underline{r}} = \begin{pmatrix} \sigma_3 & 0 \\ 0 & \sigma_3 \end{pmatrix}$$
$$\gamma^{\underline{x}} = \begin{pmatrix} -\sigma_2 & 0 \\ 0 & \sigma_2 \end{pmatrix} \qquad \gamma^{\underline{y}} = \begin{pmatrix} 0 & -\sigma_2 \\ -\sigma_2 & 0 \end{pmatrix} \qquad \gamma^{\underline{z}} = \begin{pmatrix} 0 & i\sigma_2 \\ -i\sigma_2 & 0 \end{pmatrix}. \tag{3.8}$$

Then eq. (3.7) reduces to two decoupled equations

$$\left[\sqrt{-g^{tt}}\sigma_1(\omega + qA_t) + \sqrt{g^{rr}}\sigma_3\partial_r + (-1)^{\alpha}\sqrt{g^{xx}}i\sigma_2 k - m\right]\psi_{\alpha} = 0, \tag{3.9}$$

where ψ_1 and ψ_2 are two-component spinors. The equation for ψ_2 is related to the equation for ψ_1 by $k \to -k$.

The (massive or massless) Dirac spinor Ψ in the AdS_5 maps to a chiral spinorial operator $\mathcal{O}_{\Psi}$ at the boundary [31, 32, 46]. The asymptotic behavior of ψ_{α} near the AdS boundary is

$$\psi_{\alpha} \xrightarrow{r\to\infty} a_{\alpha}r^{m}\begin{pmatrix} 1 \\ 0 \end{pmatrix} + b_{\alpha}r^{-m}\begin{pmatrix} 0 \\ 1 \end{pmatrix}. \tag{3.10}$$

The expectation value of the boundary spinorial operator dual to the bulk spinor Ψ has the form $\langle\mathcal{O}_{\Psi}\rangle = (0, b_1, 0, b_2)^T$. In fact, $\mathcal{O}_{\Psi} = \frac{1}{2}(1 - \gamma^{\underline{r}})\mathcal{O}_{\Psi}$, which means that the boundary spinorial operator is left-handed. By imposing the in-falling boundary

condition at the horizon, we can obtain the retarded Green's function as

$$G = \begin{pmatrix} 0 & & & \\ & G_1 & & \\ & & 0 & \\ & & & G_2 \end{pmatrix}, \qquad G_\alpha = \frac{b_\alpha}{a_\alpha}. \tag{3.11}$$

Note that if we use the alternative quantization, the Green's function is $\tilde{G}_\alpha = -a_\alpha/b_\alpha$, and the boundary spinorial operator is right-handed. If $m = 0$, G_1 and G_2 are related by $G_2 = -1/G_1$ [22]; therefore, the alternative quantization for G_1 is the standard quantization for G_2, and vice versa. By taking into account both G_1 and G_2, the alternative quantization gives the same Fermi momenta as the standard quantization does, when $m = 0$ [22].

We will focus on $\psi_1 \equiv (u_1, u_2)^T$ in the following. The square roots in the Dirac equation can be eliminated, following a method which has appeared, for example, in ref. [58]. Define $u_\pm = u_1 \pm i u_2$. From eq. (3.9), we obtain

$$u'_+ + \bar{\lambda}(r) u_+ = \bar{f}(r) u_- \tag{3.12}$$

$$u'_- + \lambda(r) u_- = f(r) u_+, \tag{3.13}$$

where

$$\lambda(r) = i\sqrt{\frac{|g^{tt}|}{g^{rr}}}(\omega + qA_t), \qquad f(r) = \frac{m}{\sqrt{g^{rr}}} - ik\sqrt{\frac{g^{xx}}{g^{rr}}}. \tag{3.14}$$

The eqs. (3.12) and 3.13 can be decoupled to obtain two second-order differential equations:

$$u''_+ + \bar{p}(r) u'_+ + \bar{q}(r) u_+ = 0 \tag{3.15}$$

$$u''_- + p(r) u'_- + q(r) u_- = 0, \tag{3.16}$$

where

$$p(r) = -\frac{f'}{f}, \qquad q(r) = |\lambda|^2 - |f|^2 + p\lambda + \lambda'. \tag{3.17}$$

After we solve eq. (3.16) for u_-, we need to plug in u_- to eq. (3.13) to obtain u_+.[1] For the metric we consider,

$$\lambda = \frac{i(\omega + q\Phi)}{he^{A-B}}, \qquad f = \frac{m}{\sqrt{h}e^{-B}} - \frac{ik}{\sqrt{h}e^{A-B}}. \tag{3.18}$$

In the following, we will only study the $m = 0$ case, in which $p(r)$ and $q(r)$ are rational functions of r. We are most interested in the following two questions: whether there are Fermi surfaces, and whether there are quasiparticles near the Fermi surfaces. We will solve the Dirac equation at $\omega = 0$ first, and the solution indicates that there are one or more Fermi surfaces when $q > 1/2$, as summarized more precisely in the text following eq. (3.1). Then the perturbation at small ω will give the Green's function near the Fermi surfaces.

When $\omega = 0$, the boundary condition for at the horizon is that the solution is regular. The solution for $u_\pm$ can be written as[2]

$$u_- = \left(\frac{r}{r + i\sqrt{2}Q}\right)^{\nu_k} \left(\frac{r + i\sqrt{2}Q}{r - i\sqrt{2}Q}\right)^{q/2} {}_2F_1\left(\nu_k - q + \frac{1}{2},\, \nu_k;\, 2\nu_k + 1;\, \frac{2r}{r + i\sqrt{2}Q}\right) \tag{3.19}$$

and

$$u_+ = (-1)^{-\nu_k + q + 1/2} u_-^*, \tag{3.20}$$

where

$$\nu_k = \frac{k}{\sqrt{2}Q}. \tag{3.21}$$

[1] We cannot only solve eqs. (3.15) and (3.16) and discard eqs. (3.12) and (3.13), because there are only two boundary conditions. After we solve u_- from the second-order equation (3.16), u_+ is fully determined by the first-order equation (3.13).

[2] Note that $(-1)^\alpha := (-1 + i\epsilon)^\alpha = e^{i\pi\alpha}$ and $(-1 - i\epsilon)^\alpha = e^{-i\pi\alpha}$.

The chemical potential $\sqrt{2}Q$ is a unit of the energy scale. To have physical bound states, Q and q must have the same sign; we assume $Q > 0$ and $q > 0$. This system has rotational invariance; we can choose $\mathbf{k} = (k, 0, 0)$, where $k > 0$. Thus we have $\nu_k > 0$, without loss of generality.

By defining $\nu_k - q + 1/2 = -n$, the solution for u_1 and u_2 is

$$u_1 = \frac{u_+ + u_-}{2} = \frac{(-1)^{n+1}u_-^* + u_-}{2} \tag{3.22}$$

$$u_2 = \frac{u_+ - u_-}{2i} = \frac{(-1)^{n+1}u_-^* - u_-}{2i}. \tag{3.23}$$

The Green's function $G_1(\omega, k)$ at $\omega = 0$ is real:

$$G_1 = \lim_{r\to\infty} \frac{u_2}{u_1} = \lim_{r\to\infty} \left(-i \frac{(-1)^{n+1}u_-^* - u_-}{(-1)^{n+1}u_-^* + u_-} \right) = G_1^*. \tag{3.24}$$

This apparently implies that the spectral density is zero at $\omega = 0$. However, we need to shift the pole at $\omega = 0$ by $\omega \to \omega + i\epsilon$, and then we will obtain a delta function in the imaginary part.[3]

The normal modes are determined by $u_1|_{r\to\infty} = 0$. In general, the hypergeometric function ${}_2F_1(\alpha, \beta; \gamma; z)$ has a branch cut from $z = 1$ to ∞. At the AdS boundary,

$$u_-|_{r\to\infty} = {}_2F_1(-n, \nu_k; 2\nu_k + 1; 2 - i\epsilon). \tag{3.25}$$

Thus, u_- and u_-^* take values at different sides of the branch cut, as shown in figure 3.1. However, if $\alpha = -n$, where $n = 0, 1, 2, \cdots$, the hypergeometric function is an nth-order polynomial of z, and the branch cut from $z = 1$ to ∞ is absent. More generally, the equation that determines the normal modes is eq. (A.37) in appendix A.2, in

[3]For example, for a free electron near k_F ($k_\perp \equiv k - k_F$):

$$\frac{1}{-\omega + v_F k_\perp - i\epsilon} = \mathcal{P}\frac{1}{-\omega + v_F k_\perp} + i\pi\delta(\omega - v_F k_\perp).$$

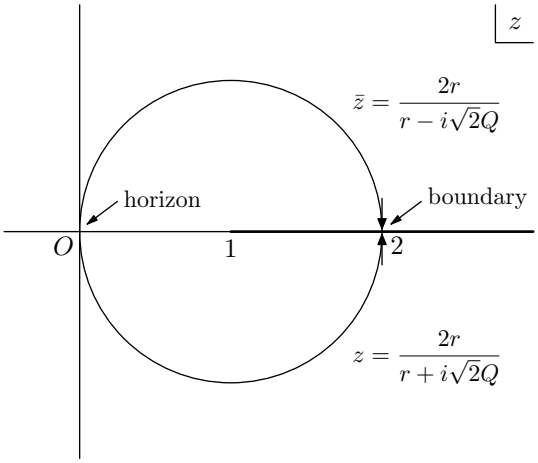

Figure 3.1: The real axis in the complex r-plane maps to a circle in the complex z-plane. The hypergeometric function $F(\alpha, \beta; \gamma; z)$ has a branch cut from $z = 1$ to ∞ in general, but the branch cut is absent when α is a non-negative integer.

which we conclude that there are no physical solutions when n is not a non-negative integer.

At the AdS boundary $r \to \infty$, $u_-^* = u_-$ if $\alpha = -n$, where $n = 0,\ 1,\ 2,\ \cdots$. Therefore, if n is even, $\nu_k^{(n)} = q - n - 1/2$ gives the Fermi surface for the standard quantization ($u_1 = 0$); if n is odd, $\nu_k^{(n)} = q - n - 1/2$ gives the Fermi surface for the alternative quantization ($u_2 = 0$). This conclusion is for the Green's function G_1, which obtained by the upper-half components of the bulk spinor. Recall that $G_2 = -1/G_1$, which is obtained by the lower-half components of the bulk spinor. In the following, we use the standard quantization only. Taking into account both G_1 and G_2, we conclude that the Fermi momenta are determined by $\nu_k^{(n)} = q - n - 1/2$, where n is a non-negative integer such that $q - n - 1/2 > 0$. Note that the alternative quantization gives the same Fermi momenta, with the difference that the boundary fermionic operator is right-handed.

By perturbation, we can obtain the analytic solution of the Green's function near the Fermi surface. The Green's function can be written as

$$G_R(\omega, k) = \frac{Z}{-\omega + v_F(k - k_F) - \Sigma(\omega, k_F)}, \tag{3.26}$$

where $k_F = |\mathbf{k}_F|$ is the Fermi momentum, v_F is the Fermi velocity, and

$$\Sigma(\omega, k) = h(k)\mathcal{G}_k(\omega), \qquad \mathcal{G}_k(\omega) = c(k)\omega^{2\nu_k}. \tag{3.27}$$

As fermionic Green's functions, G and $\mathcal{G}$ satisfy $\mathrm{Im}(G) > 0$ and $\mathrm{Im}(\mathcal{G}) > 0$ for all real ω. The result shows that $v_F > 0$, $Z > 0$, and $h > 0$. The Fermi momenta are determined by

$$\frac{k_F^{(n)}}{\sqrt{2}Q} = q - n - \frac{1}{2}, \tag{3.28}$$

where $n = 0, 1, 2, \cdots, \lfloor q - 1/2 \rfloor$. When n is even, eq. (3.26) is for G_1; when n is odd, eq. (3.26) is for G_2. Again note that we need to shift the $\omega = 0$ pole to the lower half complex ω-plane by $\omega \to \omega + i\epsilon$ to obtain a well-defined retarded Green's function.

3.3 IR geometry and Green's function

We expect that the Green's function near the Fermi surface can be obtained by the perturbation of small ω around the exact solution. However, the ordinary perturbation method is not enough when the black hole is extremal. As pointed out in ref. [22], when it is sufficiently close to the horizon, ω-dependent terms cannot be treated as small perturbations no matter how small ω is. This section and the next are in parallel with ref. [22], in which a systematic method is developed for treating the extremal black hole system. Usually this method relies on numerics to fix certain quantities, such as the Fermi velocity. The example we provide is exactly solvable, in the sense that a perturbative treatment of the small ω regime can be obtained through matched asymptotic expansions of analytically known functions.

We divide the geometry into inner and outer regions, as shown in figure 3.2. The inner region refers to the IR (near horizon) geometry, in which the Dirac equation can be exactly solved to give an IR Green's function. The outer region refers to the

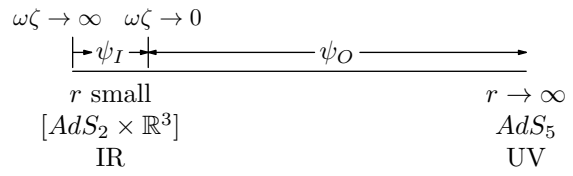

Figure 3.2: The inner (near horizon) and outer regions, where the solutions of the Dirac equation are denoted by ψ_I and ψ_O, respectively.

remaining geometry, in which we can make perturbations for small ω. Then we need to match the inner and outer regions.

The IR geometry is examined as follows. In the $r \to 0$ limit, the metric becomes

$$ds^2 = \left(\frac{r}{Q}\right)^{2/3} \left(-\frac{2r^2}{L^2}dt^2 + \frac{L^2}{2r^2}dr^2 + \frac{Q^2}{L^2}d\mathbf{x}^2\right). \tag{3.29}$$

Therefore, the IR geometry is conformal to $AdS_2 \times \mathbb{R}^3$. This can be made more explicit by change of variables

$$r = \frac{L_2^2}{\zeta}, \qquad L_2 = \frac{L}{\sqrt{2}}, \tag{3.30}$$

and the metric becomes

$$ds^2 = \left(\frac{L^2}{2Q\zeta}\right)^{2/3} \left[\frac{L_2^2}{\zeta^2}\left(-dt^2 + d\zeta^2\right) + \frac{Q^2}{L^2}d\mathbf{x}^2\right]. \tag{3.31}$$

The gauge field A_t becomes

$$\Phi = \frac{L_2^3}{Q\zeta^2}. \tag{3.32}$$

We will switch back to the r coordinate. Note that in the RN-AdS black hole system, $\Phi \sim r$, and thus the electric field $E = \nabla\Phi$ is constant at the horizon. In our system, $\Phi \sim r^2$, and thus the electric field $E = \nabla\Phi \sim r$ falls off toward the horizon. This leads to a significant difference relative to the Dirac equation in AdS_2. In the near

horizon limit $r \to 0$ ($\zeta \to \infty$), the contribution by the electric field to the Dirac equation is negligible. Nevertheless, the flux is conserved by $d(e^{4\alpha} {}^*F) = 0$.

We solve the Dirac equation in the geometry eq. (3.29) without the electric field. The solution for $u_\pm$ with in-falling boundary condition[4] is

$$u_- = C\sqrt{r}\, W_{1/2,\nu_k}(-i\omega/r) \tag{3.33}$$

$$u_+ = i\nu C\sqrt{r}\, W_{-1/2,\nu_k}(-i\omega/r), \tag{3.34}$$

where W is a Whittaker function, and C is a constant. Denote ψ_I as the solution in the inner region. In the near boundary limit of the IR geometry, the asymptotic behavior is

$$\psi_I \;\; \to \;\; \alpha \left(\frac{\omega}{r}\right)^{-\nu_k} + \beta \left(\frac{\omega}{r}\right)^{\nu_k} \qquad \text{as} \quad \frac{\omega}{r} \to 0. \tag{3.35}$$

More precisely, the inner region solution can be written as

$$\psi_I = v_+ r^{\nu_k}(1 + \cdots) + \mathcal{G}_k(\omega) v_- r^{-\nu_k}(1 + \cdots), \tag{3.36}$$

where $v_\pm$ must be chosen to match the normalization of eqs. (3.19) and (3.20). By expanding $\psi_I = (u_1, u_2)^T$ from eqs. (3.33) and (3.34), we know that $v_\pm$ take the following form

$$v_+ = \lambda_+ \begin{pmatrix} 1 \\ 1 \end{pmatrix}, \qquad v_- = \lambda_- \begin{pmatrix} -1 \\ 1 \end{pmatrix}, \tag{3.37}$$

where $\lambda_\pm$ are constants. The Green's function $\mathcal{G}_k(\omega)$ depends on the ratio λ_+/λ_-. However, the self-energy Σ is independent of $\lambda_\pm$ after matching the inner and outer

[4]The in-falling wave in terms of the coordinate ζ is $e^{i\omega\zeta}$ as $\zeta \to \infty$.

regions. We choose $\lambda_+ = \lambda_-$, and then the IR Green's function is[5]

$$\mathcal{G}_k(\omega) = e^{i\pi(1/2-\nu_k)} \frac{\Gamma(1/2-\nu_k)}{\Gamma(1/2+\nu_k)} \left(\frac{\omega}{4}\right)^{2\nu_k}. \tag{3.38}$$

The IR Green's function can be generalized to finite temperature when the back hole is near extremal:

$$\mathcal{G}_k(\omega) = i\Big(\frac{\pi T}{2}\Big)^{2\nu_k} \frac{\Gamma\big(\frac{1}{2}-\nu_k\big)\Gamma\big(\frac{1}{2}+\nu_k-\frac{i\omega}{2\pi T}\big)}{\Gamma\big(\frac{1}{2}+\nu_k\big)\Gamma\big(\frac{1}{2}-\nu_k-\frac{i\omega}{2\pi T}\big)}. \tag{3.39}$$

The main difference between the RN-AdS black hole system and our system is attributed to the IR geometry with the gauge field. In the RN-AdS_5 black hole system, the IR geometry is $AdS_2 \times \mathbb{R}^3$, and the electric field is nonzero at the horizon. The IR scaling exponent has the form $\nu_k = \sqrt{k^2 - k_o^2}$, which depends on the charge of the spinor, and will become imaginary if the charge is large. The system with this IR behavior is studied as a semi-local quantum liquid [24]. The imaginary ν_k implies an instability causing by the pair production near the black hole horizon [22, 59]. It has been argued that back-reaction from the pair production alters the IR region to a Lifshitz geometry [26]; a candidate of the final geometry was constructed as the electron star [40, 41, 27]. In our system, ν_k is always real, and the electric field approaches zero in the near horizon limit.

[5]Other ways to write down $\mathcal{G}_k(\omega)$ are

$$-ie^{-i\pi\nu}\frac{\Gamma(-2\nu)\Gamma(1+\nu)}{\Gamma(2\nu)\Gamma(1-\nu)}\omega^{2\nu}, \qquad \frac{(\tan\pi\nu+i)\pi}{\Gamma(\nu+1/2)^2}\left(\frac{\omega}{4}\right)^{2\nu}.$$

3.4 Green's function near the Fermi surface

In the outer region, the solution at small ω can be written as

$$\psi_O = \eta_+ + \mathcal{G}_k(\omega)\eta_-, \tag{3.40}$$

where

$$\eta_\pm = \eta_\pm^{(0)} + \omega\eta_\pm^{(1)} + \omega^2\eta_\pm^{(2)} + \cdots . \tag{3.41}$$

The asymptotic behavior near the horizon is

$$\eta_\pm^{(0)} = v_\pm r^{\pm\nu_k} + \cdots , \qquad r \to 0, \tag{3.42}$$

which is matched with the inner region solution, eq. (3.36). Here $\eta_+^{(0)} = (u_1, u_2)^T$, where u_1 and u_2 are solutions in the outer region as eqs. (3.22) and (3.23). We expand u_1 in the $r \to 0$ limit

$$u_1 = \frac{i^{n+1}}{\sqrt{2}(\sqrt{2}Q)^{\nu_k}} r^{\nu_k}(1 + \cdots). \tag{3.43}$$

Similarly, we can expand u_2 and the solution of $\eta_-^{(0)}$. The normalization constants $v_\pm$ are

$$v_\pm = \frac{i^{n+1}}{\sqrt{2}(\sqrt{2}Q)^{\nu_k}} \begin{pmatrix} \pm 1 \\ 1 \end{pmatrix}. \tag{3.44}$$

The asymptotic behavior near the boundary is

$$\eta_\pm^{(n)} \to a_\pm^{(n)} r^m \begin{pmatrix} 1 \\ 0 \end{pmatrix} + b_\pm^{(n)} r^{-m} \begin{pmatrix} 0 \\ 1 \end{pmatrix}, \qquad r \to \infty. \tag{3.45}$$

Consequently, the Green's function near $\omega = 0$ to the first order is [22]

$$G_R(\omega, k) = \frac{b_+^{(0)} + \omega b_+^{(1)} + \mathcal{G}_k(\omega)\big(b_-^{(0)} + \omega b_-^{(1)}\big)}{a_+^{(0)} + \omega a_+^{(1)} + \mathcal{G}_k(\omega)\big(a_-^{(0)} + \omega a_-^{(1)}\big)}. \tag{3.46}$$

We only summarize the result of the perturbation method given in appendix C of ref. [22]. Some notations are slightly changed here. Define

$$J^t = (\bar{\Psi}_0, \Gamma^t \Psi_0) = -\int_0^\infty dr \sqrt{g_{rr}(-g^{tt})}\, (\eta_+^{(0)})^\dagger \eta_+^{(0)}$$
$$J^x = (\bar{\Psi}_0, \Gamma^x \Psi_0) = \int_0^\infty dr \sqrt{g_{rr} g^{xx}}\, (\eta_+^{(0)})^\dagger \sigma_3 \eta_+^{(0)}, \tag{3.47}$$

which are integrations of hypergeometric functions in our system. Note that both J^t and J^x are negative. The various functions in the Green's function eq. (3.26) are determined as follows:

$$v_F = \frac{J^x}{J^t}, \qquad Z = -\frac{(b_+^{(0)})^2}{J^t}, \qquad h = -\frac{v_-^\dagger i\sigma^2 v_+}{J^t}, \tag{3.48}$$

where the quantities above are evaluated at $k = k_F$.

By plugging u_1 and u_2 into eq. (3.47), the integration can be evaluated for non-negative integers n. The first three results of J^t are

$$J^{t\,(0)} = -\frac{(4\nu-1)\sqrt{\pi/2}\,\Gamma(\nu-1/2)}{8Q\,\Gamma(\nu+1)}$$
$$J^{t\,(1)} = -\frac{(8\nu^2+6\nu-1)\sqrt{\pi/2}\,\Gamma(\nu-1/2)}{8(2\nu+1)^2 Q\,\Gamma(\nu+1)}$$
$$J^{t\,(2)} = -\frac{(8\nu^2+10\nu-1)\sqrt{\pi/2}\,\Gamma(\nu-1/2)}{8(2\nu+1)^2 Q\,\Gamma(\nu+2)}. \tag{3.49}$$

By induction, we find that the nth J^t is given by

$$J^{t\,(n)} = -\frac{n!\sqrt{\pi}[8\nu^2+(4n+2)\nu-1]\Gamma(\nu+1/2)\Gamma(\nu-1/2)}{2^{n+3}\sqrt{2}Q(2\nu+1)\Gamma(\nu+n/2+1/2)\Gamma(\nu+n/2+1)}, \tag{3.50}$$

where $\nu = \nu_k^{(n)}$.

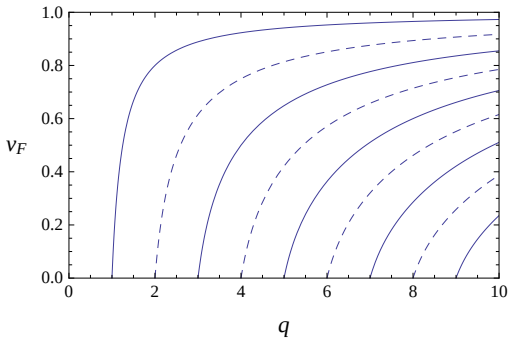

Figure 3.3: Fermi velocity as a function of charge q, where $q > n+1$ for the nth Fermi surface. The solid lines are for $n = 0, 2, \cdots$, and the dashed lines are for $n = 1, 3, \cdots$ (from left to right).

After we obtain J_x, the Fermi velocity is

$$v_F^{(n)} = \frac{2(2\nu+1)(2\nu-1)}{8\nu^2+(4n+2)\nu-1}, \tag{3.51}$$

where $\nu = \nu_k^{(n)}$. When n is even, $v_F^{(n)}$ is for G_1; when n is odd, $v_F^{(n)}$ is for G_2. If we take $\sqrt{2}Q = 1$, the only independent parameter is the charge of the spinor, in terms of which the v_F can be written as

$$v_F^{(n)} = \frac{4(q-n)(q-n-1)}{4q^2-3(2n+1)q+2n(n+1)}. \tag{3.52}$$

We can see that $0 \leq v_F < 1$, and $v_F \to 1$ as $q \to \infty$. The Fermi velocities as a function of the charge is plotted in figure 3.3.

If n is even, for the Green's function G_1,

$$Z^{(n)} = \frac{2\sqrt{2}Q\Gamma(n/2+1/2)\Gamma(\nu+n/2+1)}{\pi\Gamma(n/2+1)\Gamma(\nu+n/2+1/2)} v_F^{(n)}; \tag{3.53}$$

if n is odd, for the Green's function G_2,

$$Z^{(n)} = \frac{2\sqrt{2}Q\Gamma(n/2+1)\Gamma(\nu+n/2+1/2)}{\pi\Gamma(n/2+1/2)\Gamma(\nu+n/2+1)} v_F^{(n)}, \tag{3.54}$$

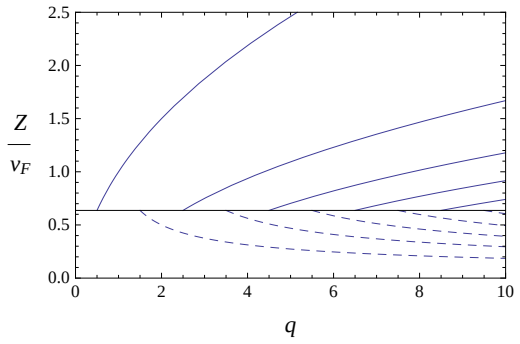

Figure 3.4: Z/v_F as a function of charge q, where $q > n + 1/2$ for the nth Fermi surface. When $q = n + 1/2$, $Z/v_F = 2/\pi$, as indicated by the horizonal line. The solid lines are for $n = 0, 2, \cdots$, and the dashed lines are for $n = 1, 3, \cdots$ (from left to right).

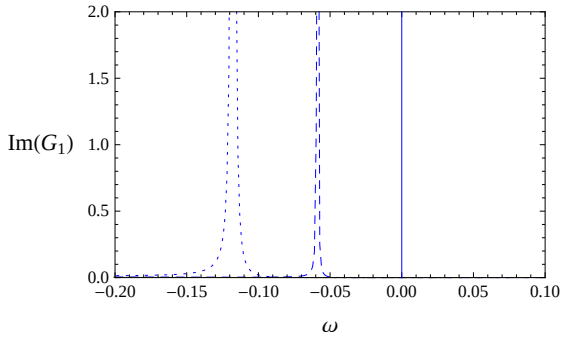

Figure 3.5: Spectral density as a function of ω at three different values of k. We plot the near $\omega = 0$ region for $q = 4.5$ and $n = 2$, which give $k_F = 2$. The dotted, dashed, and solid curves are for $k = 1.8$, 1.9, and 2, respectively. When $k = k_F$, the quasiparticle peak becomes a pole.

where $\nu = \nu_k^{(n)}$. The ratio Z/v_F as a function of charge is plotted in figure 3.4. The self-energy is given by

$$\Sigma^{(n)} = \frac{\Gamma(2\nu + n + 1)\Gamma(1/2 - \nu)e^{i\pi(1/2-\nu)}\omega^{2\nu}}{2^{6\nu-1}(\sqrt{2}Q)^{2\nu-1}\Gamma(n+1)\Gamma(\nu+1/2)^3} v_F^{(n)}, \tag{3.55}$$

where $\nu = \nu_k^{(n)}$. The spectral density $\rho = \mathrm{Im}(G)$ as a function of ω at different values of k is plotted in figure 3.5. As $k \to k_F$, the quasiparticle peak will become a delta function at $k = k_F$.

Another way to write down the Green's function is

$$G(\omega, k) = \frac{h_1}{k_\perp - \frac{1}{v_F}\omega - h_2 e^{i\gamma_{k_F}} \omega^{2\nu_{k_F}}}, \tag{3.56}$$

where $k_\perp = k - k_F$, $h_1 = Z/v_F$, $h_2 = |\Sigma/(\omega^{2\nu} v_F)|$, and

$$\gamma_k = \pi(1/2 - \nu_k) + \arg\Gamma(1/2 - \nu_k). \tag{3.57}$$

The Green's function in the form of eq. (3.56) is analyzed in ref. [22] in detail. The poles never appear in the upper half complex ω-plane of the physical sheet. The three cases $\nu_k > 1/2$, $\nu_k = 1/2$, and $\nu_k < 1/2$ correspond to Fermi liquid, marginal Fermi liquid, and non-Fermi liquid, respectively.

The Green's function for the non-Fermi liquid ($\nu_k < 1/2$) can be written as

$$G = -\frac{c_1 k_\perp^{1/2\nu_k - 1}}{\omega - c_2 k_\perp^{1/2\nu_k}}, \tag{3.58}$$

where

$$c_1 = \frac{h_1}{2\nu (h_2 e^{i\gamma_k})^{1/2\nu_k}}, \qquad c_2 = \frac{1}{(h_2 e^{i\gamma_k})^{1/2\nu_k}}. \tag{3.59}$$

The residue vanishes as $k \to k_F$. The pole ω_* moves along a line approaching the origin with the angle

$$\theta_* = \arg(\omega_*) = \begin{cases} \left(\frac{1}{2} + \frac{1}{4\nu_k}\right)\pi & k < k_F \\ \left(\frac{1}{2} - \frac{1}{4\nu_k}\right)\pi & k > k_F. \end{cases} \tag{3.60}$$

We can see that $\theta_* \notin (0, \pi)$, which is the upper half plane of the physical sheet $\theta \in (-\pi/2, 3\pi/2)$. There is a particle-hole symmetry due to $\mathrm{Im}(\omega_*)|_{k_\perp} = \mathrm{Im}(\omega_*)|_{-k_\perp}$.

What is especially interesting is the marginal Fermi liquid. In the $\nu_k \to (1/2)^+$ limit,

$$\Sigma^{(n)} = -\omega - \omega(2\ln\omega - i\pi + \tilde{c}^{(n)})\epsilon + \mathcal{O}(\epsilon^2), \tag{3.61}$$

where $\epsilon = \nu_k - 1/2$, and $\tilde{c}^{(n)}$ is a real constant. We can see that the $-\omega$ in Σ exactly cancels the $-\omega$ in the denominator of eq. (3.26), which is a delicate cancellation between the UV and the IR data. The Green's function for the marginal Fermi liquid is

$$G = \frac{h_1}{k_\perp + \frac{1}{2}(n+1)\omega\ln\omega + c^{(n)}\omega}, \tag{3.62}$$

where h_1 and $c^{(n)}$ can be easily obtained by the exact solution. The residue also vanishes as $k \to k_F$.

3.5 Green's function at arbitrary ω

To obtain the Green's function when ω is not small, we can solve the Dirac equation numerically with the boundary condition near the horizon as eqs. (3.33) and (3.34). Alternatively, we will solve the flow equation for $\xi = u_2/u_1$ as follows

$$\partial_r\xi = -\frac{2m}{\sqrt{g^{rr}}}\xi + \left(\sqrt{\tfrac{|g^{tt}|}{g^{rr}}}(\omega + qA_t) + \sqrt{\tfrac{g^{xx}}{g^{rr}}}k\right) + \left(\sqrt{\tfrac{|g^{tt}|}{g^{rr}}}(\omega + qA_t) - \sqrt{\tfrac{g^{xx}}{g^{rr}}}k\right)\xi^2, \tag{3.63}$$

with the boundary condition $\xi|_{r=0} = i$ ($\omega \neq 0$). The Green's function is obtained by $r^{2m}\xi|_{r\to\infty}$. A typical case of the spectral density $\rho = \mathrm{Im}(G)$ as a function of ω is plotted in figure 3.6, in which the peaks correspond to quasibound states.

The non-analytic features of the Green's function from the RN-AdS black hole at finite temperature are studied in detail in ref. [30]. The poles of the Green's function are schematically plotted in figure 3.7, in which we ignore a small difference that

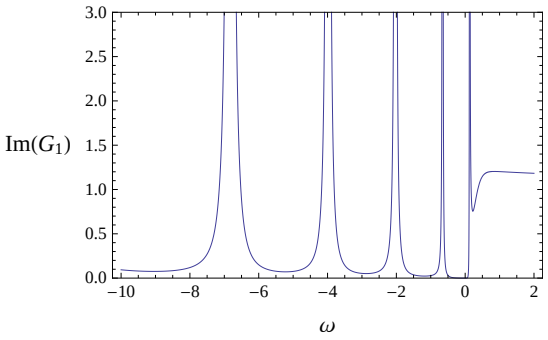

Figure 3.6: Spectral density as a function of ω at $k = 2$ with $q = 10$ and $\sqrt{2}Q = 1$. We can see five peaks for the quasibound states. As we increase k from small k, the peaks will move to the right. Each time a pole go across $\omega = 0$, we obtain a Fermi momentum. Therefore, there are five Fermi surfaces from G_1, as the formula of $k_F^{(n)}$ predicts.

the poles in the finite temperature case cannot be exactly at the origin $\omega = 0$. The RN-AdS black hole system and our system have some similar features, as follows. Consider the $m = 0$ case. There are no poles in the Green's function at $k = 0$, so we start with a small k. If the charge of the spinor q is sufficiently large, there are quasibound states. As we increase k, the poles with $\mathrm{Re}(\omega) < 0$ will move to the right. When a pole goes through the origin $\omega = 0$, we obtain a normal mode, which indicates a Fermi surface. The number of the quasibound states equals the number of the Fermi surfaces.

The schematic plots of the dispersion relation and the Fermi surface are shown in figure 3.8. Our system has at least one Fermi surface when $q > 1/2$. If we increase q, more Fermi surfaces will appear, and the Fermi surfaces are equally spaced.

The number of quasibound states can be estimated by the WKB method. The effective potential is[6]

$$V_{\text{eff}} = \frac{m^2}{g^{rr}} + \frac{g^{xx}}{g^{rr}}k^2 - \frac{|g^{tt}|}{g^{rr}}(\omega + q\Phi)^2. \tag{3.64}$$

[6]This is the leading order of the effective potential, in the sense of ref. [27]. Higher order terms contain singularities. A more rigorous WKB treatment is in ref. [30], which shows that the singularities in higher order terms are essential to the negative sign of the imaginary part of the quasinormal modes.

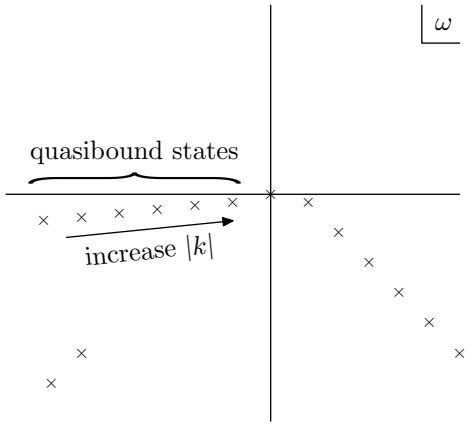

Figure 3.7: Schematic plot of the poles of the Green's function. The generic feature is that there are quasibound states when the charge of the spinor is sufficiently large. The highly damped modes are plotted from the RN-AdS black hole system.

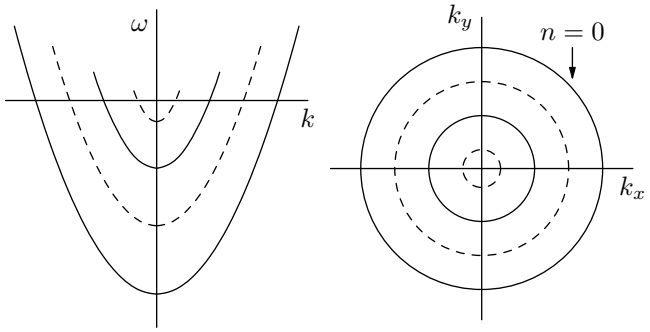

Figure 3.8: Schematic plot of dispersion relation and the Fermi surface by the massless spinor in the bulk (for massive spinor in the bulk, see ref. [30]). The system has rotational invariance, and we only show some intersections. If we decrease the charge q, the Fermi surfaces will shrink but keep the same space.

The distinctive shapes of the effective potential are plotted in figures 3.9 and 3.10. At the AdS boundary, $V_{\text{eff}} = 0$. The near horizon behavior is

$$V_{\text{eff}} \to -\frac{\omega^2}{4r^4} + \left(\frac{k^2}{2Q^2} - \frac{q\omega}{\sqrt{2}Q} - \frac{\omega^2}{4Q^2}\right)\frac{1}{r^2} + \frac{m^2}{2Q^{2/3}r^{4/3}} + \cdots . \tag{3.65}$$

We need to treat $\omega = 0$ and $\omega \neq 0$ cases separately. Assume at least one of k and m is nonzero, otherwise the Green's function has no poles.

When $\omega = 0$, the leading term in V_{eff} is positive as $r \to 0$, which implies that the state cannot tunnel to the horizon and thus is stable. This is similar to the electron

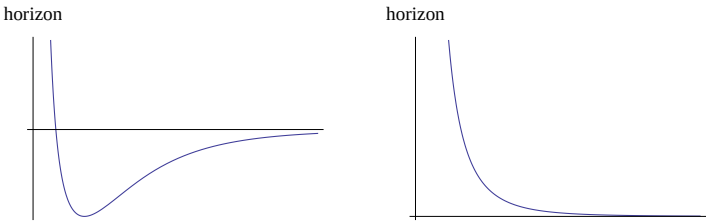

Figure 3.9: Effective potential when $\omega = 0$.

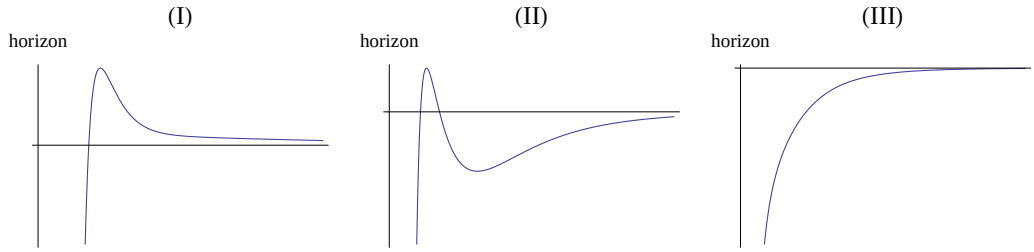

Figure 3.10: Effective potential when $\omega \neq 0$.

star, but different from the extremal RN-AdS black hole, in which there are no stable bound states when ν_k is imaginary.

When $\omega \neq 0$, the leading term in V_{eff} is negative, which implies that there are no exact bound states with $\omega \neq 0$. The state can tunnel through a barrier to the horizon, which will lead to an imaginary part of the modes. The qualitative features of the effective potential are similar to the RN-AdS black hole. If q is large enough, there is a potential well with a barrier. The quasibound states in the well can tunnel through the barrier. In figure 3.7, the modes near the real ω axis corresponds to the quasibound states.

3.6 Discussion

Starting from a dilatonic black hole derived from a consistent truncation of type IIB supergravity, we have studied the fermionic Green's function dual to massless fermions in the bulk. We obtained exact analytic results at zero frequency, and exact asymptotic results for small frequencies. These analytic results capture key features

Table 3.1: Comparison between the RN-AdS black hole system and our system, with the same UV geometry as AdS_5.

	RN-AdS black hole	two-charge black hole
Charge	$Q_1 = Q_2 = Q_3 = Q$	$Q_1 = Q_2 = Q$, $Q_3 = 0$
Entropy	$S =$ constant	$S \propto T \to 0$
IR (near horizon) geometry	$AdS_2 \times \mathbb{R}^3$	conformal to $AdS_2 \times \mathbb{R}^3$
Electric field near horizon	$E =$ constant	$E \propto r \to 0$
Stability near horizon	unstable due to pair production	stable against pair production
IR scaling exponent ν_k	$\nu_k \propto \sqrt{k^2 - k_o^2}$	$\nu_k \propto k$
$\nu_k \gtreqless 1/2$	Fermi liquid (FL), marginal FL, non-FL	

of the strongly coupled fermionic system modeled by the gauge/gravity duality, and they provide a new universality class for the strange metal phase at quantum criticality. Provided that the charge of the bulk fermion is not too small, there are Fermi surfaces. Their Fermi momenta are equally spaced, and there are a finite number of them, approximately proportional to the charge of the bulk fermion. The IR scaling dimension is always real. The properties of the RN-AdS black hole system and our system are compared and summarized in table 3.1.

There are several instabilities that can modify the bosonic background, including the superconducting and the Gregory-Laflamme instabilities; however, these instabilities all involve extra fields not present in our consistent truncation of the supergravity lagrangian, eq. (3.4).

Chapter 4

Analytic quantum critical points from holography

This chapter is a lightly edited version of ref. [60].

4.1 Introduction

Phase transitions for some strongly interacting systems can be modeled by the gauge/gravity duality [7, 9, 10]. For example, holographic superconductors have been constructed in terms of asymptotic anti-de Sitter (AdS) spaces [37, 38]. In this chapter, we consider quantum phase transitions, i.e., the phase transitions that happen at zero temperature. Understanding the quantum critical points is a significant challenge in condensed matter physics, such as non-conventional superconductors. In the gravity description, a phase transition happens when a scalar field in an AdS background develops an instability. Solving the Klein-Gordon equation for the scalar field in the bulk gives the Green's function of a scalar operator in the boundary. The critical point can be identified by the non-analyticity of the Green's function at $\omega = 0$.

Previous studies have made major conceptual progress in understanding the quantum critical points in terms of the Reissner-Nordström (RN) black hole in AdS_4 [2] (for another system, see ref. [61]; the low-energy effective field theory is also identified in ref. [62]). The extremal RN-AdS black hole has an AdS_2 factor in its near horizon (hereafter IR for infrared) geometry [22]. This AdS_2 factor plays an essential role in the properties of the system, and defines a universal intermediate energy phase [24, 63]. The behavior of the system near the quantum critical point is encoded in the Green's function near $\omega = 0$, which contains both UV and IR data. The UV data can be solved from the Klein-Gordon equation at $\omega = 0$ in the bulk, and the IR data can be analytically solved from the Klein-Gordon equation at arbitrary ω in AdS_2 [2, 22]. The zero mode, which triggers the onset of the instability of the system, belongs to the UV data, and relies on numerical calculations in AdS_4.

We find that if we use AdS_5 instead, the Klein-Gordon equation at $\omega = 0$ can be analytically solved; the Green's function captures essential features of the RN-AdS system. We consider the standard/alternative quantization first. For a scalar field with mass m and charge q, the zero modes are solved as

$$\nu_k = \frac{q}{\sqrt{3}} - n_\pm - \frac{\Delta_\pm - 1}{2}, \tag{4.1}$$

where $n_\pm$ is a nonnegative integer, $\Delta_\pm$ is the scaling dimension of the boundary operator, and ν_k is the IR scaling exponent:

$$\Delta_\pm := 2 \pm \sqrt{m^2 + 4}, \tag{4.2}$$

$$\nu_k := \frac{1}{2\sqrt{3}} \sqrt{m^2 + k^2 - 2q^2 + 3}. \tag{4.3}$$

The zero modes are always at nonzero $\mathbf{k}$, and the $n_\pm = 0$ mode triggers the onset of the instability. The instabilities and the corresponding quantum critical points are

classified as follows (the name and interpretation of the quantum critical points are from ref. [2]):

- The first type of instability is triggered by a zero mode, which exists only if q is large enough. This instability gives a hybridized critical point, which is described by an order parameter in a Ginzburg-Landau sector hybridized with a strongly coupled sector, the CFT_1 dual to the IR AdS_2.

- The second type of instability happens when the IR scaling exponent ν_k becomes imaginary, which implies the instability of the IR geometry. This instability gives a bifurcating critical point, for which the Green's function bifurcates into the complex plane.

- The two types of instability can happen at the same time, and give a mixed critical point, such as a marginal critical point, which is described by a marginal term.

We then study the quantum critical points at $\omega = 0$ and $\mathbf{k} = 0$. Without introducing an extra parameter, we can only have a bifurcating critical point. We can tune the superfluid velocity to reach all three quantum critical points. The phase diagram can be analytically obtained for the onset of the instability from the normal phase.

Instead of the superfluid velocity, the zero mode can also be obtained by tuning another parameter κ_+, the coefficient of a double trace deformation in the CFT, giving a hybridized critical point [2, 64]. The analytic result allows us to draw the phase diagram for arbitrarily large m^2, where the numerical result is difficult to achieve. The Green's function (or susceptibility) for various critical points can be obtained.

This chapter is organized as follows. In section 4.2, we give the general solution of the Klein-Gordon equation at $\omega = 0$, and the Green's function near $\omega = 0$. In section 4.3, we classify the instabilities according to the parameters m^2 and q, and give the critical values of the superfluid velocity. In section 4.4, we consider the parameter

of the double trace deformation, and draw the phase diagram. In section 4.5, we conclude with some discussion.

4.2 Solution for the Klein-Gordon equation

The extremal RN-AdS_5 black hole in Poincaré coordinates is[1]

$$ds^2 = \frac{1}{z^2}\left(-f(z)dt^2 + d\mathbf{x}^2 + \frac{dz^2}{f(z)}\right), \tag{4.4}$$

$$f = 1 - 3z^4 + 2z^6, \qquad A_t = \sqrt{6}\,(1 - z^2), \tag{4.5}$$

where $\mathbf{x} = (x_1, x_2, x_3)$, and the gauge potential is $A = A_t dt$. We set the AdS radius $L = 1$, and the horizon is at $z_h = 1$.

To obtain the Green's function for a scalar operator in the dual CFT, we will solve the Klein-Gordon equation for a scalar field Φ. After the Fourier transform

$$\Phi(z, x^\mu) = \int \frac{d\omega d^3\mathbf{k}}{(2\pi)^4} e^{-i\omega t + i\mathbf{k}\cdot\mathbf{x}} \phi(z), \tag{4.6}$$

the equation of motion for ϕ is

$$\phi'' + \left(\frac{f'}{f} - \frac{3}{z}\right)\phi' + \left(\frac{(\omega + qA_t)^2}{f^2} - \frac{k^2}{f} - \frac{m^2}{z^2 f}\right)\phi = 0, \tag{4.7}$$

where we assume $\mathbf{k} = (k, 0, 0)$ without loss of generality, $q > 0$, and m^2 is above the Breitenlohner-Freedman (BF) bound [13]: $m^2 \geq m^2_{\rm BF} = -4$. The horizon $z = 1$ is an irregular singularity for this equation. The in-falling boundary condition near the horizon $z = 1$ is

$$\phi \sim W_{-\frac{iq}{\sqrt{6}},\nu_k}\Big(-\frac{i\omega}{6(1-z)}\Big), \tag{4.8}$$

[1]The action is $S = \int d^5x\sqrt{-g}\,(R - 12 - \frac{1}{4}F^2)$.

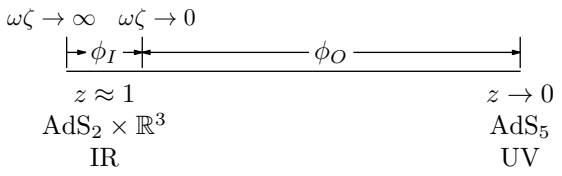

Figure 4.1: The inner (near horizon) and outer regions, where the solutions of the Klein-Gordon equation are denoted by ϕ_I and ϕ_O, respectively.

where $W_{\lambda,\mu}(z)$ is a Whittaker function. The asymptotic behavior near the AdS boundary is[2]

$$\phi = Az^{\Delta_-}(1 + \cdots) + Bz^{\Delta_+}(1 + \cdots). \tag{4.9}$$

The retarded Green's function is[3]

$$G = \frac{B}{A}. \tag{4.10}$$

When $-4 \leq m^2 \leq -3$, there is an alternative quantization, by which the Green's function is $G = A/B$ [14].

To study the instability near a quantum critical point, we need to solve the Green's function near $\omega = 0$. When it is sufficiently close to the extremal horizon, ω-dependent terms cannot be treated as small perturbations no matter how small ω is. In ref. [22], a systematic method is developed for treating the extremal black hole system. We divide the geometry into inner and outer regions, as shown in figure 4.1. The inner region refers to the IR (near horizon) geometry, in which the Klein-Gordon equation can be exactly solved as eq. (4.8). The outer region refers to the remaining geometry, in which we can make perturbations for small ω. Then we need to match the inner and outer regions.

[2]When $\Delta_+ - \Delta_- = 2n$, where $n = 1, 2, \cdots$, there are extra terms $bz^{\Delta_+} \ln z\,(1 + \cdots)$. When $\Delta_+ = \Delta_-$, $\phi = Az^2 \ln z + Bz^2 + \cdots$.

[3]We use the same normalization as in ref. [2]. By another normalization, the Green's function is $G = (2\Delta_+ - 4)B/A$.

In the inner region, the IR Green's function $\mathcal{G}_k(\omega)$ is solved as eq. (A.61) (see appendix A.4) [22]. In the outer region, the solution at small ω can be written as

$$\phi(z) = \eta_+(z) + \mathcal{G}_k(\omega)\eta_-(z), \tag{4.11}$$

where

$$\eta_\pm = \eta_\pm^{(0)} + \omega\eta_\pm^{(1)} + \mathcal{O}(\omega^2). \tag{4.12}$$

At the leading order, the asymptotic behavior near the horizon $z = 1$ is

$$\eta_\pm^{(0)} \to [12(1-z)]^{-1/2\pm\nu_k}, \tag{4.13}$$

which we also use to fix the normalization of the solution. The asymptotic behavior near the AdS boundary $z = 0$ is

$$\eta_\pm^{(0)} \to a_\pm^{(0)} z^{\Delta_-} + b_\pm^{(0)} z^{\Delta_+}. \tag{4.14}$$

The Green's function to the first order in ω is [22]

$$G(\omega, k) = \frac{b_+^{(0)} + \omega b_+^{(1)} + \mathcal{G}_k(\omega)\left(b_-^{(0)} + \omega b_-^{(1)}\right)}{a_+^{(0)} + \omega a_+^{(1)} + \mathcal{G}_k(\omega)\left(a_-^{(0)} + \omega a_-^{(1)}\right)}. \tag{4.15}$$

Note that if we consider a neutral scalar, the first order terms in ω are zero, and then we need to expand to the second order. The analytic solution of ϕ at $\omega = 0$ below gives the leading order of the Green's function. By perturbation around $\omega = 0$, we can obtain the higher-order coefficients. The Green's function can be generalized to nonzero temperature when $T << \mu$ (chemical potential) by replacing the IR Green's function $\mathcal{G}_k(\omega)$ with eq. (A.62) in appendix A.4. The results we just described can be found in ref. [22]. We now go beyond ref. [22] and obtain analytic solutions for $a_\pm^{(0)}$ and $b_\pm^{(0)}$.

When $\omega = 0$, we can solve ϕ in terms of hypergeometric equations. The general solution of ϕ for eq. (4.7) at $\omega = 0$ is[4]

$$\begin{aligned}\phi(z) =& C_1 z^{\Delta_-} \frac{(1-z^2)^{-1/2+\nu_k}}{(2z^2+1)^{-1/2+\nu_k+\Delta_-/2}}\, {}_2F_1\Big(\frac{\Delta_- - 1}{2} + \nu_k - \frac{q}{\sqrt{3}}, \frac{\Delta_- - 1}{2} + \nu_k + \frac{q}{\sqrt{3}}; \Delta_- - 1; \frac{3z^2}{2z^2+1}\Big) \\ &+ C_2 z^{\Delta_+} \frac{(1-z^2)^{-1/2+\nu_k}}{(2z^2+1)^{-1/2+\nu_k+\Delta_+/2}}\, {}_2F_1\Big(\frac{\Delta_+ - 1}{2} + \nu_k - \frac{q}{\sqrt{3}}, \frac{\Delta_+ - 1}{2} + \nu_k + \frac{q}{\sqrt{3}}; \Delta_+ - 1; \frac{3z^2}{2z^2+1}\Big). \end{aligned} \tag{4.16}$$

The asymptotic behavior near the horizon $z \to 1$ is

$$\begin{aligned}\phi \to& \Big[\frac{2}{3}(1-z)\Big]^{-1/2+\nu_k} \left(\frac{C_1\, 3^{-\Delta_-/2}\Gamma(\Delta_- - 1)\Gamma(-2\nu_k)}{\Gamma(\frac{\Delta_- -1}{2} - \nu_k + \frac{\sqrt{3}}{3}q)\Gamma(\frac{\Delta_- -1}{2} - \nu_k - \frac{q}{\sqrt{3}})} + \frac{C_2\, 3^{-\Delta_+/2}\Gamma(\Delta_+ - 1)\Gamma(-2\nu_k)}{\Gamma(\frac{\Delta_+ -1}{2} - \nu_k + \frac{q}{\sqrt{3}})\Gamma(\frac{\Delta_+ -1}{2} - \nu_k - \frac{q}{\sqrt{3}})} \right) \\ &+ \Big[\frac{2}{3}(1-z)\Big]^{-1/2-\nu_k} \left(\frac{C_1\, 3^{-\Delta_-/2}\Gamma(\Delta_- - 1)\Gamma(2\nu_k)}{\Gamma(\frac{\Delta_- -1}{2} + \nu_k + \frac{q}{\sqrt{3}})\Gamma(\frac{\Delta_- -1}{2} + \nu_k - \frac{q}{\sqrt{3}})} + \frac{C_2\, 3^{-\Delta_+/2}\Gamma(\Delta_+ - 1)\Gamma(2\nu_k)}{\Gamma(\frac{\Delta_+ -1}{2} + \nu_k + \frac{q}{\sqrt{3}})\Gamma(\frac{\Delta_+ -1}{2} + \nu_k - \frac{q}{\sqrt{3}})} \right). \end{aligned} \tag{4.17}$$

The asymptotic behavior near the boundary $z \to 0$ is

$$\phi \to C_1 z^{\Delta_-} + C_2 z^{\Delta_+}. \tag{4.18}$$

By eqs. (4.13) and (4.14), the solutions of $a_\pm^{(0)}$ and $b_\pm^{(0)}$ are

$$\begin{aligned}&\begin{pmatrix} a_+^{(0)} & a_-^{(0)} \\ b_+^{(0)} & b_-^{(0)} \end{pmatrix} \\ &= \frac{\nu_k}{\sqrt{m^2+4}} \begin{pmatrix} \frac{18^{1/2+\nu_k}\cdot 3^{-\Delta_+/2}\Gamma(\Delta_+ - 1)\Gamma(2\nu_k)}{\Gamma(\frac{\Delta_+ -1}{2} + \nu_k + \frac{q}{\sqrt{3}})\Gamma(\frac{\Delta_+ -1}{2} + \nu_k - \frac{q}{\sqrt{3}})} & \frac{-18^{1/2-\nu_k}\cdot 3^{-\Delta_+/2}\Gamma(\Delta_+ - 1)\Gamma(-2\nu_k)}{\Gamma(\frac{\Delta_+ -1}{2} - \nu_k + \frac{q}{\sqrt{3}})\Gamma(\frac{\Delta_+ -1}{2} - \nu_k - \frac{q}{\sqrt{3}})} \\ \frac{-18^{1/2+\nu_k}\cdot 3^{-\Delta_-/2}\Gamma(\Delta_- - 1)\Gamma(2\nu_k)}{\Gamma(\frac{\Delta_- -1}{2} + \nu_k + \frac{q}{\sqrt{3}})\Gamma(\frac{\Delta_- -1}{2} + \nu_k - \frac{q}{\sqrt{3}})} & \frac{18^{1/2-\nu_k}\cdot 3^{-\Delta_-/2}\Gamma(\Delta_- - 1)\Gamma(-2\nu_k)}{\Gamma(\frac{\Delta_- -1}{2} - \nu_k + \frac{q}{\sqrt{3}})\Gamma(\frac{\Delta_- -1}{2} - \nu_k - \frac{q}{\sqrt{3}})} \end{pmatrix}. \end{aligned} \tag{4.19}$$

It can be checked that $a_+^{(0)} b_-^{(0)} - a_-^{(0)} b_+^{(0)} = \nu_k/\sqrt{m^2+4}$ is satisfied.

[4]When Δ_+ is an integer, the two hypergeometric functions in eq. (4.16) are linearly dependent. We can choose another two linearly independent solutions as eq. (A.47) in appendix A.3.

4.3 Analytic Green's functions

4.3.1 Zero modes and the phase diagram

The zero mode is a gapless mode in the Green's function at $\omega = 0$. The singularity of a fermionic Green's function at $\omega = 0$ indicates a Fermi surface, while the singularity of a bosonic Green's function at $\omega = 0$ indicates instability. In the fermionic case, solving $G^{-1}(\omega = 0, \mathbf{k}) = 0$ gives $\mathbf{k} = \mathbf{k}_F$, where $\mathbf{k}_F$ is the Fermi momentum. Similarly, in the bosonic case, solving $G^{-1}(\omega = 0, \mathbf{k}) = 0$ gives the $\mathbf{k} = \mathbf{k}_S$, where we use the subscript S for superfluid. The analytic solution enables us to solve for the zero modes, which are the only normal modes.

The zero modes are determined by $a_+^{(0)} = 0$ for the standard quantization, and $b_+^{(0)} = 0$ for the alternative quantization. By eq. (4.19), we have

$$\frac{\Delta_\pm - 1}{2} + \nu_k - \frac{q}{\sqrt{3}} = -n_\pm, \tag{4.20}$$

where $n_\pm$ is a nonnegative integer, the "+" sign is for the standard quantization, and the "−" sign is for the alternative quantization. Although the above result is derived under the assumption that Δ_+ is not an integer, eq. (4.20) is generally valid when $m^2 \geq -4$ for the standard quantization, and when $-4 < m^2 < -3$ for the alternative quantization (see appendix A.3). The solution of k is denoted by k_S. The existence of a real k_S requires $\nu_k \geq 0$, which implies

$$\frac{q}{\sqrt{3}} \geq n_\pm + \frac{\Delta_\pm - 1}{2}. \tag{4.21}$$

The first type of instability is initiated by the nodeless zero mode, $n_\pm = 0$. We set $n_\pm = 0$ in the following. Solving k from eq. (4.20) gives

$$\begin{aligned} k_S^2 &= 12\Big(\frac{q}{\sqrt{3}} - \frac{1 \pm \sqrt{m^2+4}}{2}\Big)^2 + 2q^2 - m^2 - 3 \\ &= 6\Big[q - \frac{\sqrt{3}}{3}(1 \pm \sqrt{m^2+4})\Big]^2 + 2(1 \pm \sqrt{m^2+4}), \end{aligned} \tag{4.22}$$

where

$$q \geq \frac{\sqrt{3}}{2}(1 \pm \sqrt{m^2+4}). \tag{4.23}$$

For the standard quantization, k_S is always nonzero. For the alternative quantization, k_S is nonzero except for a special case: $m^2 = -3$ and $q = 0$, in which, however, eq. (4.16) is not valid and the solution of ϕ by eq. (4.44) below shows that $k = 0$ is not a zero mode. Moreover, k_S is always nonzero for all $n_\pm \geq 0$.

If eq. (4.23) is not satisfied, i.e., the zero mode does not exist, there can still be the second type of instability when ν_k is imaginary. The critical value of k is

$$k_{\rm IR}^2 = 2q^2 - m^2 - 3, \tag{4.24}$$

where

$$q^2 > \frac{m^2+3}{2}. \tag{4.25}$$

As explained in ref. [22], this instability is due to the backreaction of pair production in the IR geometry for a charged scalar, or the mass below the AdS_2 BF bound for a neutral scalar; the parameter set for which ν_k is imaginary is called the oscillatory region. The imaginary IR scaling dimension $\delta_k = 1/2 + \nu_k$ implies the conformality lost after the annihilation of two fixed points of the CFT dual to the AdS_2, leading to an instability of the IR geometry [65, 66].

Table 4.1: The critical value of the superfluid velocity ($\pm$ is for the standard and alternative quantization, respectively).

m^2	q	Superfluid velocity S_x
$-4 \le m^2 \le -3$ [a]	$0 \le q \le \frac{\sqrt{3}}{2}(1 \pm \sqrt{m^2+4})$	IR geometry instability at $S_x = k_{\rm IR}/q$
	$q \ge \frac{\sqrt{3}}{2}(1 \pm \sqrt{m^2+4})$	Zero mode instability at $S_x = k_S/q$
$m^2 > -3$	$0 \le q < \sqrt{\frac{m^2+3}{2}}$	No instability
	$\sqrt{\frac{m^2+3}{2}} \le q \le \frac{\sqrt{3}}{2}(1 + \sqrt{m^2+4})$	IR geometry instability at $S_x = k_{\rm IR}/q$
	$q \ge \frac{\sqrt{3}}{2}(1 + \sqrt{m^2+4})$	Zero mode instability at $S_x = k_S/q$

[a] For the alternative quantization, the $m^2 = -4$ and -3 cases are not included.

When a zero mode exists, there is always the second type of instability for $k < k_{\rm IR}$, by comparing eqs. (4.23) and (4.25):

$$\sqrt{\frac{m^2+3}{2}} < \frac{\sqrt{3}}{2}(1 \pm \sqrt{m^2+4}), \tag{4.26}$$

and $k_{\rm IR} \le k_S$, by comparing eqs. (4.22) and (4.24). The solution of k as a function of m^2 and q is illustrated in figures 4.2 and 4.3. The blue lines are solutions of k_S from eq. (4.20); the outermost one is $n = 0$. The boundary of the shaded region is the solution of $k_{\rm IR}$ from eq. (4.24).

By perturbation around the solution at $\omega = 0$, we can obtain the retarded Green's function near the zero mode

$$G = \frac{h_1}{k_\perp - \frac{1}{v_S}\omega - h_2 e^{i\gamma_{k_S}} \omega^{2\nu_{k_S}}}, \tag{4.27}$$

where $k_\perp = k - k_S$, and the quantities v_S, h_1, and h_2 can be calculated by the formulas given in appendix C of ref. [22]. As explained in ref. [22], when the momentum changes from $k > k_S$ to $k < k_S$, a pole of the Green's function moves across the origin to the upper half complex ω-plane, signaling an instability. As a comparison, analytic

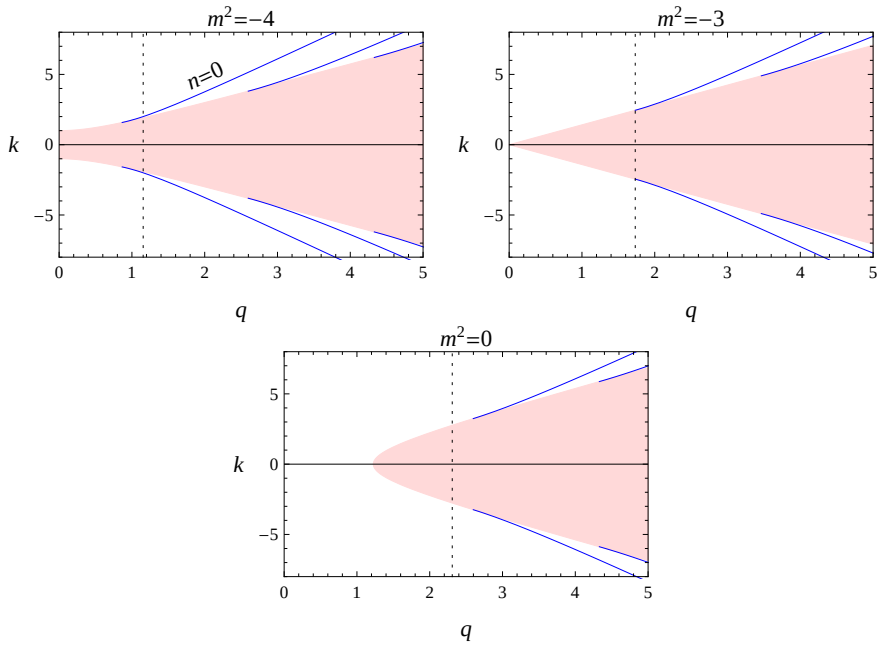

Figure 4.2: Phase diagram for the standard quantization. The solid lines correspond to zero modes. The oscillatory region is shaded, and will move to the right as we increase m^2. In the right plot, the tip of the oscillatory region corresponds to a bifurcating critical point at $k = 0$. The dotted line is the BPS bound for $q \leq \Delta_+/\sqrt{3}$, where q is the R-charge [67, 68].

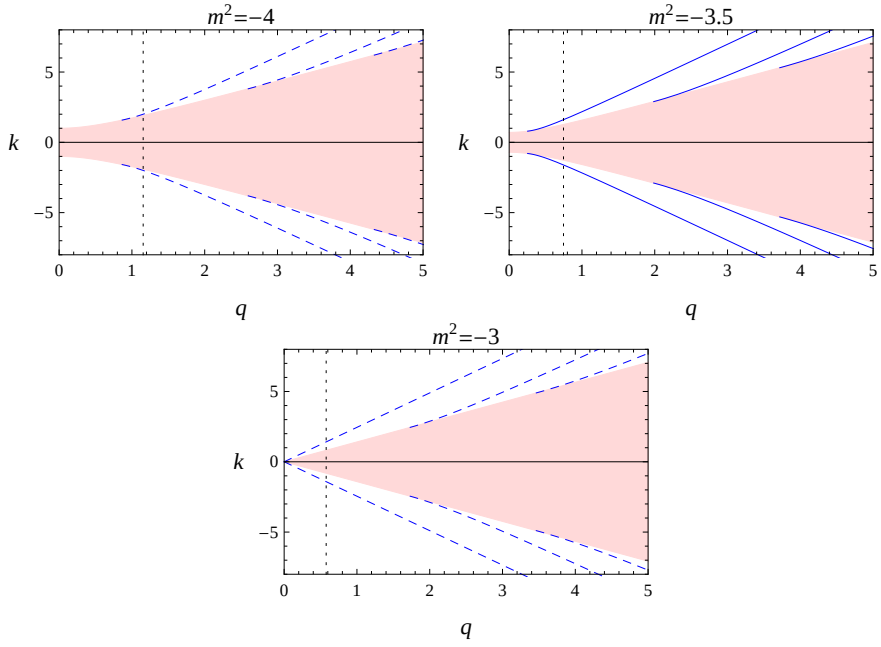

Figure 4.3: Phase diagram for the alternative quantization. The oscillatory region is shaded. The dashed lines are solutions to eq. (4.20), but do not represent zero modes. The dotted line is the BPS bound for $q \leq \Delta_-/\sqrt{3}$.

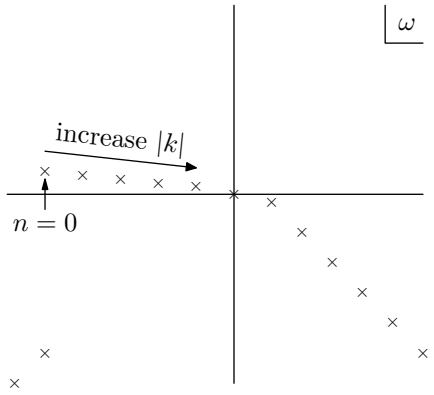

Figure 4.4: Schematic plot of the poles of the Green's function when q is large.

fermionic Green's functions can be obtained for a massless spinor in the background of the two-charge black hole in AdS_5; the Fermi momenta are $k_F = q - n - 1/2$ (in units of the chemical potential), where q is the charge of the spinor, and n labels the Fermi surface [55]. The RN-AdS black hole background is more complicated due to the extra feature of the oscillatory region.

It is helpful to understand the normal modes by looking at the poles of the Green's function at arbitrary ω. The numerical calculations suggest the following features, as illustrated in figure 4.4. At $q = 0$ and $k = 0$, all the poles of the Green's function are in the lower half ω-plane, and not close to $\omega = 0$. As we increase the charge q, there are more and more poles moving across the origin to the upper half ω-plane, and the first one is labeled by $n = 0$. Suppose we start from a large q. As we increase k, the poles will move to the right, across the origin to the lower half ω-plane. Therefore, the largest k corresponds to the $n = 0$ mode, which triggers the onset of the instability. The situation is similar to the fermionic case with a crucial difference that the quasibound states in the upper half plane in figure 4.4 are now in the lower half plane [30].

According to ref. [2], we can associate the first type of instability with the hybridized critical point, and the second type of instability with the bifurcating critical point. Recall that the system has rotational symmetry. In the fermionic case, a

nonzero k_F gives a spherical Fermi surface. However, in the bosonic case, the condensation of the scalar cannot happen at a spherical shell of the momentum space. Instead, the quantum phase transition happens at $\omega = 0$ and $k = 0$. Without tuning extra parameters, only the second type of instability can happen. By tuning an extra parameter, both types of instability can happen at $k = 0$.

4.3.2 Bifurcating critical point

When the IR scaling exponent ν_k at $k = 0$ becomes imaginary, there is a bifurcating critical point [2]. We will denote $\nu := \nu_{k=0} = \frac{1}{2\sqrt{3}}\sqrt{u}$, where $u = m^2 - 2q^2 + 3$. From $u > 0$ to $u < 0$, the Green's function at $\omega = 0$ keeps finite, but bifurcates into the complex plane and has a cusp [2].

Near $\nu_k = 0$, the quantities $a_\pm^{(0)}$ and $b_\pm^{(0)}$ in the Green's function can be expanded as

$$\begin{aligned} a_\pm^{(0)} &= \alpha \pm \nu_k \tilde{\alpha} + \cdots , \\ b_\pm^{(0)} &= \beta \pm \nu_k \tilde{\beta} + \cdots . \end{aligned} \tag{4.28}$$

By eq. (4.19), we have

$$\begin{aligned} \alpha &= \frac{3^{1-\Delta_+/2}\Gamma(\Delta_+ - 1)}{\sqrt{2(m^2+4)}\,\Gamma\left(\frac{\Delta_+ - 1}{2} + \frac{q}{\sqrt{3}}\right)\Gamma\left(\frac{\Delta_+ - 1}{2} - \frac{q}{\sqrt{3}}\right)} \\ \tilde{\alpha} &= -\frac{\Gamma(\Delta_+ - 1)\left(\psi\left(\frac{\Delta_+ - 1}{2} + \frac{q}{\sqrt{3}}\right) + \psi\left(\frac{\Delta_+ - 1}{2} - \frac{q}{\sqrt{3}}\right) + 2\gamma - \ln 18\right)}{\sqrt{2(m^2+4)}\,3^{-1+\Delta_+/2}\Gamma\left(\frac{\Delta_+ - 1}{2} + \frac{q}{\sqrt{3}}\right)\Gamma\left(\frac{\Delta_+ - 1}{2} - \frac{q}{\sqrt{3}}\right)} \\ \beta &= -\frac{3^{1-\Delta_-/2}\Gamma(\Delta_- - 1)}{\sqrt{2(m^2+4)}\,\Gamma\left(\frac{\Delta_- - 1}{2} + \frac{q}{\sqrt{3}}\right)\Gamma\left(\frac{\Delta_- - 1}{2} - \frac{q}{\sqrt{3}}\right)} \\ \tilde{\beta} &= \frac{\Gamma(\Delta_- - 1)\left(\psi\left(\frac{\Delta_- - 1}{2} + \frac{q}{\sqrt{3}}\right) + \psi\left(\frac{\Delta_- - 1}{2} - \frac{q}{\sqrt{3}}\right) + 2\gamma - \ln 18\right)}{\sqrt{2(m^2+4)}\,3^{-1+\Delta_-/2}\Gamma\left(\frac{\Delta_- - 1}{2} + \frac{q}{\sqrt{3}}\right)\Gamma\left(\frac{\Delta_- - 1}{2} - \frac{q}{\sqrt{3}}\right)}, \end{aligned} \tag{4.29}$$

where $\psi(x) := \Gamma'(x)/\Gamma(x)$ is the digamma function, and γ is the Euler-Mascheroni constant. It can be checked that $\alpha\tilde{\beta} - \beta\tilde{\alpha} = -1/(2\sqrt{m^2+4})$ is satisfied.

Near the bifurcating critical point $\nu \to 0$, the IR Green's function can be written as

$$\mathcal{G}_{k=0}(\omega) = -1 + 2\nu\mathcal{G}_0(\omega), \tag{4.30}$$

where $\mathcal{G}_0(\omega)$ is the IR Green's function when $\nu = 0$, which can be obtained by eq. (4.8) with $\nu_k = 0$:

$$\mathcal{G}_0(\omega) = -\ln(-2i\omega) - 2\gamma - \psi\Big(\frac{1}{2} - \frac{iq}{\sqrt{6}}\Big). \tag{4.31}$$

Particularly, for a neutral scalar,

$$\mathcal{G}_0(\omega) = -\ln\Big(-\frac{i\omega}{2}\Big) - \gamma. \tag{4.32}$$

By expanding the Green's function, eq. (4.15), at small ν, we obtain the Green's function for the bifurcating critical point:

$$G = \frac{\beta\,\mathcal{G}_0(\omega) + \tilde{\beta}}{\alpha\,\mathcal{G}_0(\omega) + \tilde{\alpha}}. \tag{4.33}$$

The finite temperature generalization of $\mathcal{G}_0(\omega)$ is given by eqs. (A.64) and (A.65) in appendix A.4.

Note that eq. (4.33) is obtained by taking the $\nu \to 0$ limit at fixed ω. If we want to examine the poles of the Green's function, we need a Green's function valid to arbitrarily small ω. To do so, we need to use $\mathcal{G}_{k=0}(\omega)$ instead of $\mathcal{G}_0(\omega)$. In the condensed side ($u < 0$), there are infinite number of poles in the upper half ω-plane; these massive states will condense and lead to instability [2].

4.3.3 Critical points with superfluid velocity

A superfluid with a supercurrent flow can be studied holographically by turning on a vector potential

$$A_x = S_x + J^x z^2 + \cdots, \tag{4.34}$$

where S_x is the superfluid velocity, which is the source, and J^x is the supercurrent, which is the expectation value [69, 35, 70, 71, 72]. The Klein-Gordon equation for a scalar ϕ coupled with both A_t and A_x at $\omega = 0$ and $k = 0$ is

$$\phi'' + \left(\frac{f'}{f} - \frac{3}{z}\right)\phi' + \left(\frac{q^2 A_t^2}{f^2} - \frac{q^2 A_x^2}{f} - \frac{m^2}{z^2 f}\right)\phi = 0. \tag{4.35}$$

When the superfluid velocity is too large, the superfluid phase will return to the normal phase. At the critical point, $A_x = S_x$ is a constant. From eq. (4.35), we can see that the superfluid velocity plays the same role as the momentum k,[5] which is consistent with the fact that the superfluid velocity is the gradient of the phase of the order parameter. The phase diagrams are figures 4.2 and 4.3 by replacing k with qS_x.

According to previous studies of holographic superconductors, there are two mechanisms for instabilities: (1) When the charge of the scalar is large, the effective mass $m_{\text{eff}}^2 = m^2 + g^{tt}q^2A_t^2$ is negative enough to produce an unstable mode [36, 37]. (2) When it is close to the zero temperature, and the effective mass $m_{\text{eff}}^2 = (m^2 - 2q^2)/12$ is below the AdS_2 BF bound $m_{\text{BF}}^2 = -1/4$, the IR geometry is unstable [38, 22, 75]. Here the quantum critical point can be reached by tuning the superfluid velocity, and the above two mechanisms for instabilities correspond to the two types of instabilities we discussed before: zero mode instability and IR geometry instability, respectively. They can happen at the same time, giving a mixed critical point, as shown in figures 4.2 and 4.3, when a solid line touches the oscillatory region.

We call the stable region (k or $qS_x > \max(k_S, k_{\text{IR}})$) the normal phase, and we call the unstable region the superfluid phase. When the mass is small ($-4 \leq m^2 \leq -3$), there are two cases: (i) For small charge, the scalar is unstable due to the second

[5]We reinterpret k as the superfluid velocity (in the x-direction). Another way to reinterpret k is the magnetic field added by $A_y = Bx$, assuming that the metric is not changed. After a separation of variables $\Phi \sim X(x)\phi(z)$, the magnetic filed plays the same role as k^2 ($qB \leftrightarrow k^2$) in the equation for ϕ [73, 38]. In terms of a dyonic black hole in AdS_4, the quantum critical point by the second type of instability is studied in ref. [74].

type of instability; (ii) For large charge, the scalar is unstable due to the first type of instability. When the mass is large ($m^2 > -3$), there are three cases: (i) For small charge, the scalar is stable; (ii) For intermediate charge, the scalar is unstable due to second type of instability; (iii) For large charge, the scalar is unstable due to the first type of instability. The result is summarized in table 4.1.

4.4 Adding a double trace deformation

4.4.1 Hybridized critical point

Without the superfluid velocity, the zero mode at $k = 0$ can also be achieved by tuning another parameter κ_+, which describes a double trace deformation in the boundary CFT:

$$\frac{\kappa_+}{2} \int d^d x \, \mathcal{O}^2, \tag{4.36}$$

where $\langle \mathcal{O} \rangle = B$ [2, 76]. The Green's function becomes

$$G^{(\kappa_+)} = \frac{1}{G^{-1} + \kappa_+}. \tag{4.37}$$

Similarly, starting from the alternative quantization, we can add a double trace deformation with coefficient κ_-, which is related to κ_+ by $\kappa_- = -1/\kappa_+$. The alternative quantization is allowed only if the m^2 of the scalar is in the interval $m^2_{\mathrm{BF}} \leq m^2 \leq m^2_{\mathrm{BF}} + 1$ [14], which leads to a slight difference between AdS_4 and AdS_5 as illustrated in figure 4.5. Since we are interested in the instability triggered by a zero mode at $k = 0$, we do not want other instabilities to exist. Therefore, we require $u > 0$, i.e., the parameters are not in the oscillatory region, in which the system is already unstable. In AdS_4, if we start from the alternative quantization, there is still

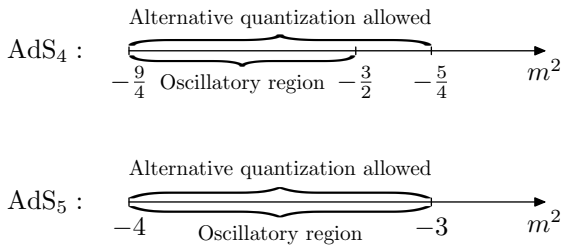

Figure 4.5: A slight difference between AdS_4 and AdS_5. We set the AdS radius $L = 1$. In AdS_5, we can only start from the standard quantization.

an interval of m^2 not in the oscillatory region. In AdS_5, however, we can only start from the standard quantization.[6]

The Green's function at the leading order in ω is

$$G(\omega, k) = \frac{b_+^{(0)} + \mathcal{G}_k(\omega) b_-^{(0)}}{a_+^{(0)} + \kappa_+ b_+^{(0)} + \mathcal{G}_k(\omega)(a_-^{(0)} + \kappa_+ b_-^{(0)})}. \tag{4.38}$$

The boundary condition for a pole in the Green's function at $\omega = 0$ is $a_+^{(0)} + \kappa_+ b_+^{(0)} = 0$. Thus, by eq. (4.19), the critical value of κ_+ is

$$\kappa_c = 3^{-\sqrt{m^2+4}} \times \frac{\Gamma\big(\frac{\Delta_- - 1}{2} + \nu_k + \frac{q}{\sqrt{3}}\big)\Gamma\big(\frac{\Delta_- - 1}{2} + \nu_k - \frac{q}{\sqrt{3}}\big)\Gamma(\Delta_+ - 1)}{\Gamma\big(\frac{\Delta_+ - 1}{2} + \nu_k + \frac{q}{\sqrt{3}}\big)\Gamma\big(\frac{\Delta_+ - 1}{2} + \nu_k - \frac{q}{\sqrt{3}}\big)\Gamma(\Delta_- - 1)}. \tag{4.39}$$

When $\kappa_+ = \kappa_c$, we obtain a hybridized critical point, which is described by an order parameter in the Ginzburg-Landau sector hybridized with a strongly coupled sector, the emergent CFT_1 dual to the IR AdS_2 [2]. The Green's function near a hybridized critical point can be written as

$$G(\omega, k) = \frac{1}{\kappa_+ - \kappa_c + h_k k^2 - h_\omega \omega + hC(\nu)(-i\omega)^{2\nu}}, \tag{4.40}$$

[6]When $m^2 \geq -3$, eq. (4.36) is an irrelevant term. We assume that the UV geometry is not changed, and examine (both UV and IR) instabilities by the Green's function.

where

$$h = \frac{a_-^{(0)} + \kappa_c b_-^{(0)}}{b_+^{(0)}} = -\frac{\nu}{\sqrt{m^2+4}\,(b_+^{(0)})^2}, \qquad C = \frac{\Gamma(-2\nu)\Gamma\left(\frac{1}{2}+\nu-\frac{iq}{\sqrt{6}}\right)}{\Gamma(2\nu)\Gamma\left(\frac{1}{2}-\nu-\frac{iq}{\sqrt{6}}\right)} 2^{2\nu}. \quad (4.41)$$

For a neutral scalar, the first order in ω vanishes, so we need to write $h_\omega \omega^2$ instead.

We assume $\nu < 1/2$ for a charged scalar, or $\nu < 1$ for a neutral scalar. For example, $\nu < 1$ for a neutral scalar means $-3 < m^2 < 9$, which is already a large range. Then we do not need h_ω since the $\omega^{2\nu}$ term is dominant as $\omega \to 0$. For the Green's function, $\omega = 0$ is a branch point in the complex ω-plane, and we define the physical sheet as $\theta \in (-\pi/2, 3\pi/2)$. The Green's function has a pole at

$$\omega_* = i\left(\frac{\kappa_c - \kappa_+}{hC(\nu)}\right)^{\frac{1}{2\nu}}. \quad (4.42)$$

Note that $h < 0$, and for $q > 0$,

$$0 < \arg\frac{1}{(-C)^{1/2\nu}} < \frac{\pi}{2}, \qquad \nu < \frac{1}{2}, \quad (4.43)$$

(see appendix A.4); for $q = 0$, C is real and negative. Therefore, when $\kappa_+ < \kappa_c$, the pole will be in the upper half ω-plane of the physical sheet. When $\kappa_+ > \kappa_c$, the pole will be either in the lower half ω-plane of the physical sheet, or on a non-physical sheet.

We can easily plot the critical value of κ_+ for the hybridized critical point as a function of u, as shown in figure 4.6. The boundary for the bifurcating critical point is $u = 0$. The two curves $u = 0$ and $\kappa_+ = \kappa_c$ intersect at $(u, \kappa_+) = (0, -2)$, which is a marginal critical point. When κ_+ changes across the curve from $\kappa_+ > \kappa_c$ to $\kappa_+ < \kappa_c$, a pole will move across the origin to the upper half ω-plane, causing an instability. We can see that κ_c is a single-valued function of u, which implies the following. If we keep increasing or decreasing κ_+, after a pole moves across the origin

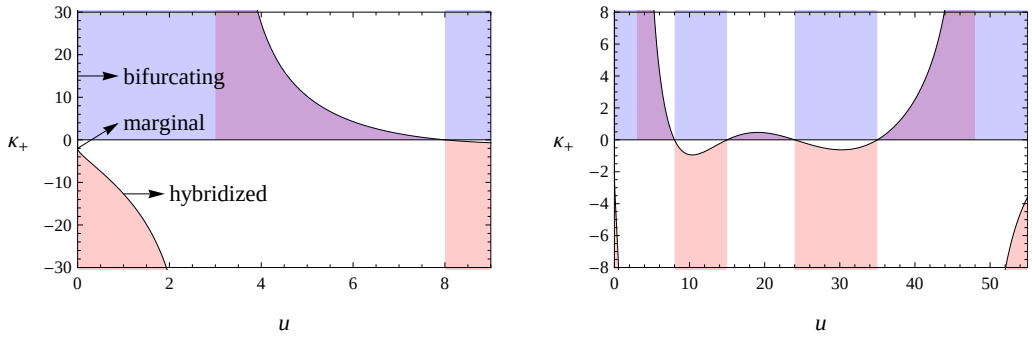

Figure 4.6: The tentative phase diagram for a neutral scalar ($q = 0$), with different ranges of $u = m^2 + 3$. The small u part is consistent with ref. [2]. The bifurcating critical point is at $u = 0$, and the oscillatory region is $u < 0$. The hybridized critical point is at $\kappa_+ = \kappa_c$. The curve crosses the horizontal axis at $u = 8$. The red shaded region when $\kappa_+ < \kappa_c$ is for IR instability, and the blue shaded region when $\kappa_+ > 0$ is for UV instability. The white regions are stable.

of the complex ω-plane, it will never come back to the origin. However, we cannot exclude the possibility that a pole can appear from infinity in the upper half ω-plane, or a pole in the upper half ω-plane can move to infinity and disappear. The analytic solution cannot capture these features. We hope further numerical calculations can be helpful to make this clear.[7]

We will refer to the IR instability as the singularity of the Green's function at $|\omega| \to 0$, and UV instability as the singularity of the Green's function at $|\omega| \to \infty$ in the upper half complex ω-plane. For a CFT at zero density, the boundary for the UV instability is $\kappa_+ = 0$ [2]. If the UV and IR instabilities are related, a tentative phase diagram for a neutral scalar is shown in figure 4.6. The boundary for the hybridized critical point is much more intricate than previous numerical results showed [2]. Especially, the curve will cross the u axis ($\kappa_+ = 0$). From eq. (4.39), we can see that when $1 - \Delta_- = -n$, i.e., $m^2 = (n+1)^2 - 4$, where $n = 0, 1, \cdots$, the denominator of κ_c is infinity; thus, if there is no other infinity in the numerator, we have $\kappa_c = 0$, which implies that the static Green's function $G(\omega = 0) \to \infty$. However,

[7]There are two challenges in numerical calculations. One is that the result becomes inaccurate very quickly as the $\mathrm{Im}(\omega)$ becomes large; the other is that it is more difficult to obtain the expectation value accurately when the scaling dimension is large.

when Δ_+ (or Δ_-) is a integer, we need to use eq. (A.47) in appendix A.3 to calculate the Green's function, and the result is usually finite. This puzzle is largely related to the renormalization near integer values of $\Delta_\pm$ (see appendix A.3).

4.4.2 Marginal critical point

The marginal critical point happens at both $u = 0$ and $\kappa_+ = \kappa_c$. Recall that the IR scaling dimension $\delta_k = 1/2 + \nu_k$; when $\nu = 0$, the double trace deformation is marginally relevant in the IR CFT [2]. The only possible parameters for the marginal critical point are $m^2 = -3$ and $q = 0$. The critical value of κ_+ is $\kappa_c = -2$, which can be obtained from eq. (4.39) by setting $q = 0$ and $k = 0$ first, and then taking the $m^2 \to -3$ limit. The direct calculations are as follows. The solution of ϕ in the outer region at $\omega = 0$ and $k = 0$ is

$$\phi_O = \frac{z}{\sqrt{1-z^2}} \left(C_1 + C_2 \ln \frac{1-z^2}{2z^2+1} \right). \tag{4.44}$$

The solution in the inner region is

$$\phi_I = \frac{\ln[12(1-z)]}{\sqrt{12(1-z)}} + \mathcal{G}_0(\omega) \frac{1}{\sqrt{12(1-z)}}, \tag{4.45}$$

where $\mathcal{G}_0$ is given by eq. (4.32). By matching ϕ_O and ϕ_I, we obtain

$$\begin{aligned} \alpha &= \frac{1}{\sqrt{6}} & \beta &= \frac{1}{2\sqrt{6}} \\ \tilde{\alpha} &= \frac{1}{\sqrt{6}} \ln 18 & \tilde{\beta} &= \frac{1}{2\sqrt{6}} \ln 18 - \frac{3}{\sqrt{6}}. \end{aligned} \tag{4.46}$$

By expanding eq. (4.38) at small ν, the Green's function near the marginal critical point is

$$G = \frac{\beta\, \mathcal{G}_0(\omega) + \tilde{\beta}}{(\alpha + \kappa_+ \beta)\mathcal{G}_0(\omega) + \tilde{\alpha} + \kappa_+ \tilde{\beta}}, \tag{4.47}$$

which gives

$$G = \frac{\ln\omega - 2\ln 6 + 6 + \gamma - i\pi/2}{(\kappa_+ + 2)(\ln\omega - 2\ln 6 + 6 + \gamma - i\pi/2) - 12}, \tag{4.48}$$

where the critical value of κ_+ is -2.

We can replace the zero temperature Green's function $\mathcal{G}_k(\omega)$ with the finite temperature Green's function, eq. (A.62) in appendix A.4, and the phase diagram of T-κ_+ can be obtained [2]. At finite temperature $T << \mu$, the result is

$$G = \frac{\psi\left(\frac{1}{2} - \frac{i\omega}{2\pi T}\right) + \ln\frac{\pi T}{18} + 6 + \gamma}{(\kappa_+ + 2)\left[\psi\left(\frac{1}{2} - \frac{i\omega}{2\pi T}\right) + \ln\frac{\pi T}{18} + 6 + \gamma\right] - 12}, \tag{4.49}$$

whose imaginary part is

$$\mathrm{Im}G = \frac{\pi}{24}\tanh\frac{\omega}{2T} = \begin{cases} \dfrac{\pi\omega}{48T} & \omega << T \\ \dfrac{\pi}{24}\mathrm{sgn}(\omega) & \omega >> T. \end{cases} \tag{4.50}$$

4.5 Discussion

Starting from the extremal RN-AdS_5 black hole, we have studied the quantum critical points by solving the Klein-Gordon equation in the bulk. The result gives us a glimpse of some strongly interacting systems, whose properties are beyond the reach of the perturbative method in quantum field theory. Just like the harmonic oscillator and the hydrogen atom as exactly solvable models capture essential features in quantum mechanics, the exactly solvable model in this work, together with a previous fermionic one [55], captures many essential features in AdS/CMT.

We have calculated the Green's function to the leading order in ω. The non-analyticity of the Green's function indicates two types of instabilities: one is triggered by a zero mode, and the other is triggered by the instability of the IR geometry. In the standard/alternative quantization, the zero modes of the system are always at finite

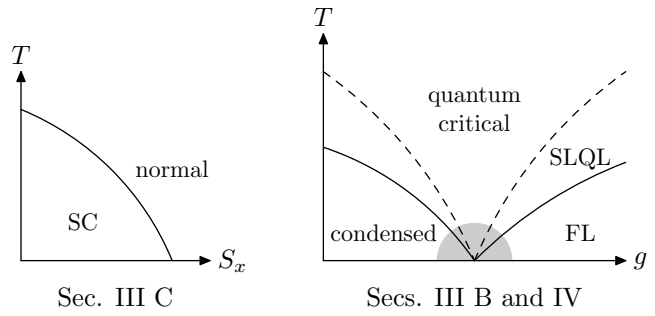

Figure 4.7: The left plot is the phase diagram for section 4.3.3. The parameter S_x is the superfluid velocity. SC denotes (holographic) superconductor. The right plot is the phase diagram for sections 4.3.2 and 4.4, according to ref. [2]. The parameter g is u for the bifurcating critical point, or κ_+ for the hybridized critical point.

$\mathbf{k}$. However, we can tune an extra parameter to make the zero mode be at $\mathbf{k} = 0$. We considered the quantum critical points of two systems, whose finite temperature phase diagrams are illustrated in figure 4.7. The extra parameter in the first system is the superfluid velocity. The RN-AdS_5 geometry describes the normal phase, and depending on the parameters (m^2, q), the system can develop zero mode instability, IR geometry instability, or be stable. The extra parameter in the second system is the double trace deformation. The zero mode instability gives a hybridized critical point. In the second system, besides the above IR instabilities, there is also UV instability, which is not captured by the analytic solution.

There are several remaining questions in the second system as follows. (i) What is the full phase diagram including both UV and IR instabilities? We already have the boundary for the IR instabilities. To find the stable region, we need not only the boundary for the UV instabilities, but how the poles move as we change the parameters. (ii) What happens to the Green's function when Δ_+ approaches an integer? This is related to the curve crossing the u-axis ($\kappa_+ = 0$) in figure 4.6. It seems that the Δ_+ approaching an integer limit is not the same as the result obtained by setting Δ_+ be the integer. (iii) What are the analogous models in condensed matter physics?

There is another related work [77] for the two-charge black hole in AdS_5, in which the massless Klein-Gordon equation is analytically solved. We can obtain the zero modes as $\nu_k = q - 2n - 3$, where $\nu_k = \sqrt{k^2 + 1}$ and n is a nonnegative integer. Only the first type of instability exists, because the electric field approaches zero in the near horizon limit [55].

Appendix A

Mathematical notes

A.1 Analytic results from Heun polynomials

In the AdS/CFT correspondence, some perturbation equations can be written in terms of the Heun equation, which has four regular singularities. Under certain conditions, the solution of the Heun equation is a polynomial, which can help us to obtain an exact solution to the Green's function. The Heun differential equation is

$$\frac{d^2y}{dx^2} + \left(\frac{\gamma}{x} + \frac{\delta}{x-1} + \frac{\epsilon}{x-a}\right)\frac{dy}{dx} + \frac{\alpha\beta x - Q}{x(x-1)(x-a)}y = 0\,, \tag{A.1}$$

where $\alpha+\beta+1 = \gamma+\delta+\epsilon$ [78]. The regular singularities are at $x = 0$, 1, a, and ∞. The solution to this equation is called the Heun function, if it is regular at both $x = 0$ and $x = 1$ (assuming $a > 1$). We denote the Heun function by $\mathrm{HeunG}(a, Q; \alpha, \beta, \gamma, \delta; x)$, which is symmetric in α and β. The Heun function can be written as a power series $\mathrm{HeunG}(x) = \sum_{r=0}^{\infty} c_r x^r$ where the coefficients satisfy a three term recursion relation [78]:

$$(r-1+\alpha)(r-1+\beta)c_{r-1} - \{r[(r-1+\gamma)(1+a)+a\delta+\epsilon]+Q\}c_r + (r+1)(r+\gamma)ac_{r+1} = 0\,.$$

Given this recursion relation, it is clear that if α or $\beta = -n$ and if $c_{n+1} = 0$, then HeunG(x) is an nth order polynomial.[1] In general, the condition $c_{n+1} = 0$ is an $(n+1)$th order algebraic equation in the parameters of the Heun function. Since we need to solve an $(n+1)$th-order algebraic equation to obtain an nth-order Heun polynomial, we usually cannot obtain explicit solutions when $n \geq 4$. (For comparison, the series expansion for the hypergeometric function ${}_2F_1(\alpha, \beta, \gamma; x)$ is defined by a two term recursion relation, and the polynomial condition is just $\alpha = -n$.) The set of solutions $c_{n+1} = 0$ may include unphysical regions of parameter space, for example regions where the charge or momentum is imaginary. We will need to further restrict the solution set.

Setting

$$\psi = \begin{pmatrix} u_1 \\ u_2 \end{pmatrix}, \tag{A.2}$$

the two coupled equations (2.5) for u_1 and u_2 can be reduced to a single second-order ODE. To avoid the awkward square root, we define $u_\pm = u_1 \pm u_2$, and then the Dirac equations are

$$\partial_z u_+ - \frac{i(\omega + qA_t)}{f} u_+ = \frac{m + ikz}{z\sqrt{f}} u_- , \tag{A.3}$$

$$\partial_z u_- + \frac{i(\omega + qA_t)}{f} u_- = \frac{m - ikz}{z\sqrt{f}} u_+ . \tag{A.4}$$

[1] There are other types of "Heun polynomials" [78]. For example, another solution to the Heun equation is $x^{1-\gamma}\text{HeunG}(a, (a\delta + \epsilon)(1-\gamma) + Q; \alpha + 1 - \gamma, \beta + 1 - \gamma, 2 - \gamma, \delta; x)$, which indicates that the HeunG on the right-hand side is a polynomial of order n when $\alpha + 1 - \gamma = -n$. In this work, other polynomials give unphysical results or the same results as the case $\alpha = -n$.

The equation for u_- is given by[2]

$$u_-'' + \left(\frac{f'}{2f} + \frac{m}{z(m-ikz)}\right) u_-' + \left[\frac{(\omega+qA_t)^2}{f^2} - \frac{m^2}{z^2 f} - \frac{k^2}{f} + \frac{i(\omega+qA_t)}{f}\left(-\frac{f'}{2f} + \frac{m}{z(m-ikz)}\right) + \frac{iqA_t'}{f}\right] u_- = 0\,. \quad \text{(A.5)}$$

We need to solve this equation with in-falling wave boundary condition at the horizon, and then plug u_- into eq. (A.4) to obtain u_+.

For the massless fermion in AdS_5, we obtain a second-order ODE with four regular singularities as follows:[3]

$$u_-'' + \frac{f'}{2f}u_-' + \left[\frac{(\omega+qA_t)^2}{f^2} - \frac{k^2}{f} - \frac{if'(\omega+qA_t)}{2f^2} + \frac{iqA_t'}{f}\right] u_- = 0\,, \quad \text{(A.6)}$$

where $f = 1-z^4$ and $A_t = 1-z^2$. The solution is

$$u_- \sim (z+1)^{i\omega/4+1/2}(z-1)^{-i\omega/4+1/2}(z+i)^{-q/2+1/2-\omega/4}(z-i)^{-3/2+q/2+\omega/4} \times \text{HeunG}\left(\frac{1}{2}, \frac{3-(1-i)\omega}{2} - \frac{ik^2}{4} - q; 2, \frac{3-\omega}{2} - q, \frac{3+i\omega}{2}, \frac{3-i\omega}{2}; \frac{(1-i)(z+1)}{2(z-i)}\right). \quad \text{(A.7)}$$

We can see that when

$$\omega = 2n + 3 - 2q\,, \qquad n = 0, 1, 2, \cdots\,, \quad \text{(A.8)}$$

we can obtain an nth-order polynomial solution p_n,

$$\text{HeunG}(x) = p_n = \sum_{r=0}^{n} c_r x^r\,, \qquad x = \frac{(1-i)(z+1)}{2(z-i)}\,, \quad \text{(A.9)}$$

[2]Note that this equation can be put in Schrödinger form and gives an alternate starting point for a WKB approximation. The corresponding Schrödinger potential is complex which makes phase integral methods substantially more involved.

[3]While we have focused on AdS_4 backgrounds in chapter 2, with an appropriate choice of gamma matrices [16], eq. (2.5) also holds for AdS_5.

if k satisfies an $(n+1)$th-order algebraic equation.

The zeroth-order polynomial is

$$p_0 = 1\,, \qquad \text{when} \quad k^2 = 6 - 4q\,. \tag{A.10}$$

With this exact solution, we can obtain the Green's function

$$G(\omega = 3 - 2q, k = \sqrt{6-4q}, q) = \frac{4 - 2q - \sqrt{6-4q}}{4 - 2q + \sqrt{6-4q}} i\,. \tag{A.11}$$

For the other sign of k, $G(-k) = -1/G(k)$. We can see that $\mathrm{Im}(G) > 0$ is always satisfied (if k is real). The first-order polynomial is

$$p_1 = 1 - \frac{2\omega - 2i\omega - 6 + ik^2 + 4q}{i\omega + 3} x\,, \qquad \text{when} \quad k^2 = 15 - 6q \pm \sqrt{4q^2 - 20q + 33}\,. \tag{A.12}$$

The Green's function

$$G(\omega = 5 - 2q, k = \sqrt{15 - 6q \pm \sqrt{4q^2 - 20q + 33}}, q) \tag{A.13}$$

can be exactly expressed. If we take the plus sign, for example, the result is

$$\frac{15 - 4q + (7-2q)\sqrt{4q^2 - 20q + 33} - (3 + \sqrt{4q^2 - 20q + 33})\sqrt{15 - 6q + \sqrt{4q^2 - 20q + 33}}}{15 - 4q + (7-2q)\sqrt{4q^2 - 20q + 33} + (3 + \sqrt{4q^2 - 20q + 33})\sqrt{15 - 6q + \sqrt{4q^2 - 20q + 33}}} i\,. \tag{A.14}$$

To obtain the second-order polynomial, we need to solve a third-order algebraic equation for k. There are higher-order polynomials, and the results are more complicated. The denominator of the above two Green's functions are non-zero for all real q. It is unlikely that we can solve for a Fermi momentum k_F in this way.

The exact results can be used to check the numerical program. For example, some exact results are

$$G(\omega=1,k=\sqrt{2},q=1) = (3-2\sqrt{2})i\,, \tag{A.15}$$

$$G(\omega=1,k=\sqrt{6},q=2) = \frac{59-24\sqrt{6}}{5}i\,, \tag{A.16}$$

$$G(\omega=-1,k=0,q=3) = i\,, \tag{A.17}$$

where the last one is consistent with $G(\omega,k=0)=i$ for massless spinors [22]. As more examples, we list the numerical value of the exact result and the numerical result in some special cases as follows:

ω	k	q	exact	numerical
7	$\sqrt{21+\sqrt{57}}$	-1	$0.21336115i$	$0.21336116i$
5	$\sqrt{15+\sqrt{33}}$	0	$0.16186619i$	$0.16186620i$
3	$\sqrt{9+\sqrt{17}}$	1	$0.10121094i$	$0.10121094i$
1	$\sqrt{6}$	2	$0.04244923i$	$0.04244924i$
0	$2^{3/4}$	5/2	$0.04177353i$	$0.04177353i$

There is a hidden algebraic structure in the Heun equation. A representation of the SU(2) algebra is

$$S_+ = z^2\partial_z - 2sz\,, \tag{A.18}$$

$$S_- = -\partial_z\,, \tag{A.19}$$

$$S_0 = z\partial_z - s\,, \tag{A.20}$$

where $[S_+,S_-]=2S_z$, $[S_0,S_\pm]=\pm S_\pm$, and $\mathbf{S}^2=s(s+1)$. If we consider the following Hamiltonian problem $Hy(z)=Ey(z)$ with

$$H=\sum_{\substack{i,j=-,0,+\\ i\geq j}} a_{ij}S_iS_j+\sum_{i=+,0,-} b_iS_i\,, \tag{A.21}$$

we obtain a differential equation with polynomial coefficients [79]:

$$P_4\, y''(z) + P_3\, y'(z) + P_2\, y(z) = E y(z)\,, \tag{A.22}$$

where

$$P_4 = a_{++}z^4 + a_{+0}z^3 + (a_{00} - a_{+-})z^2 - a_{0-}z + a_{--}\,, \tag{A.23}$$

$$P_3 = 2(1-2s)a_{++}z^3 + [(1-3s)a_{+0} + b_+]z^2 + [2s(a_{+-} - a_{00}) + a_{00} + b_0]z + sa_{0-} - b_-\,, \tag{A.24}$$

$$P_2 = 2s(2s-1)a_{++}z^2 + 2s(sa_{+0} - b_+)z + s^2 a_{00} - sb_0\,. \tag{A.25}$$

There is a correspondence between the Heun equation and the spin system by the following identification:

$$a_{++} = 0\,, \qquad a_{+0} = 1\,, \qquad a_{--} = 0\,, \tag{A.26}$$

$$a_{00} - a_{+-} = -(1+a)\,, \qquad a_{0-} = -a\,, \tag{A.27}$$

$$2s(a_{+-} - a_{00}) + a_{00} + b_0 = -(\gamma(1+a) + \delta a + \epsilon)\,, \tag{A.28}$$

$$sa_{0-} - b_- = a\gamma\,, \qquad s^2 a_{00} - sb_0 - E = Q\,, \tag{A.29}$$

$$b_+ - 3s = \alpha + \beta\,, \qquad 2s(s - b_+) = \alpha\beta\,. \tag{A.30}$$

Solving eq. (A.30) gives $s = -\alpha/2$ or $s = -\beta/2$. If the total spin s is an integer or half-integer, the H in eq. (A.21) has a finite dimensional representation. Therefore, the eigenvalues satisfy an algebraic equation by diagonalizing H. This algebraic equation is equivalent to the condition for the existence of a Heun polynomial solution. If s is not an integer or half-integer, the Hilbert space is infinite dimensional.

The interpretation of why there exist some exact solutions to the Green's function is as follows. When $m = 0$, in the three-dimensional parameter space (ω, k, q),

there are discrete one-dimensional lines (subspaces) that are labeled by $n = 1, 2, \cdots$. On these lines, the Hilbert space (accidentally) becomes finite dimensional. So the eigenvalues satisfy an nth-order algebraic equation. When $n \leq 4$, we can explicitly solve the algebraic equation.

A.2 Mathematical notes for chapter 3

Hypergeometric function ${}_2F_1(\alpha, \beta; \gamma; z)$. We will denote ${}_2F_1$ by F for simplicity in the following. The derivative of the hypergeometric function can also be expressed by a hypergeometric function:

$$\frac{d}{dz}F(\alpha, \beta; \gamma; z) = \frac{\alpha\beta}{\gamma}F(\alpha + 1, \beta + 1; \gamma + 1; z). \tag{A.31}$$

The following formula can be used to combine the sum of two hypergeometric functions:

$$\gamma F(\alpha, \beta; \gamma; z) + \alpha z F(\alpha + 1, \beta + 1; \gamma + 1; z) = \gamma F(\alpha, \beta + 1; \gamma; z). \tag{A.32}$$

In general, the hypergeometric function has branch points at $z = 0$, 1, and ∞. By convention, we make a branch cut from $z = 1$ to ∞, and take the principle branch as $-2\pi < \arg z \leq 0$ for $|z| > 1$. The following formula can be used to transform a value above the branch cut to another value below the branch cut:

$$F(\alpha, \beta; \gamma; z) = (1 - z)^{-\alpha} F\big(\alpha, \gamma - \beta; \gamma; \frac{z}{z - 1}\big). \tag{A.33}$$

The $z = 2$ point has the following special property:

$$z \to \frac{z}{z - 1}: \qquad 2 \pm i\epsilon \to 2 \mp i\epsilon. \tag{A.34}$$

By eq. (A.33) and $(-1-i\epsilon)^{-\alpha} = e^{i\alpha\pi}$, we have

$$F(\alpha,\beta;\gamma;2+i\epsilon) = e^{i\alpha\pi}F(\alpha,\gamma-\beta;\gamma;2-i\epsilon). \tag{A.35}$$

We define

$$F(\alpha,\beta;\gamma;2) := F(\alpha,\beta;\gamma;2-i\epsilon). \tag{A.36}$$

The condition for the normal modes is

$$F(-n,\nu_k;2\nu_k+1;2) = \pm F(-n,\nu_k+1;2\nu_k+1;2), \tag{A.37}$$

where $n = -\nu_k + q - 1/2$. The plus sign is for G_1 and the minus sign is for G_2. We assume that n is a non-negative integer at first. If n is even, the above equation with the plus sign is satisfied; If n is odd, the above equation with the minus sign is satisfied. We can numerically check that they are the only solutions when $q > 0$. When $q < 0$, there is another set of solutions due to the $q \to -q$, $\omega \to -\omega$, $u_1 \leftrightarrow u_2$ symmetry of the Dirac equation; however, these solutions are unphysical because they give $\mathrm{Im}(G) < 0$. Intuitively, only if a particle and the black hole have the same charge can there be a balance between the attractive gravitational force and the repulsive electromagnetic force on the particle.

For non-negtive integer n,

$$F(-n,\nu;2\nu+1;2) = \begin{cases} \dfrac{\Gamma(n/2+1/2)\Gamma(\nu+1/2)}{\sqrt{\pi}\,\Gamma(\nu+n/2+1/2)} & \text{if } n \text{ is even} \\ \dfrac{\Gamma(n/2+1)\Gamma(\nu+1/2)}{\sqrt{\pi}\,\Gamma(\nu+n/2+1)} & \text{if } n \text{ is odd.} \end{cases} \tag{A.38}$$

Gamma function. Useful identities for the Gamma functions include

$$\Gamma\Big(n+\frac{1}{2}\Big) = \frac{(2n)!}{4^n n!}\sqrt{\pi} = \frac{(2n-1)!!}{2^n}\sqrt{\pi}$$
$$\Gamma(z)\Gamma(1-z) = \frac{\pi}{\sin \pi z}$$
$$\Gamma(z)\Gamma(z+1/2) = 2^{1-2z}\sqrt{\pi}\,\Gamma(2z). \tag{A.39}$$

Whittaker function. Whittaker's equation is

$$\frac{d^2W}{dz^2} + \left(-\frac{1}{4} + \frac{\lambda}{z} + \frac{1/4-\mu^2}{z^2}\right) W = 0. \tag{A.40}$$

We can write down the general solution as $C_1 W_{\lambda,\mu}(z) + C_2 W_{-\lambda,\mu}(-z)$, where for large $|z|$ one has

$$W_{\lambda,\mu}(z) \sim e^{-z/2} z^{\lambda}(1+\cdots), \qquad |z| \to \infty. \tag{A.41}$$

As special cases, $W_{\pm 1/2,\mu}(z)$ are related to the modified Bessel function $K_\nu(z)$ by

$$W_{1/2,\mu}(z) = \frac{z}{2\sqrt{\pi}}\left(K_{\mu+1/2}\left(\frac{z}{2}\right) + K_{\mu-1/2}\left(\frac{z}{2}\right)\right)$$
$$W_{-1/2,\mu}(z) = \frac{z}{2\mu\sqrt{\pi}}\left(K_{\mu+1/2}\left(\frac{z}{2}\right) - K_{\mu-1/2}\left(\frac{z}{2}\right)\right). \tag{A.42}$$

A.3 Mathematical notes for chapter 4

Hypergeometric function ${}_2F_1(\alpha,\beta;\gamma;x)$. We will denote ${}_2F_1$ by F for simplicity. The following formulas are helpful to obtain and understand the analytic solutions:

$$F(\alpha,\beta;\gamma;x) = (1-x)^{-\beta} F\big(\gamma-\alpha,\beta;\gamma;\frac{x}{x-1}\big). \tag{A.43}$$

If $\mathrm{Re}(\gamma) > \mathrm{Re}(\alpha+\beta)$,

$$F(\alpha,\beta;\gamma;1) = \frac{\Gamma(\gamma)\Gamma(\gamma-\alpha-\beta)}{\Gamma(\gamma-\alpha)\Gamma(\gamma-\beta)}. \tag{A.44}$$

A connection formula for the hypergeometric function is

$$\begin{aligned} F(\alpha,\beta;\gamma;x) = {} & AF(\alpha,\beta;\alpha+\beta-\gamma+1;1-x) \\ & + B(1-x)^{\gamma-\alpha-\beta}F(\gamma-\alpha,\gamma-\beta;\gamma-\alpha-\beta+1;1-x), \end{aligned} \tag{A.45}$$

where

$$A = \frac{\Gamma(\gamma)\Gamma(\gamma-\alpha-\beta)}{\Gamma(\gamma-\alpha)\Gamma(\gamma-\beta)}, \qquad B = \frac{\Gamma(\gamma)\Gamma(\alpha+\beta-\gamma)}{\Gamma(\alpha)\Gamma(\beta)}. \tag{A.46}$$

Other solutions for the Klein-Gordon equation (4.7). If Δ_+ is an integer, eq. (4.16) is no longer a general solution. If $2\nu_k$ is not an integer, the general solution for eq. (4.7) at $\omega = 0$ can be written as

$$\begin{aligned} \phi(z) = {} & C_1 \frac{z^{\Delta_+}(1-z^2)^{-1/2-\nu_k}}{(2z^2+1)^{-1/2-\nu_k+\Delta_+/2}}\, {}_2F_1\Big(\frac{\Delta_+-1}{2}-\nu_k-\frac{q}{\sqrt{3}}, \frac{\Delta_+-1}{2}-\nu_k+\frac{q}{\sqrt{3}}; 1-2\nu_k; \frac{1-z^2}{2z^2+1}\Big) \\ & + C_2 \frac{z^{\Delta_+}(1-z^2)^{-1/2+\nu_k}}{(2z^2+1)^{-1/2+\nu_k+\Delta_+/2}}\, {}_2F_1\Big(\frac{\Delta_+-1}{2}+\nu_k-\frac{q}{\sqrt{3}}, \frac{\Delta_+-1}{2}+\nu_k+\frac{q}{\sqrt{3}}; 1+2\nu_k; \frac{1-z^2}{2z^2+1}\Big). \end{aligned} \tag{A.47}$$

If $2q/\sqrt{3}$ is not an integer, the general solution can also be written as

$$\begin{aligned} \phi(z) = {} & C_1 z^{\Delta_+} \frac{(1-z^2)^{-\Delta_+/2+q/\sqrt{3}}}{(2z^2+1)^{q/\sqrt{3}}}\, {}_2F_1\Big(\frac{\Delta_+-1}{2}-\nu_k-\frac{q}{\sqrt{3}}, \frac{\Delta_+-1}{2}+\nu_k-\frac{q}{\sqrt{3}}; 1-\frac{2q}{\sqrt{3}}; \frac{2z^2+1}{1-z^2}\Big) \\ & + C_2 z^{\Delta_+} \frac{(1-z^2)^{-\Delta_+/2-q/\sqrt{3}}}{(2z^2+1)^{-q/\sqrt{3}}}\, {}_2F_1\Big(\frac{\Delta_+-1}{2}-\nu_k+\frac{q}{\sqrt{3}}, \frac{\Delta_+-1}{2}+\nu_k+\frac{q}{\sqrt{3}}; 1+\frac{2q}{\sqrt{3}}; \frac{2z^2+1}{1-z^2}\Big). \end{aligned} \tag{A.48}$$

If all Δ_+, $2\nu_k$, and $2q/\sqrt{3}$ are integers, it is likely that the solution is an elementary function. It is especially convenient to use eq. (A.47), because the boundary condition at the horizon to obtain zero modes is simply $C_1 = 0$. We will discuss some special cases, in which we only consider the standard quantization.

Special case 1: $m^2 = -4$ ($\Delta_+ = 2$). By using eq. (A.47), the result for the static Green's function is

$$G(\omega = 0) = \frac{1}{2}\Big[\psi\Big(\frac{1}{2} + \nu_k - \frac{q}{\sqrt{3}}\Big) + \psi\Big(\frac{1}{2} + \nu_k + \frac{q}{\sqrt{3}}\Big) + 2\gamma + \ln 3\Big], \tag{A.49}$$

where $\psi(x)$ is the digamma function.

Special case 2: $m^2 = -3$ ($\Delta_+ = 3$). Similarly, the result for the static Green's function is

$$G(\omega = 0) = (3\nu_k^2 - q^2)\Big[\psi\Big(1 + \nu_k - \frac{q}{\sqrt{3}}\Big) + \psi\Big(1 + \nu_k + \frac{q}{\sqrt{3}}\Big) + 2\gamma + \ln 3 - 1\Big] + \frac{1}{2} - 3\nu_k. \tag{A.50}$$

Special case 3: $m^2 = 0$ ($\Delta_+ = 4$) and $q = 0$. The solution for eq. (4.7) at $\omega = 0$ is

$$\phi_O = C_1 + C_2\left(\frac{3}{1 - z^2} + \ln\frac{1 - z^2}{2z^2 + 1}\right). \tag{A.51}$$

The solution for eq. (4.7) in the inner region is $\phi_I = e^{i\omega/[12(1-z)]}$. We obtain $G(\omega = 0) = 0$, which implies $\kappa_c \to \infty$ at $u = 3$, and thus is consistent with figure 4.6.

Special case 4: $m^2 = 5$ ($\Delta_+ = 5$). This corresponds to $u = 8$ in figure 4.6. The result is cumbersome, but it is clear that the Green's function at $\omega = 0$ is a finite number, which implies that $\kappa_c \neq 0$. However, figure 4.6 shows that $\kappa_c = 0$ at $u = 8$. This inconsistency can be explained as follows. If we take the limit that Δ_+ approaches an integer, eq. (4.16) diverges, and we need a renormalization, which changes κ_c.

Let's take a more careful examination about the cases when $\Delta_+ = 2, 3, \cdots$. When $\Delta_+ = 2$, i.e., $m^2 = m_{\rm BF}^2 = -4$, $\phi = Az^2 \ln z + Bz^2 + \cdots$, where A is the source. Now we consider $\Delta_+ > 2$. According to eq. (4.19), the expectation value B is divergent

when Δ_+ is an integer. If we add a small number δ to Δ_+, we have

$$B = \frac{b}{\delta} + B_r + \mathcal{O}(\delta), \tag{A.52}$$

where B_r is the renormalized value of B. By the expansion

$$z^\delta = 1 + \delta \ln z + \frac{1}{2}(\delta \ln z)^2 + \cdots, \qquad \delta \to 0, \tag{A.53}$$

we have

$$\begin{aligned}\phi &= Az^{\Delta_-}(1 + \cdots) + Bz^{\Delta_+ + \delta}(1 + \cdots) \\ &= Az^{\Delta_-}(1 + \cdots) + z^{\Delta_+}\Big(\frac{b}{\delta} + B_r + b \ln z + \mathcal{O}(\delta \ln z)\Big)(1 + \cdots),\end{aligned} \tag{A.54}$$

where "$\cdots$" denotes higher-order terms in z. The renormalized Green's function by the standard quantization is $G_r = B_r/A$. Since there is a logarithm, the near boundary expansion should be evaluated at a UV cutoff $z = L_{\rm UV}$ ($L_{\rm UV}/L << 1$). Therefore, there are two noncommuting limits: $\delta \to 0$ and $L_{\rm UV} \to 0$. The Green's function obtained by eq. (4.19) makes sense only if the following condition is satisfied:

$$\left|\delta \cdot \ln \frac{L_{\rm UV}}{L}\right| << 1. \tag{A.55}$$

A.4 IR Green's function

The IR Green's function $\mathcal{G}_k(\omega)$ for the scalar field is given in ref. [22]. We will briefly review the result first. The IR geometry described by

$$f = 12(1 - z)^2, \qquad A_t = 2\sqrt{6}(1 - z). \tag{A.56}$$

Define the AdS_2 coordinate

$$\zeta = \frac{1}{12(1-z)}. \tag{A.57}$$

The solution to the Klein-Gordon equation with the in-falling boundary condition at the horizon is

$$\phi \sim W_{-\frac{iq}{\sqrt{6}},\nu_k}(-2i\omega\zeta), \tag{A.58}$$

where $W_{\lambda,\mu}(x)$ is a Whittaker function with the following asymptotic behavior:

$$W_{\lambda,\mu}(x) \sim e^{-x/2}x^{\lambda}(1+\cdots), \qquad |x| \to \infty. \tag{A.59}$$

By expanding eq. (A.58) at $\omega\zeta \to 0$, we obtain

$$\phi = \zeta^{1/2-\nu_k} + \mathcal{G}_k(\omega)\zeta^{1/2+\nu_k}. \tag{A.60}$$

The IR Green's function at zero temperature is

$$\mathcal{G}_k(\omega) = \frac{\Gamma(-2\nu_k)\Gamma(\frac{1}{2}+\nu_k-\frac{iq}{\sqrt{6}})}{\Gamma(2\nu_k)\Gamma(\frac{1}{2}-\nu_k-\frac{iq}{\sqrt{6}})}(-2i\omega)^{2\nu_k}. \tag{A.61}$$

The finite temperature generalization at $T << \mu$ (chemical potential) is

$$\mathcal{G}_k^{(T)}(\omega) = (4\pi T)^{2\nu_k} \times \frac{\Gamma(-2\nu_k)\Gamma\big(\frac{1}{2}+\nu_k-\frac{iq}{\sqrt{6}}\big)\Gamma\big(\frac{1}{2}+\nu_k-\frac{i\omega}{2\pi T}+\frac{iq}{\sqrt{6}}\big)}{\Gamma(2\nu_k)\Gamma\big(\frac{1}{2}-\nu_k-\frac{iq}{\sqrt{6}}\big)\Gamma\big(\frac{1}{2}+\nu_k-\frac{i\omega}{2\pi T}+\frac{iq}{\sqrt{6}}\big)}. \tag{A.62}$$

Near the bifurcating critical point $\nu \to 0$,

$$\mathcal{G}_{k=0}^{(T)}(\omega) = -1 + 2\nu\mathcal{G}_0^{(T)}(\omega), \tag{A.63}$$

where

$$\mathcal{G}_0^{(T)}(\omega) = -\psi\Big(\frac{1}{2}+\frac{iq}{\sqrt{6}}-\frac{i\omega}{2\pi T}\Big) - 2\gamma - \ln(4\pi T) - \psi\Big(\frac{1}{2}-\frac{iq}{\sqrt{6}}\Big). \tag{A.64}$$

Particularly, for a neutral scalar,

$$\mathcal{G}_0^{(T)}(\omega) = -\psi\Big(\frac{1}{2} - \frac{i\omega}{2\pi T}\Big) - \gamma - \ln(\pi T). \tag{A.65}$$

For $q > 0$ and $\nu < 1/2$, eq. (4.43) can be proved by

$$\begin{aligned}\arg \frac{1}{(-C)} &= \arg\left(-\frac{\Gamma(2\nu)\Gamma(\frac{1}{2} - \nu - iq_*)}{\Gamma(-2\nu)\Gamma(\frac{1}{2} + \nu - iq_*)}\right) \\ &= \arg[\cos\pi(\nu - iq_*)] \\ &= \arctan(\tan\pi\nu \tanh\pi q_*) < \pi\nu,\end{aligned} \tag{A.66}$$

where we have used the reflection formula $\Gamma(x)\Gamma(1-x) = \pi/\sin\pi x$, and the fact that we can put any positive number inside $\arg(x)$ without changing its value.

Bibliography

[1] K. G. Wilson and M. E. Fisher, *Critical exponents in 3.99 dimensions*, *Phys.Rev.Lett.* **28** (1972) 240–243.

[2] N. Iqbal, H. Liu, and M. Mezei, *Quantum phase transitions in semi-local quantum liquids*, arXiv:1108.0425.

[3] S. Sachdev and B. Keimer, *Quantum Criticality*, *Physics Today* **64** (2011) 29, [arXiv:1102.4628].

[4] S. A. Hartnoll, *Lectures on holographic methods for condensed matter physics*, *Class.Quant.Grav.* **26** (2009) 224002, [arXiv:0903.3246].

[5] C. P. Herzog, *Lectures on Holographic Superfluidity and Superconductivity*, *J.Phys.* **A42** (2009) 343001, [arXiv:0904.1975].

[6] J. McGreevy, *Holographic duality with a view toward many-body physics*, *Adv.High Energy Phys.* **2010** (2010) 723105, [arXiv:0909.0518].

[7] J. M. Maldacena, *The Large N limit of superconformal field theories and supergravity*, *Adv.Theor.Math.Phys.* **2** (1998) 231–252, [hep-th/9711200].

[8] O. Aharony, O. Bergman, D. L. Jafferis, and J. Maldacena, *N=6 superconformal Chern-Simons-matter theories, M2-branes and their gravity duals*, *JHEP* **0810** (2008) 091, [arXiv:0806.1218].

[9] S. Gubser, I. R. Klebanov, and A. M. Polyakov, *Gauge theory correlators from noncritical string theory*, *Phys.Lett.* **B428** (1998) 105–114, [hep-th/9802109].

[10] E. Witten, *Anti-de Sitter space and holography*, *Adv.Theor.Math.Phys.* **2** (1998) 253–291, [hep-th/9802150].

[11] M. Cvetic, M. Duff, P. Hoxha, J. T. Liu, H. Lu, *et. al.*, *Embedding AdS black holes in ten-dimensions and eleven-dimensions*, *Nucl.Phys.* **B558** (1999) 96–126, [hep-th/9903214].

[12] D. T. Son and A. O. Starinets, *Minkowski space correlators in AdS/CFT correspondence: Recipe and applications*, *JHEP* **0209** (2002) 042, [hep-th/0205051].

[13] P. Breitenlohner and D. Z. Freedman, *Stability in Gauged Extended Supergravity*, *Annals Phys.* **144** (1982) 249.

[14] I. R. Klebanov and E. Witten, *AdS/CFT correspondence and symmetry breaking*, *Nucl.Phys.* **B556** (1999) 89–114, [hep-th/9905104].

[15] M. Ammon, J. Erdmenger, M. Kaminski, and A. O'Bannon, *Fermionic Operator Mixing in Holographic p-wave Superfluids*, *JHEP* **1005** (2010) 053, [arXiv:1003.1134].

[16] D. R. Gulotta, C. P. Herzog, and M. Kaminski, *Sum Rules from an Extra Dimension*, *JHEP* **1101** (2011) 148, [arXiv:1010.4806].

[17] M. Edalati, R. G. Leigh, and P. W. Phillips, *Dynamically Generated Mott Gap from Holography*, *Phys.Rev.Lett.* **106** (2011) 091602, [arXiv:1010.3238].

[18] M. Edalati, R. G. Leigh, K. W. Lo, and P. W. Phillips, *Dynamical Gap and Cuprate-like Physics from Holography*, *Phys.Rev.* **D83** (2011) 046012, [arXiv:1012.3751].

[19] H. Liu, J. McGreevy, and D. Vegh, *Non-Fermi liquids from holography*, *Phys.Rev.* **D83** (2011) 065029, [arXiv:0903.2477].

[20] D. Guarrera and J. McGreevy, *Holographic Fermi surfaces and bulk dipole couplings*, arXiv:1102.3908.

[21] P. K. Kovtun and A. O. Starinets, *Quasinormal modes and holography*, *Phys.Rev.* **D72** (2005) 086009, [hep-th/0506184].

[22] T. Faulkner, H. Liu, J. McGreevy, and D. Vegh, *Emergent quantum criticality, Fermi surfaces, and AdS(2)*, *Phys.Rev.* **D83** (2011) 125002, [arXiv:0907.2694].

[23] T. Faulkner, N. Iqbal, H. Liu, J. McGreevy, and D. Vegh, *Holographic non-Fermi liquid fixed points*, arXiv:1101.0597.

[24] N. Iqbal, H. Liu, and M. Mezei, *Semi-local quantum liquids*, *JHEP* **1204** (2012) 086, [arXiv:1105.4621].

[25] C. Varma, P. Littlewood, S. Schmitt-Rink, E. Abrahams, and A. Ruckenstein, *Phenomenology of the normal state of Cu-O high-temperature superconductors*, *Phys.Rev.Lett.* **63** (1989) 1996–1999.

[26] S. A. Hartnoll, J. Polchinski, E. Silverstein, and D. Tong, *Towards strange metallic holography*, *JHEP* **1004** (2010) 120, [arXiv:0912.1061].

[27] S. A. Hartnoll, D. M. Hofman, and D. Vegh, *Stellar spectroscopy: Fermions and holographic Lifshitz criticality*, *JHEP* **1108** (2011) 096, [arXiv:1105.3197].

[28] S. S. Gubser and F. D. Rocha, *Peculiar properties of a charged dilatonic black hole in AdS_5*, *Phys.Rev.* **D81** (2010) 046001, [arXiv:0911.2898].

[29] X. Dong, S. Harrison, S. Kachru, G. Torroba, and H. Wang, *Aspects of holography for theories with hyperscaling violation*, *JHEP* **1206** (2012) 041, [arXiv:1201.1905].

[30] C. P. Herzog and J. Ren, *The Spin of Holographic Electrons at Nonzero Density and Temperature*, *JHEP* **1206** (2012) 078, [arXiv:1204.0518].

[31] M. Henningson and K. Sfetsos, *Spinors and the AdS/CFT correspondence*, *Phys.Lett.* **B431** (1998) 63–68, [hep-th/9803251].

[32] W. Mueck and K. Viswanathan, *Conformal field theory correlators from classical field theory on anti-de Sitter space. 2. Vector and spinor fields*, *Phys.Rev.* **D58** (1998) 106006, [hep-th/9805145].

[33] S.-S. Lee, *A Non-Fermi Liquid from a Charged Black Hole: A Critical Fermi Ball*, *Phys.Rev.* **D79** (2009) 086006, [arXiv:0809.3402].

[34] M. Cubrovic, J. Zaanen, and K. Schalm, *String Theory, Quantum Phase Transitions and the Emergent Fermi-Liquid*, *Science* **325** (2009) 439–444, [arXiv:0904.1993].

[35] C. Herzog, P. Kovtun, and D. Son, *Holographic model of superfluidity*, *Phys.Rev.* **D79** (2009) 066002, [arXiv:0809.4870].

[36] S. S. Gubser, *Breaking an Abelian gauge symmetry near a black hole horizon*, *Phys.Rev.* **D78** (2008) 065034, [arXiv:0801.2977].

[37] S. A. Hartnoll, C. P. Herzog, and G. T. Horowitz, *Building a Holographic Superconductor*, *Phys.Rev.Lett.* **101** (2008) 031601, [arXiv:0803.3295].

[38] S. A. Hartnoll, C. P. Herzog, and G. T. Horowitz, *Holographic Superconductors*, *JHEP* **0812** (2008) 015, [arXiv:0810.1563].

[39] T. Hartman and S. A. Hartnoll, *Cooper pairing near charged black holes*, *JHEP* **1006** (2010) 005, [arXiv:1003.1918].

[40] S. A. Hartnoll and A. Tavanfar, *Electron stars for holographic metallic criticality*, *Phys.Rev.* **D83** (2011) 046003, [arXiv:1008.2828].

[41] S. A. Hartnoll and P. Petrov, *Electron star birth: A continuous phase transition at nonzero density*, *Phys.Rev.Lett.* **106** (2011) 121601, [arXiv:1011.6469].

[42] S. Sachdev, *A model of a Fermi liquid using gauge-gravity duality*, *Phys.Rev.* **D84** (2011) 066009, [arXiv:1107.5321].

[43] S. A. Hartnoll and L. Huijse, *Fractionalization of holographic Fermi surfaces*, *Class.Quant.Grav.* **29** (2012) 194001, [arXiv:1111.2606].

[44] L. Huijse, S. Sachdev, and B. Swingle, *Hidden Fermi surfaces in compressible states of gauge-gravity duality*, *Phys.Rev.* **B85** (2012) 035121, [arXiv:1112.0573].

[45] F. Benini, C. P. Herzog, R. Rahman, and A. Yarom, *Gauge gravity duality for d-wave superconductors: prospects and challenges*, *JHEP* **1011** (2010) 137, [arXiv:1007.1981].

[46] N. Iqbal and H. Liu, *Real-time response in AdS/CFT with application to spinors*, *Fortsch.Phys.* **57** (2009) 367–384, [arXiv:0903.2596].

[47] D. Boyanovsky, R. Blankenbecler, and R. Yahalom, *Physical origin of topological mass in (2+1)-dimensions*, *Nucl.Phys.* **B270** (1986) 483.

[48] H. A. Weldon, *Effective Fermion Masses of Order gT in High Temperature Gauge Theories with Exact Chiral Invariance*, *Phys.Rev.* **D26** (1982) 2789.

[49] A. Allais, J. McGreevy, and S. J. Suh, *A quantum electron star*, *Phys.Rev.Lett.* **108** (2012) 231602, [arXiv:1202.5308].

[50] S. Linnaeus, *Phase-integral solution of the radial Dirac equation*, *J.Math.Phys.* **51** (2010) 032304.

[51] Wolfram Research, Inc., *Mathematica Edition: Version 8.0*. Champaign, Illinois, 2010.

[52] J. Sinova, D. Culcer, Q. Niu, N. A. Sinitsyn, T. Jungwirth, and A. H. MacDonald, *Universal Intrinsic Spin-Hall Effect*, *Phys.Rev.Lett* **92** (2004) 126603, [cond-mat/0307663].

[53] D. Hsieh *et. al.*, *A tunable topological insulator in the spin helical Dirac transport regime*, *Nature* **460** (2009) 1101, [arXiv:1001.1590].

[54] R. E. Langer, *On the Connection Formulas and the Solutions of the Wave Equation*, *Phys.Rev.* **51** (1937) 669.

[55] S. S. Gubser and J. Ren, *Analytic fermionic Green's functions from holography*, *Phys.Rev.* **D86** (2012) 046004, [arXiv:1204.6315].

[56] K. Goldstein, S. Kachru, S. Prakash, and S. P. Trivedi, *Holography of Charged Dilaton Black Holes*, *JHEP* **1008** (2010) 078, [arXiv:0911.3586].

[57] O. DeWolfe, S. S. Gubser, and C. Rosen, *Fermi Surfaces in Maximal Gauged Supergravity*, *Phys.Rev.Lett.* **108** (2012) 251601, [arXiv:1112.3036].

[58] D. Batic, H. Schmid, and M. Winklmeier, *The Generalized Heun equation in QFT in curved space-times*, *J.Phys.* **A39** (2006) 12559–12564, [gr-qc/0607017].

[59] B. Pioline and J. Troost, *Schwinger pair production in AdS(2)*, *JHEP* **0503** (2005) 043, [hep-th/0501169].

[60] J. Ren, *Analytic quantum critical points from holography*, arXiv:1210.2722.

[61] N. Evans, K. Jensen, and K.-Y. Kim, *Non Mean-Field Quantum Critical Points from Holography*, *Phys.Rev.* **D82** (2010) 105012, [arXiv:1008.1889].

[62] K. Jensen, *Semi-Holographic Quantum Criticality*, *Phys.Rev.Lett.* **107** (2011) 231601, [arXiv:1108.0421].

[63] T. Faulkner and J. Polchinski, *Semi-Holographic Fermi Liquids*, *JHEP* **1106** (2011) 012, [arXiv:1001.5049].

[64] T. Faulkner, G. T. Horowitz, and M. M. Roberts, *Holographic quantum criticality from multi-trace deformations*, *JHEP* **1104** (2011) 051, [arXiv:1008.1581].

[65] D. B. Kaplan, J.-W. Lee, D. T. Son, and M. A. Stephanov, *Conformality Lost*, *Phys.Rev.* **D80** (2009) 125005, [arXiv:0905.4752].

[66] K. Jensen, A. Karch, D. T. Son, and E. G. Thompson, *Holographic Berezinskii-Kosterlitz-Thouless Transitions*, *Phys.Rev.Lett.* **105** (2010) 041601, [arXiv:1002.3159].

[67] F. Denef and S. A. Hartnoll, *Landscape of superconducting membranes*, *Phys.Rev.* **D79** (2009) 126008, [arXiv:0901.1160].

[68] S. S. Gubser, C. P. Herzog, S. S. Pufu, and T. Tesileanu, *Superconductors from Superstrings*, *Phys.Rev.Lett.* **103** (2009) 141601, [arXiv:0907.3510].

[69] P. Basu, A. Mukherjee, and H.-H. Shieh, *Supercurrent: Vector Hair for an AdS Black Hole*, *Phys.Rev.* **D79** (2009) 045010, [arXiv:0809.4494].

[70] J. Sonner and B. Withers, *A gravity derivation of the Tisza-Landau Model in AdS/CFT*, *Phys.Rev.* **D82** (2010) 026001, [arXiv:1004.2707].

[71] D. Arean, P. Basu, and C. Krishnan, *The Many Phases of Holographic Superfluids*, *JHEP* **1010** (2010) 006, [arXiv:1006.5165].

[72] D. Arean, M. Bertolini, C. Krishnan, and T. Prochazka, *Type IIB Holographic Superfluid Flows*, *JHEP* **1103** (2011) 008, [arXiv:1010.5777].

[73] T. Albash and C. V. Johnson, *A Holographic Superconductor in an External Magnetic Field*, *JHEP* **0809** (2008) 121, [arXiv:0804.3466].

[74] N. Iqbal, H. Liu, M. Mezei, and Q. Si, *Quantum phase transitions in holographic models of magnetism and superconductors*, *Phys.Rev.* **D82** (2010) 045002, [arXiv:1003.0010].

[75] G. T. Horowitz and M. M. Roberts, *Zero Temperature Limit of Holographic Superconductors*, *JHEP* **0911** (2009) 015, [arXiv:0908.3677].

[76] E. Witten, *Multitrace operators, boundary conditions, and AdS/CFT correspondence*, hep-th/0112258.

[77] M. Alishahiha, M. R. M. Mozaffar, and A. Mollabashi, *Holographic Aspects of Two-charged Dilatonic Black Hole in AdS_5*, *JHEP* **1210** (2012) 003, [arXiv:1208.2535].

[78] A. Ronveaux, ed., *Heun's Differential Equations*. Oxford University Press, New York, 1995.

[79] A. V. Turbiner, *Quasi-exactly-solvable problems and sl(2) algebra*, *Commun.Math.Phys.* **118** (1988) 467.